IDENTIFICATION OF VASCULAR ENDOTHELIAL GROWTH FACTOR RECEPTOR 3 (VEGFR3) AS AN *IN VITRO* AND *IN VIVO* SUBSTRATE OF THE ALZHEIMER'S DISEASE-LINKED PROTEASE BACE2

Andree Schmidt

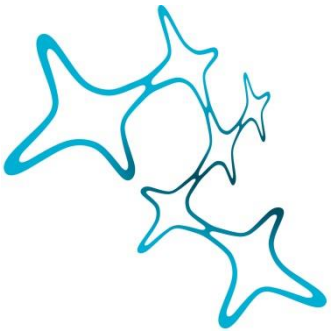

Graduate School of
Systemic Neurosciences

LMU Munich

Dissertation der
Graduate School of Systemic Neurosciences der
Ludwig-Maximilians-Universität München

‹24.08, 2021›

Supervisor and first reviewer:
Prof. Dr. Stefan Lichtenthaler
Neuroproteomics
German Center for Neurodegenerative Diseases, Munich

Second reviewer:
Prof. Dr. Felix Meissner
Systems Immunology and Proteomics
Max-Planck-Institute for Biochemistry, Munich

Third/External reviewer:
Prof. Dr. Christoph Becker-Pauly
Institute for Biochemistry, University of Kiel

Date of Submission: ‹24.08, 2021›

Date of Defense : ‹18.01, 2022›

Table of Content

ABSTRACT

The protease ß-Site Amyloid Precursor Protein Cleaving Enzyme 1 (BACE1) is a key drug target in Alzheimer's disease (AD). It catalyzes the first step in the generation of the pathogenic amyloid ß (Aß) peptide and its inhibition is therefore a promising approach to prevent or delay the onset of AD. To date however, most inhibitory compounds do not discriminate between BACE1 and its close non-amyloidogenic homologue BACE2 and therefore may lead to undesired off target effects, resulting from BACE2 biology. Therefore, future compounds require a higher selectivity for BACE1 and a biomarker is required to confirm unimpaired *in vivo* BACE2 activity. To replace a long lasting depigmentation assay, which is the current standard for *in vivo* BACE2 activity monitoring, the blood plasma of BACE2 knockout mice (B2KO) was screened and the tyrosine kinase receptor Vascular Endothelial Growth Factor 3 (VEGFR3) was identified as a putative BACE2 substrate. Subsequently, VEGFR3 was thoroughly validated as an *in vitro* and *in vivo* BACE2 substrate and the BACE2 cleavage site was determined. In direct comparison to the pigmentation readout, plasma VEGFR3 performed superior and displayed higher sensitivity and lower variance. Importantly, reduction of VEGFR3 was also detectable in the plasma of BACE inhibitor treated non-human primates (NHP) and clinical trial participants, highlighting potential for applicability in the clinical context. To test whether BACE2 cleavage may be a novel mechanism to control VEGFR3 function, downstream events of VEGFR3 signaling were monitored in primary lymphatic endothelial cells (LECs). Impairment of BACE2 dependent VEGFR3 processing was accompanied by increased activation of the VEGFR3 dependent pathways AKT and ERK and resulted into enhanced transcription of the VEGFR3 inducible genes (FOXC2) and Delta-like 4 (DLL4). As a consequence, alterations in the morphological structure and drainage efficiency of lymphatic vessels and cannot be excluded in the periphery and central nervous system (CNS). Future developments in the BACE inhibitor field need to consider these implications and plasma VEGFR3 levels may be used to control for possible of target effects from BACE2 inhibition.

List of abbreviations

A*1bg*	Alpha-1B-glycoprotein
Aß	Amyloid beta
AB	Antibody
ABC	Ammonium bicarbonate
ACN	Acetonitrile
AD	Alzheimer´s disease
ADAM	A disintegrin and metalloprotease
AICD	APP intracellular domain
A*lcam*	CD166 antigen
APP	Amyloid precursor protein
B1KO	BACE1 KO
B2KO	BACE2 KO
BACE	Beta site amyloid-precursor cleaving enzyme
BDKO	BACE double KO
B-CTF	BACE dependent CTF
B-Ecto	BACE dependent Ectodomain
B-JXT	BACE dependent juxtamembrane domain
B-NTF	BACE dependent NTF
BSA	Bovine serum albumin
C3	ß secretase inhibitor IV
Chl1	Close homologue of L1
ConA	Concanavalin A
CSF	Cerebrospinal fluid
CNS	Central nervous system
CTF	C-terminal fragment
Ctrl	Control
DDA	Data dependent acquisition
DEA	Diethylamine
DIA	Data independent acquisition
Dll4	Delta-like 4
DMSO	Dimethyl sulfoxide
DNA	Deoxyribonucleic acid
Dsg2	Desmoglein-2
DTT	Dithiothreitol
EDTA	Ethylendiaminetetraacetic acid
EGF	Endothelial growth factor
ELISA	Enzyme linked immune sorbent assay
ERBB4	Receptor tyrosine-protein kinase erbB-4
FA	Formic acid
FBS	Fetal bovine serum
FDG	Fluordesoxyglucose
FDR	False discovery rate
FLT4	Fms like tyrosine kinase 4
FOXC2	Forkhead box protein C2
GFAP	Glial fibrillary acidic protein
HET	Heterozygous
HPLC	High performance liquid chromatography
IAA	Iodoacetamide
I-Ecto	Immature ectodomain

I-FL	Immature full length
IL6ST	Interleukin-6-receptor subunit beta
KO	Knockout
LEC(s)	Lymphatic endothelial cell(s)
LFQ	Label free quantification
LYVE1	Lymphatic vessel endothelial hyaluronic acid receptor 1
Man2b	Lysosomal alpha-mannosidase
Mbl2	Mannose binding protein C
MCI	Mild cognitive impairment
M-CTF	Mature CTF
M-Ecto	Mature ectodomain
mRNA	messenger RNA
MS	Mass spectrometry
m/z	mass to charge ratio
NHP	Non human primate
NRG	Neuregulin
NTF	N-terminal fragment
OVN	Overnight
PBS	Phosphate buffered saline
PET	Positron-emission tomography
PMEL	Pigment cell specific melanocyte protein
PNS	Peripheral nervous system
PODXL2	Podocalyxin-like protein 2
PROX1	Prospero-related homeobox-1
PTM	Post translational modification
qPCR	quantitative polymerase chain reaction
RNA	Ribonucleic acid
RT	Room temperature
sAPP	Soluble APP
SEZ6	Seizure 6 protein
SEZ6L	Seizure 6-like protein
s(ProteinX)	Soluble (ProteinX)
SVG	Synaptic vessel protein
SWATH	Sequential Window Acquisition of All Theoretical Mass Spectra
TM	Transmembrane
TMEM27	Collectrin
TREM	Triggering receptor expressed on myeloid cells
Vcam	Vascular cell adhesion protein
VEGF(R)	Vascular endothelial growth factor (receptor)
WT	Wild type
YKL-40	Chitinase-3-like protein 1

1. Introduction

1.1. History and epidemiology of Alzheimer's Disease

Records of senile cognitive decline and demented behavior in elderly people were already discovered as early as in ancient Greece in the 7th century BC[1]. Therein, the Greek physician Pythagoras divided the human life cycle into five different stages, the last two of which were classified as senescence and old age. These were described to be accompanied by the decline and decay of the body, ultimately leading to the detrition of mental capacities in the last cycle stage[2]. For centuries to go, underlying reasons remained elusive and no distinction into different dementia subtypes was done until the 19th century[3]. In 1907, Alois Alzheimer first described the now commonly known pathological features with brain tissue samples of his deceased 51-year-old patient Aguste Deter, who suffered of dementia and altered personality. Therein, he described gliosis, atrophic tissue, neurofibrillary tangles and amyloid plaques[4] as physiological manifestations of his patient's condition, which is nowadays termed Alzheimer's Disease (AD). His findings were further confirmed and his observations are still considers as the main characteristics of AD[5].

Today, it is clear, that there is also a plethora of different sub forms of dementia, derived from different causes, like e.g. frontotemporal dementia or vascular dementia. Nevertheless, Alzheimer's disease is the most common form of dementia and comprises about 50-60% of all dementia cases according to Alzheimer's Disease International (https://www.alzint.org/about/). In 2006, a worldwide prevalence of 26.6 million cases was registered and numbers are predicted to quadruple until 2050 due to increased live expectancy and AD's strong dependence on aging. Of these, a considerable amount will need a high level of personal care[6]. Besides the strong deterioration of individual psychological and physiological wellbeing, the severe progression of the disease is putting a high psychological and social burden on family, friends and caregivers[7]. Furthermore, taking care of AD patients is financially challenging and today 5.8 million patients are already contributing 200 billion USD in yearly health care costs for the USA, alone[8]. Only counting the US, incidences are projected to rise to 13.8 million patients in 2050 (Fig. 01A), further increasing the cost to 777 billion USD (Fig. 01B; source: www.statista.com; US Alzheimer Association).

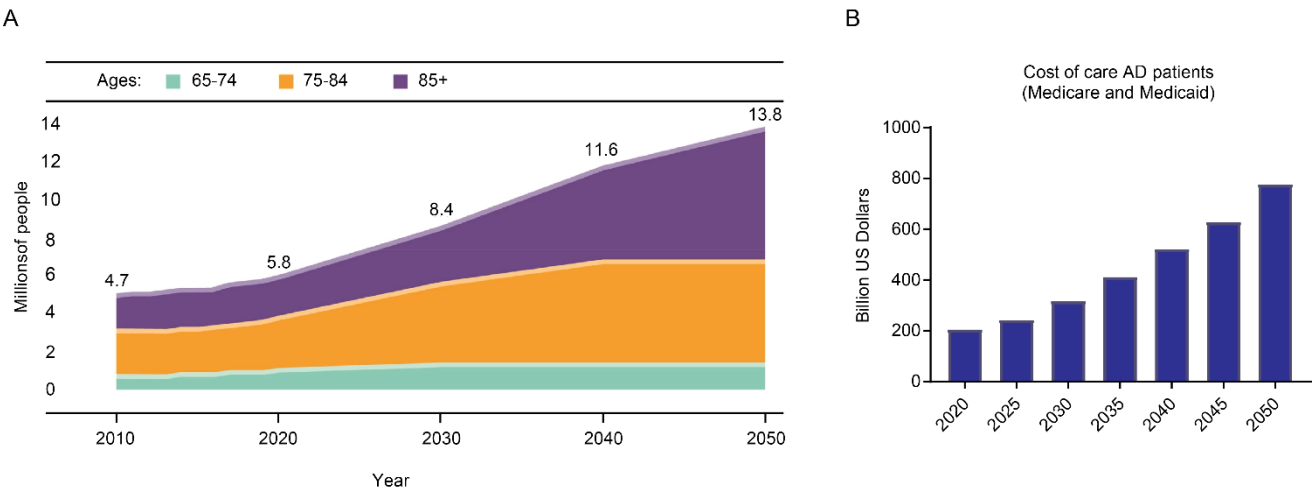

Figure 01. Past and predictive data on Alzheimer's Disease. (A) Total number and age group differentiation for US AD cases from 2010-2050[8]. **(B)** US health care cost from 2020-2050 (adapted figure from statista).

While there have been countless great scientific advances in the treatment of various diseases like e.g. different forms of cancer or most prominently in infectious diseases, there has still been barely any progress in treating or even slowing the onset and progression of AD. Only a minor amelioration of cognitive decline symptoms can be achieved via the use of e.g. acetylcholine inhibitors or NMDA receptor antagonists[9].Therefore, todays' physicians are almost as helpless to aid their AD patients, as Alois Alzheimer was more than a hundred years ago in aiding Aguste Deter.

Taken together, there is a dire need for preventive and treatment measures in AD, which until today remains unfulfilled. However, the ever-increasing speed and diversification of scientific research and the increasing capabilities to generate and analyze inconceivable amounts of data gives rise to copious putative targets to achieve those goals. One of the oldest known and most widely researched approaches is the targeting of the amyloid beta aggregates[10].

1.2. The amyloid cascade hypothesis

The two major neuropathological hallmarks of AD, besides brain shrinkage, are the formation of intracellular hyper-phosphorylated Tau tangles and the extracellular accumulation of Amyloid-ß (Aß)[4] in the parenchymal brain tissue. While both aggregates initially form on the molecular level, they also become visible on the macroscopic level as Tau tangles and Amyloid plaques and are seen as the main pathogenic event of the disease. Therefore, they are still used for diagnostic purposes nowadays[11,12].

Currently, the amyloid cascade hypothesis is still one of the most widespread and convincing explanations, on which molecular events drive Aß generation and development of AD[13,14]. According to the hypothesis, the transmembrane protease beta site amyloid precursor cleaving enzyme 1 (BACE1) is processing its physiological substrate amyloid-precursor protein (APP) at the membrane, where the subsequent cleavage by another protease, called γ secretase, releases aggregation-prone Aß peptides of various sizes into the extracellular space. There, monomers are able to aggregate into oligomers and plaques (Fig. 02). Especially the oligomers are seen as the neurotoxic component of this pathway, whereas plaques may rather function as a reservoir for spreading into adjacent tissue [15]. The neurotoxic effects are then thought to lead to neuroinflammation, –degeneration and therefore ultimately to cognitive decline.

The hypothesis mainly derives from genetic observations in different human populations, where mutations in in the Aß precursor protein, the y secretase subunits presenilin 1 and 2, as well as associated pathway components affects the susceptibility for AD pathogenesis and cognitive decline. Therein, mutations, which lead to a shift towards more aggregation prone Aß subspecies, like e.g. the Swedish and the A673V APP mutations[16,17], increase the strength and velocity of AD pathogenesis. Expressing aggregation-promoting APP mutation in mice is one of the approaches to artificially induce amyloid plaques and AD in mice, which naturally do not suffer from AD[18,19]. In contrast, the Icelandic mutation with a shift towards less APP processing into aggregating Aß, decreases the overall AD susceptibility[20].

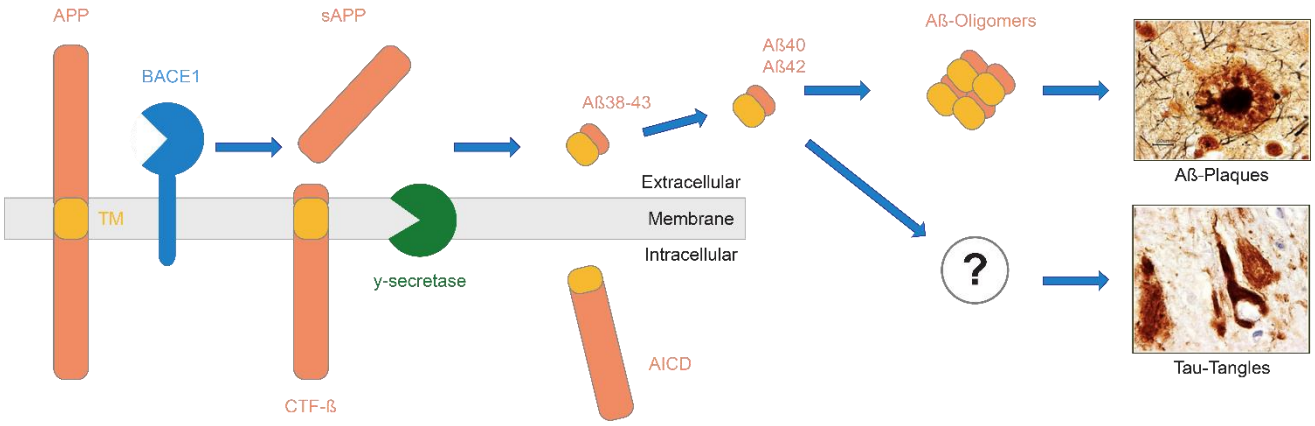

Figure 02. The amyloid cascade. APP is cleaved by BACE1, close to the transmembrane (TM) domain and releases soluble APP (sAPP) into the extracellular space. The remaining transmembrane C-terminal fragment ß (CTF-ß) is subsequently cleaved by γ secretase inside the TM domain and Aß subspecies of different sizes (Aß38-43)[21] are released into the extracellular space, of which Aß40 and Aß42 are most dominant. The APP intracellular domain (AICD) remains inside the cellular space. Predominantly Aß42 aggregates into Aß-plaques and tangles of hyperphosphorylated Tau are induced in an unknown manner (Microscopy pictures: www.alz101.blogspot.de).

While Tau burden correlates more closely with neurological death and AD severity than Aß[22], the role and origin of increased Tau burden are highly context dependent on the associated disease[23]. Pathological increases in Tau levels are not AD exclusive and can be observed in a range of diseases, which are commonly grouped as Tauopathies, like e.g. frontotemporal dementia[24]. In the context of AD, no formation of Tau tangles occurs in human Aß aggregate forming stem cell derived cell culture models, when Aß formation is impaired via the application of a BACE inhibitor[25,26]. *In vivo*, transgenic human APP expressing mice, display also increased total and hyperphosphorylated Tau levels[27], which can be ameliorated via the inhibition of BACE[28]. While Tau appears to be highly Aß dependent in its initial accumulation, BACE inhibition can no longer prevent Tau generation at later time points, indicating a switch from Aß dependent to Aß independent pathogenesis[29]. The reasons for this change of behavior are still elusive, but suggests that a successful AD prevention via BACE inhibitors requires a very early intervention. Afterwards, alternative means for AD prevention and treatment may be necessary, like e.g. a combination of therapies against Aß and Tau. Given Tau's less clear role in AD and its dependency on Aß, early anti-amyloidogenic therapies currently remain the most promising approach in prevention of AD.

While initial anti-amyloidogenic efforts were focused on the inhibition of the subsequent γ secretase cleavage[30-32], this approach was quickly set back, as clinical trials using γ secretase inhibitors had to be discontinued due to unexpected side effects, like enhanced cognitive decline and toxicity[33]. Later, many of the occurring problems were traced back to the unselective inhibition of γ secretase, which among others, plays an important role in Notch1 processing[34]. Consequently, BACE1 became the focus as an alternative pharmacological target of the amyloid cascade.

Taken together, prevention of formation of aggregating Aß via the amyloid cascade was and still is one of the major targets in the effort to delay or prevent the onset of clinical AD manifestations

1.3. BACE proteases

The amyloid cascade component BACE1 is a type 1 transmembrane protease, the expression of which is low throughout various tissues, but pronounced in the brain[35]. Therein, the protease is mostly located at the presynaptic terminals of neurons[36,37]. Besides its prominent role in APP cleavage (1.2.), BACE1 has also a variety of other substrates, which can be cleaved and released into the extracellular space, like e.g. seizure protein 6 (SEZ6), seizure protein 6 like (SEZ6L)[38] and neuregulin-1 (NRG1)[39]. The process of cleaving and releasing a substrate's ectodomain into the extracellular space is also referred to as shedding. The resulting ectodomains are indicated as the soluble form, like e.g. sAPP[40]. BACE1 shedding is strongest at acidic pH and was shown to process its substrates inside components of the secretory pathway, mainly in endosomes but also in the trans Golgi network[35,41]. Generated soluble ectodomains are subsequently released into the extracellular space, e.g. the cerebrospinal fluid (CSF), via fusion to the plasmamembrane. There, substrate concentrations can be determined e.g. via mass spectrometric or immunological techniques and alterations in substrate concentration consequently display the proteolytic activity of BACE1[38,42]. Shed substrates are also detectable in the blood stream[43], presumably via physiological CSF clearing mechanisms across the blood brain barrier via the glymphatic system[44] or lymphatic drainage[45].

Due to the substrate diversity of BACE1, strong inhibition of its proteolytic activity results into a broad spectrum of side effects, which manifest in BACE1 knockout mice (B1KO). B1KO mice display a largely abolished Aß generation[46], but also suffer from a range of predominantly neurological phenotypes. Among others, mice display impaired synaptic plasticity and decreased cognitive functions[47,48], reduced spine density[49], epileptic- like seizures[50,51], hypomyelination[52,53] and schizophrenic behavior[49,54]. Extensive research has been done to identify BACE1 substrates from BACE1 deficient mouse CSF[38,42] and *in vitro* cell models[55-59]. For several BACE1 substrates, association or logically likely connections were made between their decreased BACE1 processing and the observed phenotypes. Possible effects of altered substrate processing may however be highly dependent on the individual protein properties and functions.

Lack of function phenotypes have been widely described for impaired BACE1 processing. Proper processing of the ß-subunit of voltage gated ion channels has been proposed as the responsible substrate for the development of seizures[60,61]. Proteolytically generated sAPP and Aß play physiological roles and are connected to synaptic density, synaptic scaling and synaptic vesicle release[62-65]. Processed NRG1 serves as a ligand for its receptor tyrosine-protein kinase erbB-4 (ErbB4) and is associated with axon myelination in the peripheral nervous system PNS and spine density in hippocampal neurons[49,52,53]. The ß-CTF fragment of the BACE1 substrate close homologue of L1 (*Chl1*) has been implicated in the collapse and recovery of axonal growth cones[59,66]. Notch associated γ secretase toxicity is thought to derive from the missing transcriptional function of the corresponding CTF[67] and various γ secretase dependent CTFs have been associated with transcriptional functions[68]. Therefore, it seems reasonable to assume that further BACE1 associated CTFs may contribute to functional effects from impaired BACE1 activity.

While decreased BACE cleavage leads to a decline of the processed substrates in the extracellular space, the non-processed forms can often be observed to accumulate on the surface of source cells[38,57,69]. Possible gain of function phenotypes were not described yet, but are highly likely due to the diverse functions of BACE substrates. Two of the fundamental functions of membrane associated proteins may be especially noteworthy from this perspective. Many membrane proteins are able to

interact in cis or trans with other membrane proteins or can be receptors with downstream signaling function. Therefore, accumulation of BACE1 substrates may not only lead to already described loss of function phenotypes, but may additionally comprise substrate related functional gains. The rational for some possible consequences of altered BACE substrate processing can be seen below (Fig. 03). Taken together, described secondary effects and the high likelihood of further unknown side effects, highlight the need for broad knowledge about BACE substrates and their individual functions.

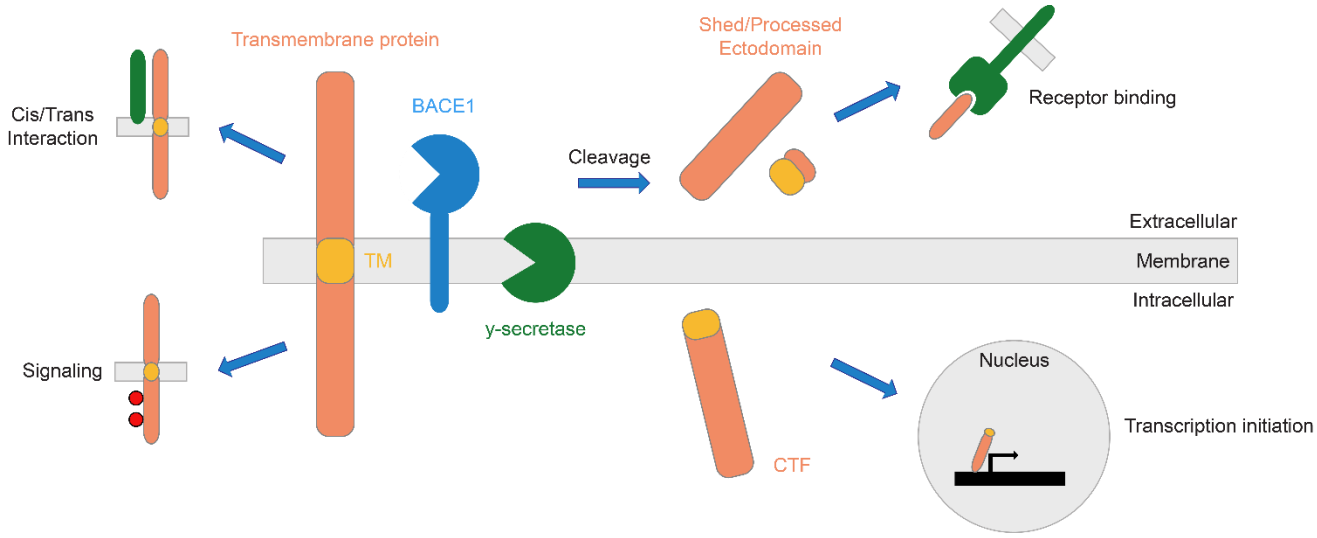

Figure 03. Transmembrane proteins in context of secretase cleavage. When processed, substrate ectodomains and secreted BACE1 generated cleavage products (e.g. sAPP and Aß40) may bind to distant cellular receptors. Additionally, generated intracellular products may translocate into the nucleus and act as transcription factors (right part of figure). Impaired BACE cleavage is known to decrease these events and to promote cellular substrate accumulation. Functional implications of these accumulations are not yet described, but may include altered protein-protein interactions and enhanced signaling capabilities of receptor substrates (left part of figure).

In contrast to BACE1, much less is known about the close homologue[70] BACE2, which does not play a major role in the generation of Aß[70]. However, BACE2 can ameliorate the lethality in BACE1 KO mice, suggesting a considerable substrate overlap between the two proteases[71]. In comparison to *BACE1*, *BACE2* expression levels are low in the central nervous system and mainly apparent in a subset of neurons, astrocytes, and oligodendrocytes[72,73]. Instead, BACE2 was deemed rather important in the periphery, like kidney and pancreatic tissue[72]. B2KO mice appear healthy and only two major phenotypes were describe, improved glucose tolerance and hypopigmentation of the hair[71].

In the pancreas, BACE2 is especially highly expressed in the insulin generating ß-islets, where it is responsible for the processing of the transmembrane protein collectrin (TMEM27). Therein, BACE2 deficiency increases overall ß-cell mass and insulin levels, which results into improved glucose homeostasis[74]. Additionally BACE2 suppression enhances survival of ß cells due to altered processing of the substrate islet amyloid polypeptide[75,76]. Recently, BACE2 was also shown to directly cleave the insulin receptor in zebrafish melanophores, thereby adding another layer of regulation in respect to insulin signaling[77]. As a consequence, BACE2 is an ongoing target in diabetes research[78]. Furthermore, silver fur can be deduced from the formation of abnormal melanosomes, which derive from the lack of processing for the substrate pigment cell specific melanocyte protein (PMEL)[79]. Accordingly, fur pigmentation can also be observed in response to different unselective BACE inhibitors, i.e. which impair both, BACE1 and BACE2 with similar strenghts[80,81].

Recently it has become apparent, that BACE2 may be more important in the brain than initially expected. Neuregulin2, a member of the endothelial growth factor (EGFR) family, which is associated with abnormal behavior in psychiatric disorders[82,83], is processed by BACE2 in a subset of brain structures[84]. Besides, before mentioned astrocytes and oligodendrocytes, BACE2 mRNA expression was also identified in a subset of neurons and several BACE2 specific substrates like vascular cell adhesion protein 1 (Vcam1) were identified. Inflammatory conditions, like apparent in AD, enhanced the processing of identified substrates[73]. Furthermore, BACE2 protein levels have also been shown to display high to medium expression in the cerebral cortex, cerebellum und caudate on the protein level (https://www.proteinatlas.org/ENSG00000182240-BACE2/tissue, 2021)[85]. Proper BACE2 processing of the neuronal potassium channel Kv2.1, has been shown to disrupt proper potassium channel formation and led to alterations in potassium exchange and acted neuroprotective against apoptosis[86]. Therein, processed Kv2.1 was able to localize to the plasma membrane, but not to form functioning channels. If opposite functional changes, i.e. enhanced channel formation and apoptosis can be induced by decreased BACE2 processing remains to be seen.

Taken together, these shifts in the importance of BACE2 in the CNS further highlights possible implications of secondary effects from unintentional BACE2 inhibition.

1.4. AD associated biomarker

Additionally to Aß and Tau tangles, AD pathology is also accompanied by synaptic dysfunction[87], enhanced neuro-inflammation[88] and a volumetric decrease of the brain tissue[89]. Mentioned effects are not limited to but especially pronounced in brain areas, which are important for memory and cognitive function, like e.g. the cerebral cortex and hippocampal regions[12,90].

In AD, many of these changes only become apparent relatively late in the pathogenesis and can be monitored via different types of biomarkers. These however, often only become abnormally changed; when mild cognitive impairment already becomes visible and when preventive measures would therefore become obsolete[11] (Fig. 04). The earliest known changing markers are plasma and CSF levels of Aß42 [12,43,91] and Tau [12,43,92]. The individual levels or ratios of Aß40 to Aß42 are also commonly used to monitor the decrease of BACE1 activity in clinical BACE inhibitor trials[11,93-95]. In response to Aß aggregation, the soluble triggering receptor expressed on myeloid cells (Trem2) is secreted into the CSF by activated microglia, which may be used as a readout for neuronal inflammation[96]. This is most prominent during the mild cognitive impairment (MCI) stage and afterwards decreases again[97]. During the MCI stage, macroscopically visible Aß plaques can be imaged via positron emission tomography (PET) tracers[91] and increased CSF neurogranin levels, which reflect the synaptic dysfunction[98,99]. At later stages, PET tracers can also detect abnormality in brain Tau levels[100], hypo-metabolic activity via Fluorodeoxyglucose (FDG)[12,101,102] and synaptic dysfunction via decreased hippocampal levels of synaptic vesicle protein 2A (SVG)[103]. Concurrent, magnetic resonance imaging can be used to track the decrease in hippocampal brain volume[12,89,104] . Increasing amounts of neurofilaments in CSF and blood is an established marker for neuroaxonal degeneration[105]. Late changing biomarkers are CSF levels of the neuroinflammation related glycoprotein YKL-40[96] and plasma levels of the astrocyte associated glial fibrillary acidic protein GFAP[106].

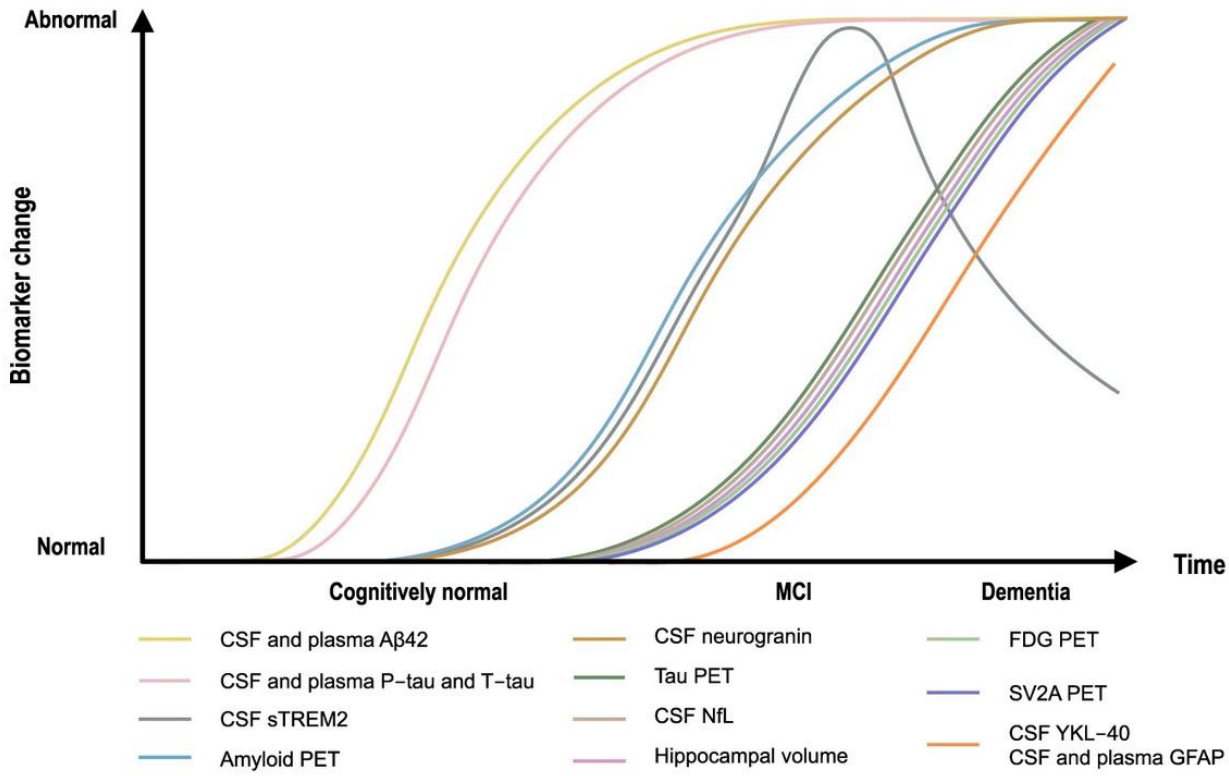

Figure 04. Profiles of individual AD biomarkers across time. Changes are indicated as abnormality across time. First visible biomarkers, which are usable for preventive measures in cognitively normal stages, are Aß42 and Tau. Macroscopically visible Aß plaques become apparent before Tau tangles with the latter only becoming apparent in the MCI stage. Most other indicated biomarker are rather predictive for disease progression and are not feasible for disease prevention. Figure source: Zetterberg and Bendlin, 2021[11].

Given the available biomarkers, AD associated pathology can be extensively monitored across several decades and can be used as a predictor of disease progression. CSF biomarker monitoring is very invasive and efforts have been made to transfer Aß42 and Tau monitoring to blood plasma measurements. Due to the high complexity and difficulty of plasma protein measurements, these are still in their early phase and new tests require a large-scale applicability to be feasible for clinical usage. However, great advances have been made in the last years. Plasma Aß42/Aß40 ratios have been shown to adequately correlate with amyloid PET and CSF levels[107,108] and an automated plasma screen test has been developed[109]. Plasma total-Tau assays proved to be less straightforward for use in AD[110] and poorly correlate with respective CSF level[111]. This may derive from a shorter plasma half-life time[112,113] and shifting the focus on the P-tau181 subspecies resolved the issue, where high correlation with respective CSF level and amyloid PET could be observed[114,115].

For preventive interventions, it will be necessary to act in early, cognitively normal stages. Monitoring the CSF, or preferably the plasma levels, of Aß42 and Tau appear to be the most feasible approach to detect the onset of AD pathology at early stages and to assess BACE1 activity during pharmacological intervention by BACE inhibitors. Aß42 and possibly other BACE1 substrates like SEZ6 and SEZ6L can be used to monitor the *in vivo* activity of BACE1[38,93-96], but no sophisticated means are available to assess *in vivo* activity for BACE2. *In vitro* activity determinations are available[116,117], but the only *in vivo* determination of BACE2 activity is done via the BACE2 dependent hair pigmentation status of newly grown hair following initial hair removal[79-81]. Due to the slow velocity of hair growth, hair depigmentation assays require a period of three to four weeks and are therefore not an adequate biomarker readout.

Taken together, while feasible BACE1 *in vivo* activity biomarkers exist and become more sophisticated, BACE2 *in vivo* activity can only be determined in a crude manner and a better alternative is required.

1.5. Current state of clinical BACE inhibitor research

Various clinical trial for BACE inhibitors have suffered major setbacks in recent years. A wave of clinical trial terminations commenced in 2018, as studies for Atabecestat (Janssen/Shionogi), Lanabecestat (AstraZeneca/Eli Lilly), LY3202626 (Eli Lily) and Verubecestat (Merck) were all terminated. This series of terminations ended in 2019, when also Umibecestat (Amgen/Novartis) and Elenbecestat (Biogen/Eisai) were terminated, thereby bringing the BACE inhibitor field towards an abrupt stop (Table 01). All compounds sufficiently lowered CSF Aß levels. However, no reduction of-amyloid plaques, and no cognitive improvements were visible in any of the studies. Furthermore, cognitive capabilities even dropped slightly, but significantly, in some of the studies. Consequently, the BACE inhibitor trials had to be stopped due to lack of efficacy and observable adverse effects.

Table 01. Overview on most recent BACE inhibitor trials.

Compound and Company	Potency, Selectivity [nM]	Doses [mg]	Extend of Aß lowering	Population	Cognitive worsening	Reason for termination
Atabecestat (JNJ-54861911) Janssen/Shionogi	N/A	5 25	CSF Aß40: 67-90%	Asymptomatic with increased AD risk	yes	Hepatoxicity
Elenbecestat (E2609) Biogen/Eisai	BACE1 IC50: 7 BACE1 Kd: 19 BACE2 Kd: 67	50	CSF Aß40: 70%	Ad and prodromal AD	no	Risk/benefit ratio unfavorable
Lanabecestat (AZD3293, LY3314814) Astrazeneca/Eli Lilly	BACE1 IC50: 0.6 BACE2 IC50: 0.9	20 50	CSF Aß40/Aß42: 50-73% Plasma Aß40/Aß42: 70-80%	MIC and mild AD	Yes, but not consistently	Futility
LY3202626 Eli Lilly	BACE1 IC50: 0.61 BACE2 IC50: 0.87	3 12	CSF Aß40: 50-90%	Mild AD	Trend in 3mg subgroup	Futility
Umibecestat (CNP520) Amgen/Novartis	BACE1 IC50: 11 BACE2 IC50: 30	15 50	CSF Aß40: 60-90%	Asymptomatic with increased AD risk	yes	Futility
Verubecestat (MK-8931) Merck	BACE1 Ki: 2.2 BACE2 Ki: 0.38	12 40	CSF Aß40/Aß42: 60-88%	Prodromal, MCI, mild to moderate AD	yes	Futility
References: see[93,95,116,118-123]; https://www.alzforum.org/therapeutics; https://clinicaltrials.gov, Table adapted from McDade et al. 2021[124]						

Reasons for the lack of efficacy and adverse effects are currently under discussion. While recent failures may appear as the last nail in the coffin of AD prevention and treatment via BACE inhibitors, logical flaws in the design of the trials have to be considered. As described in 1.4., AD pathology is developing across several decades and most study participant were composed of patients, which were already suffering from early stage AD symptoms. At this stage, neurological damages and sometimes decreased brain volumes are already visible. These are pathological outcomes, which would not be expected to

improve upon reduced Aß generation, but in the best scenario would not further progress. As mentioned before however (1.3.), Tau pathology and apparently other pathological changes, become Aß independent after the initial phase and prevention of Aß formation at later stages should therefore not influence diseases progression anymore. Another important point is the strength of BACE inhibition in all of the studies. As described, (1.3.), BACE1 plays a role in various physiological functions and should not be impaired too strongly. All performed studies decreased CSF Aß accumulation by 50 – 90%, which may be the major culprit for also observed side effects, like cognitive worsening, anxiety, falls, suicidal thoughts and sleep disturbances. These side effects were however not consistent across compounds and their occurrence was of a subtle nature[93,118]. This raises the hope that a decrease of BACE1 inhibition may avoid observed side effects. Taking into account the variety of BACE substrates and their functions, a rational connection between side effects and BACE1 substrate processing appears likely. Among other possible responsible BACE1 substrates, abnormal NRG1 processing in B1KO mice has also been connected do defective muscle spindles and motor deficits[125]. Impaired murine SEZ6 and APP cleavage have been connected to defects in neuronal connectivity and impaired long-term potentiation[38,126,127]. Described phenotypes intuitively raises associations to the clinically observed cognitive worsening and increased occurrence of falls. Proof of transferability into the human system needs however yet to be demonstrated.

To prevent BACE1 associated side effects, lower BACE1 inhibition appears promising. According to one study, heterozygous BACE1 deletion in mice (50% reduction of BACE1 activity), only lowered Aß levels by 12%, but nevertheless resulted in a strong reduction of Aß plaques, synaptic deficits and neuritic burden in aged mice[128]. Furthermore, heterozygous carriers of the Icelandic APP mutation display decreased BACE1 dependent APP processing by only 20%, which suffices to provide lifelong protection against AD[129,130]. Accordingly, a much milder inhibition of BACE1 should be sufficient to lower the levels of aggregating amyloid ß, while being low enough, to prevent the development of noteworthy side effects. Additionally, all clinical side effects were of subtle nature, making the approach of mild BACE1 inhibition appear feasible.

While also briefly considered, little attention has been paid to the issue of missing BACE selectivity. Most inhibitors did not display any selectivity for BACE1 over BACE2 and especially Verubecestat proved to be an even better inhibitor for BACE2, than for BACE1 (table 01). Only Elenbecestat and Umibecestat showed a recognizable *in vitro* assay selectivity towards BACE1, whereas only Elenbecestat did not result into noteworthy cognitive worsening, compared to the placebo group. Considering, that Elenbecestat displayed similar decreases in BACE1 activity as other inhibitor trials, the main difference is its comparably high BACE1 selectivity. BACE1 *in vitro* selectivity appears similar for Umibecestat, but corresponding BACE1 activity and therefore probably BACE2 activity were decreased even more prominently with up to 90% decreased of CSF Aß. It has also to be noted, that any selectivity data derives from *in vitro* assay and *in vivo* selectivity may not reflect physiological differences in activity of BACE1 and BACE2. This may e.g. derive from compound specific drug distribution effects and individual physiological differences. This also became apparent in discussed studies, as altered BACE2 dependent hair pigmentation only occurred in some of the inhibitor treated patients[93,116,118].

Assessing inhibitors from the perspective of BACE selectivity is far from clear and there is a strong possibility that many of the observed BACE inhibitor side effects predominantly derive from the lack of BACE1 substrate processing. Nevertheless, BACE2 dependent side effects are also a reasonable possibility and further strengthen the argument for a closer validation of BACE2 substrates. The lack

of a comparable *in vivo* BACE2 activity biomarker makes consideration of *in vivo* selectivity more difficult and highlights the need for an appropriate biomarker.

2. Aim of the study

The amyloid cascade hypothesis is one of the most promising approaches in the prevention and delay of AD, via inhibition of BACE1. While BACE1 and associated substrates are well described, little is known about the non-amyloidogenic, but also often inhibited, close homologue BACE2. In accordance with physiological importance of BACE1, its substrates, associated side effects and *in vivo* activity biomarkers have been extensively researched. However, complementary information is largely missing for BACE2. Additionally considering the unclear rationale for the recent failures of unselective and marginally BACE1 selective inhibitors, this doctoral thesis has several aims:

1) Identification of a new BACE2 substrate detectable in mouse plasma and validation as an *in vivo* BACE2 activity biomarker

2) Validation of the new BACE2 substrate in cell lines and in primary cells, including determination of the BACE2 cleavage site

3) Determine whether BACE2 cleavage alters the function of the substrate in vitro.

Taken together, successful conduction of this thesis should not only improve the monitoring of *in vivo* BACE2 activity in the context of clinical BACE inhibitor trials, but also help to shed light on physiological functions of BACE2 and it substrates, thereby helping to elucidate the still neglected consequences of unselective BACE inhibitors, which is essential to understand and control side effects that occurred in recent BACE inhibitor trials.

3. Material and methods

3.1. Material

3.1.1. General reagents and chemicals

Reagents used in this thesis are listed in the following table:

Table 02. Reagents and chemicals used in this thesis. Overview of all reagents and chemicals used in the thesis.

Reagent	Catalogue number	Manufacturer
Acetic Acid	49199	Fluka
Acetonitrile 100%	01204101	Biosolve
Acetonitrile 80 %	nc0959509	Thermo Fisher Scientific
Acrylamide/Bis Solution, 37.5:1	10681.03	Serva
Ammoniumbicarbonate (ABC)	15645440	Thermo Fisher Scientific
Ammoniumperoxidsulfate	9592	Roth
Ampicillin sodium salt	K029.2	Roth
Anilin	9931.1	Roth
APP-peptide, Swedish mutation	M-2465	Bachem,
Asp-N, Mass Spec Grade	VA1160	Promega
Bacto Trypton	211699	BD
BACE1, recombinant	Custom made	Aurigene
BACE2, recombinant	BML-SE550	Enzo
BC Accay Reagent A	UP95424A	Interchim
BC Accay Reagent B	UP95425A	Interchim
Bovine Serum Albumin (BSA)	A8022	Sigma
Bromopehnolblue	32712	Thermo Fisher Scientific
$CaCl_2$	102382	Merck
Casein	C3400	Sigma
C3 (β secretase inhibitor IV)	565788	Merck
Concanavalin A from *Canavalia ensiformis* (ConA)	C7555	Sigma
Diethylamine (DEA)	D0806	Sigma
Dimethylsulfoxid (DMSO)	4720.4	Roth
DMEM - Dulbecco's Modified Eagle Medium, high glucose, GlutaMAX Supplement	61965059	Thermo Fisher Scientific
2,4-dinitrophenyl	4026832	Bachem
Dithiothreitol	10666885	Thermo Fisher Scientific
EBM-2 – 2MV Microvascular Endothelial Cell Growth Medium- 2 BulletKit,	CC-3202	Lonza
ECL Prime Western Blotting System	GERPN2232	Sigma
ECL Western Blotting Reagents	GERPN2106	Sigma
EDTA	108421	Merck
Ethanol, 80% techn.	107017	Merck
Ethanol, 100% techn.	9474.3	Roth
FBS - Fetal Bovine Serum	10270-106	Thermo Fisher Scientific
Formic Acid 0.1% (FA)	CP03	Roth
Formic Acid 8% (FA)	34692	Thermo Fisher Scientific

Glycerol	3783	Roth
Glycine	131340.0914	AppliChem
GlycoLink Coupling buffer	88944	Thermo Fisher Scientific
H_2O MS grade	270733	Sigma
HCl 32%	100319	Merck
Hydrazine resin , ultralink	53149	Thermo Fisher Scientific
IGEPAL® CA-630	I3021	Merck
Iodoacetamide (IAA)	I1149	Sigma
Isopropanol	L311393	Thermo Fisher Scientific
rLys-C, Mass Spec Grade	VA1170	Promega
Lys-N, Mass Spec Grade	VA1180	Promega
Lipofectamine 2000, Transfection reagent	11668027	Thermo Fisher Scientific
2-Mercaptoethanol	4227.1	Roth
Methanol	13680501	Biosolve
(7-Methoxycoumarin-4-yl)acetic acid	4026019	Bachem
Methyl-alpha-D-mannopyranoside	M6882	Sigma
$MgCl_2$	105833	Merck
$MnCl_2$	M3634	Sigma
MSD Read Buffer T (4x)	R92TC	Mesoscale
MSD Strepatavidin Sulfo Tag	R32AD	Mesoscale
NaCl	3957.2	Roth
Opti-MEM, Reduced Serum Medium, GlutaMAX Supplement	51985042	Thermo Fisher Scientific
PBS - Phosphate-Buffered Saline, pH 7.4	10010056	Thermo Fisher Scientific
Penicillin/Streptomycin (5000 U/mL)	15070-063	Thermo Fisher Scientific
PhosSTOP™	4906837001	Merck
Precision Plus Protein Dual Xtra Prestained Protein Standards	161-0377	Bio-Rad
Protease Inhibitor Cocktail (Pi)	P8340	Sigma
Protein A magnetic beads	88846	Thermo Fisher Scientific
Protein G magnetic beads	88848	Thermo Fisher Scientific
Protein L magnetic beads	88850	Thermo Fisher Scientific
Recombinant Human VEGFR3/Flt-4 Fc Chimera Protein, CF	349-F4	R&D
Recombinant murine SEZ6L protein, CF	4804-S6-050	Bio-Techne
Recombinant murine VEGFR3	-	Janssen
Recombinant Mouse VEGFR3/Flt-4 Fc Chimera Protein, CF	743-R3	R&D
ReproSIl-Pur 120 C18-AQ, 1.9 µm	r119.aq.	Dr. Maisch
SDS, Molecular Biology Grade	20765.03	Serva
SeraMag Beads A	09-981-121	Thermo Fisher Scientific
SeraMag Beads B	09-981-123	Thermo Fisher Scientific
siRNA-on target plus smartpool-BACE1	003747-00-0010	Horizon
siRNA- on target plus smartpool-BACE2	003802-00-0010	Horizon
siRNA- on target plus non targeted control pool	001810-10-05	Horizon
siRNA- on target plus smartpool-VEGFR3	003138-00-0010	Horizon
Sodium azide (NaAzide)	1.06688	Merck
Sodium deoxychoate	30970	Sigma
Sodium dodecylsulfate	20765	Serva
Sodium fluoride	106449	Merck

Sodium hydroxide 1.0 N solution	S2770	Sigma
Sodium meta-periodate	S1878	Sigma
Sodium vanadate	S6508	Merck
Synthetic peptide KGCVNSSASVA	-	Peps4Life
TBS - Phosphate-Buffered Saline	28358	Thermo Fisher Scientific
TEMED, 99% p.a.	2367.2	Roth
Tris ultrapure, 5 kg	A1086	Applichem
Triton X-100	1.08603	Merck
Trypan Blue	1450021	Biorad
0.05% Trypsin-EDTA 1×	25300-062	Thermo Fisher Scientific
Trypsin, Sequencing Grade Modified	V5111	Promega
Tween 20	8.22184	Merck
Urea	1.08487	Merck
Verubecestat BACE inhibitor	MBS579527-25	Biozol
Yeast Extract	212720	BD

3.1.2. Kits

The kits used in this thesis are listed in the following table:

Table 03. Kits used in this thesis. Overview of the kits used in the thesis.

Name	Catalogue number	Manufacturer
BC Assay Kit	UP40840A	Interchim
Deglycosylation Kit	P6044S	NEB
Dynabead Protein G Immunoprecipitation kit	10007D	Thermo Fisher Scientific
InstaBlue Protein Stain solution	APE-B8226	Biozol
iScript Reverse Transcription Supermix	1708841	Biorad
iRT peptide kit	Ki-3002	Biognosys
Plasmid DNA purification	MN740410	Macherey-Nagel
Pierce Reversible Nitrocellulose Staining Kit	24580	Thermo Fisher Scientific
Pierce™ Top 12 Abundant Protein Depletion Spin Columns	85164	Thermo Fisher Scientific
PNGase Deglycosylation Kit	P0704	NEB
RNA preparation kit	74104	Qiagen
Trans-Blot Turbo Transfer System	17001915	Biorad

3.1.3. Equipment

The equipment used in this thesis is listed in the following table:

Table 04. Equipment used in this thesis. Overview of the equipment that was used to carry out this thesis.

Name	Manufacturer	Type
Avanti J-26XP, High-Speed Centrifuge	Beckman Coulter	Centrifuge
Benchtop Centrifuge 5417R	Eppendorf	Centrifuge
Benchtop Stage Tip CentrifugeTomy	Sonation lab solution	Tip-Centrifuge
C18 Empore disks	Supelco	Matrix
Corning®-Costar®-Spin-X®	Thermo Fisher Scientific	Spin filter column
CKX53 Inverted Microscope= normal microscope?	Olympus	Microscope
DynaMag™-2 Magnet	Thermo Fisher Scientific	Magnetic rack
EASY-nLC 1000 Liquid Chromatograph	Thermo Fisher Scientific	Chromatograph
Mini-PROTEAN Tetra Vertical Electrophoresis Cell	Biorad	Electrophoresis chamber
Eppendorf 5417R Centrifuge	Eppendorf	Centrifuge
FastPrep-24 - Lysing matrix D 1.4mm ceramic beads	MPBio	Lysis columns
FastPrep Instrument	MPBio	Bead beating device
Fluoroskan microplate fluorometer	Thermo Fisher Scientific	Fluorometer
Hei-Tec, Magnetic Stirrer	Heidolph	Magnetic stirrer
Heracell 150i CO2 Incubators with Stainless-Steel Chambers	Thermo Fisher Scientific	Incubator
Heraeus Megafuge 16 Centrifuge Series	Thermo Fisher Scientific	Centrifuge
ImageQuant LAS 4000 series	GE Healthcare	WB imager
Incubation/Inactivation Water Bath 1008	GFL	Water bath
Infinite 200 PRO	Tecan	Plate reader
KL 1600 LED	Olympus	Light source
Liebherr™ G Series Refrigerator	Thermo Fisher Scientific	Refrigerator
Liebherr GNP 1956 Premium NoFrost	Thermo Fisher Scientific	Freezer
Liquid Nitrogen- Cryo technology	Biostore System	Liquid nitrogen tank
Low Temperature (-80°C) - Herafreeze Basic	Thermo Fisher Scientific	Freezer
Multiwell plates (6x)	Thermo Fisher Scientific	Cell culture wells
MSD ELISA plates-empty	MSD	96 well plate
MSD ELISA MESO QuickPlex SQ 120	MSD	96 well plate reader
Nanodrop 2000	Thermo Fisher Scientific	UV-Vis spectrophotometer
Nano Electrospray Source (Thermo Proxeon)	Thermo Fisher Scientific	Ionization Source
Nunc Immuno Plates	Thermo Fisher Scientific	96 well plate
Optima MAX-XP	Beckman Coulter	Ultracentrifuge
Orbital-Rocking Shaker 3011	GFL	Shaker
Overhead Rotator Reax2	Heidolph	Overhead Rotator
PowerPac Basic Power Supply	Bio-Rad	Power supply
Protein Lobind Tubes	Eppendorf	Reaction tubes
Q-Exactive Mass Spectrometer	Thermo Fisher Scientific	Mass spectrometer
Q-Exactive HF Mass Spectrometer	Thermo Fisher Scientific	Mass spectrometer
ScanSpeed MaxiVac	ScanVac	Vacuum centrifuge
Snap Cap spin columns	Thermo	Spin columns

Sonorex Super Sonicator	Bandelin	Ultrasonic bath
StepOne Plus	Thermo Fisher Scientific	Thermocycler
T75/T175 flasks	Thermo Fisher Scientific	Cell culture flasks
TC20 Automated Cell Counter	Bio-Rad	Cell counter
ThermoMixer comfort	Eppendorf	Thermomixer
Vivaspin Turbo 15, 30,000 MWCO	Sartorius	Concentration column
Vortex mixer, peqTWIST	Peqlab	Vortex
Zeba Spin Desalting Columns	Thermo Fisher Scientific	Desalting columns
ZIEGRA Ice Maker	Ziegra Eismachinen	Ice machine

3.1.4. Antibody list

Any antibody used in this thesis is listed in the following table:

Table 05. List of antibodies. Overview of antibodies and their immunogens, species, dilutions and catalogue numbers used in this thesis.

Antibody used for	**Clone**	**Immunogen**	**Host species**	**Working Conc.**	**Catalogue number**	**Source**
AKT-pan murine	40D4	Synthetic peptide at the carboxy-terminal sequence of human Akt	mouse	1:2000	2920S	Cellsignal
AKT-phospho murine	D9E	Synthetic phosphopeptide corresponding to residues around Ser473 of human Akt	rabbit	1:2000	4060S	Cellsignal
BACE1 murine, human	5606	Synthetic peptide corresponding to residues surrounding His490 of human BACE protein	rabbit	1:10000	-5606S	Cellsignal
BACE2 murine, human	ab5670	Synthetic peptide, corresponding to amino acid residues 441-457	rabbit	2µg/ml	ab5670	Abcam
β-actin murine, human	AC-74	Slightly modified β-cytoplasmic actin N-terminal peptide, Ac-Asp-Asp-Asp-Ile-Ala-Ala-Leu-Val-Ile-Asp-Asn-Gly-Ser-Gly-Lys, conjugated to KLH	mouse	1:1000	A5316	Sigma
Calnexin human	ADI-SPA-860-D	Synthetic peptide corresponding to the sequence near the C-terminus of dog calnexin	rabbit	1:2000	ADI-SPA-860	Enzo
ERK1/2 murine	9102	Synthetic peptide corresponding to a sequence in the C-terminus of rat p44 MAP Kinase	rabbit	1:1000	9102S	Cellsignal
ERK1/2-phospho murine	4370	Monoclonal antibody is produced by immunizing animals with a synthetic phosphopeptide corresponding to residues surrounding Thr202/Tyr204 of human p44 MAP kinase	rabbit	1:2000	4370S	Cellsignal
FLAG tag	M2	Synthetic peptid, corresponding to amino acid residues DYKDDDDK	mouse	WB: 1µg/ml	F1804	Sigma

HA tag	HA-7	Synthetic peptid, corresponding to amino acid residues YPYDVPDYA	mouse	WB: 1:2000	H9658	Sigma
SEZ6L murine	AF4808	Mouse myeloma cell line NS0 derived recombinant mouse SEZ6L Glu32Ser889	sheep	ELISA: 3µg/µl	AF4804	R&D
SEZ6L murine	21A11-1111 / R-2a	SEZ6L Ectodomain Epitope not mapped	rat	ELISA: 1:400	-	In-house
VEGFR3 human	MAB3757	Recombinant produced, purified, hVEGFR-3 extracellular domain protein	mouse	WB: 1:100	MAB3757	Merck
VEGFR3 murine	BAF743	recombinant mouse VEGFR3/Flt-4 Tyr25-Asp770	goat	ELISA: 0.4µg/ml WB: 0.1µg/ml	BAF743	R&D
VEGFR3 murine	AFL4	Ectodomain not further indicated	rat	ELISA: 3µg/ml IP: 0.25mg/ml WB: 1:1000	14-5988-81	Thermo Scientific

3.2. Genetic methods

3.2.1. Origin and re-cloning of DNA constructs

Only the full length *Flt4* construct was newly generated for the indicated experiments. Briefly, the software CLC main workbench (v. 7.9.1.) was used to insert the sequence for the full length VEGFR3 into the pFUGW backbone, containing an ampicillin resistance. VEGFR3 was tagged N-terminally with two HA tag sequences and C-terminally with two FLAG tag sequences. The designed vector sequence was sent to Eurofins Genomics (former GATC) for generation and 0.5µl of the obtained plasmid solution were transformed into 25µl competent NEB 5-alpha *E.coli* via a 30s heat shock of 42°C and subsequent 2 min on ice of the ice-cold bacteria-DNA mix. Transformed bacteria were combined with 950µl of LB medium and mixed at 37°C for 60min and 250rpm. Afterwards bacteria were transferred into LB, supplemented with 1:1000 ampicillin and incubated at 37°C overnight (ovn,) while shaking/rotating. Plasmids were purified, according to the manufacturer's protocol of the plasmid mini/midi-preparation kit. A nanodrop spectrometer was used to monitor purity and a control aliquot was sent to GATC Biotech for sequencing.

LB-medium
1% (w/v) Bacto Trypton
0.5% (w/v) Yeast Extract
0.5% (w/v) NaCl

Following constructs were used in this thesis:

Table 06. Constructs and plasmids. Overview of the construct and corresponding vectors, which were used in this thesis.

Plasmid	Vector	cDNA	Source
Full length 2x*Ha-Flt4*-2x*Flag*	pFUGW.	mm*Flt4*, full length protein	Genescript
Full lenght *Bace2*	pcDNA3.1	mm*Bace2*, full length protein	Farzan et al. [70]
pFUGW	pFUGW	Empty backbone	Addgene
pcDNA	pcDNA 3.1	Empty backbone	Addgene

The newly designed VEGFR3 construct was sent to DNA sequencing to validate the right sequences.

Primers for sequencing

The primers used for construct sequencing (Table 07) and qPCRs are listed in the following tables (Table 08):

Table 07. Used sequencing primers.

Gene	Primer	Sequence (in 5´- 3´order)	Usage
mm*Flt4*	Ubiquitin-fw	GGCGAGTGTGTTTTGTGAAG	sequencing
	Fw_02	ACCAGAACTTCCTTTCCA	
	Fw_03	CCTCTTCACCCAGCATCT	
	Fw_04	CCCTCAGTTTGAATATCC	
	Fw_05	CTTTGGAGGAGCAGTGTG	
	Fw_06	CGGGACATCTACAAAGAC	
	Fw_07	CCATGACCCCTACAACCT	
	WPRF_rev	CATAGTTAAGAATACCAGTCA	

Table 08. Used qPCR primers.

Reagent	Catalogue number	Manufacturer
BACE1	qHsaCID0012647	Biorad
BACE2	qHsaCID0012156	Biorad
DLL4	qHsaCED0044238	Biorad
FLT4	qHsaCID0020886	Biorad
FOXC2	qHsaCED0047198	Biorad
GAPDH	qHsaCEP0041396	Biorad

3.2.2. RNA isolation and qPCR

Cells were washed twice, using fresh, ice cold PBS and RNA was isolated, using the Qiagen RNA preparation kit, according to the manufacturer's protocol. RNA concentrations were determined spectroscopically via Nanodrop measurements and 500-600 ng of RNA material were used for the synthesis of cDNA, using the iScript Reverse Transcription mix, according to the manufacturer's protocol.

DNA concentrations were determined via Nanodrop measurements and cDNA stocks of 25 ng/µl were generated for each sample. For primer efficiency determination via standard curves, equal amounts of cDNA were pooled and a dilution series 50, 25, 12.5, 6.25, 3.125, 1.56, 0.78 ng/µl was generated.

For the qPCR reaction, a master mix was made for each gene and samples were measured in duplicates, using the default comparative Ct methods and 2 h ramp speed of the StepOnePlus thermocycler.

Mastermix	
SybrGreen Buffer	10 µl
SybrGreen Primer	2 µl
cDNA (12.5 ng/µl)	8 µl

Polymerase chain reaction		
95°C	10 min	Holding
95°C	**15 s**	
60°C	**1 min**	**x40 Cycles**
95°C	15 s	
60°C	1 min	Melting Curve
95°C	1 5s	

Following formula was used to determine relative quantities of individual target genes:

$$RQ=\frac{[1+(reference\ gene\ primer\ efficiency/100)]^{Ct\ (reference\ gene)}}{[1+(taret\ gene\ primer\ efficiency/100)]^{Ct\ (target\ gene)}]}$$

At used cDNA concentrations, all primers displayed an efficiency close to 100%.

3.3. Cell culture/line methods

3.3.1. Maintenance

Cell culture/line work was done under sterile conditions at the cell culture hood. Cells were grown and maintained in T75/T175 flasks until usage. For splitting, adherent cells were washed with 10 ml per 75 cm^2 of PBS and incubated with Trypsin-EDTA for 5 min at 37 °C. Detached cells were collected and centrifuged at room temperature (RT), for 5 min and 700 g. After resuspension cells were split in fixed flask area ratios into a fresh flask and grew until high confluency. The splitting for maintenance was done in fixed ratios, while cells which were used for experiments were always counted via trypan blue and seeded in required density.

3.3.2. Cell systems

Used cell lines were:

Human Embryonic Kidney HEK293T (immortalized with SV40 large T-Antigen). HEK293T were cultured in DMEM supplemented with 10% FBS and 1% Penicillin/Streptomycin (5000 U/mL) (v/v). HEK293-T cells were generally split 1:10 and used not longer than until passage 10.

Human Micro Vascular Endothelial Cells HMVEC-dlyAd (Lonza Bioscience). Primary lymphatic endothelial cells (LECs), which were isolated from human lymphatic breast tissue and enriched for lymphatic cells. HMVEC were cultured in EBM, supplemented with EBM growth kit. HMVEC cells were split based on achievable confluency in their current passage. Obtained stocks were received at passage 3 and further used until passage 8.

The WT-APP (hAPP695) expressing SK-NB-E human Neuroblastoma Cell Line (commercially obtained from Sloan-Kettering Cancer center) and insulinoma 6 (Min6) cells (self-generated, Janssen pharmaceutica) were not maintained on site. Min6 cells were modified to express murine VEGFR3 in the following manner: Min6 cells (Addexbio) were transfected using a murine VEGFR3 containing pcDNA 3.1 vector (RND systems Versaclone). Briefly, the transfection vector was linearized, using ScaI and transfection was performed, using Lipofectamine 2000. Positive clones were selected, using 800 µg/ml medium G418 (Gibco Geneticin G418) and individual colonies were selected after 19 days of selection. Colonies were expanded and VEGFR3 expression was evaluated via VEGFR3 specific western blotting. The clone with the strongest expression was selected for indicated experiments.

3.3.3. Cryopreservation

HMVEC and HEK cell stocks were cryopreserved in liquid nitrogen. Detached cells were pelleted by centrifugation and re-suspended in cold DMEM supplemented with 10% FBS and 10% DMSO (HEK) or ice cold EBM, supplemented with 10% FBS and 10% DMSO (HMVEC). 1 ml aliquots of 0.5 – 1 million cells were stored at -80 °C for 24 h and then transferred to liquid nitrogen for long term storage.

For de-thawing, cells were warmed up for maximal 5 min at 37 °C and re-suspended in their respective growth medium. Cells were passaged at least one generation, before usage for experiments. Confluency and viability was controlled via light microscopy.

Min6 and SK-NB-E were stored and maintained off-site.

3.3.4. Transient transfections

<u>HEK-overexpression:</u>

800,000 viable cells were seeded in each plate of a six well plate and grown in 1600 µl Optimem for 24 h. For transfection, 6.3 µg of lipofectamin was mixed with 196 µl serum free Optimem and a total amount of 1 µg of transfection plasmids (ratio *Bace2*: *Flt4* /pCDNA3.1 : pFUGW = 1:3) were combined with 200 µl of serum free Optimem. After 5 min of equilibration to RT, tubes were mixed and incubated another 20 min. Afterwards the transfection mix was added to the cells in a dropwise manner. After 24

h, cells were washed once with serum free Optimem and then supplemented with 1 ml serum free Optimum. After another 24 h, lysates and media were collected for further analysis.

HMVEC/LEC – knockdown:

200,000 viable cells were seeded in each plate of a six well plate and grown in 1600 µl EBM for 24 h. For transfection, the EBM was replaced with 1600 µl Optimem. 6.3 µg lipofectamin were combined with 194 µl serum free Optimem and 10 µl of 5 µM siRNA pools were combined with 190 µl serum free Optimem and incubated for 5 min. Tubes were mixed and incubated another 20 min, then added to the wells in a dropwise manner. After 24 h, the Optimem was replaced with 800 µl of fresh EBM and incubated for another 24 h. Lysates and media were collected for further analysis. Control samples, were transfected with equal amounts of untargeted control siRNA. For silencing, siRNA pools for *Bace1*, *Bace2* or *Flt4* were used.

HMVEC/LEC- for qPCRs:

250,000 viable cells were seeded in each well of a 6 well plate and grown for 24 h in 1600 µl EBM. Transfection was performed as indicated above and after 24 h of incubation, cells were serum starved ovn. via the exchange of serum free EBM. The next morning, medium was replaced with fresh EBM, supplemented with DMSO, 100 nM Verubecestat or 1.5 µg/ml VEGF-C156S and incubated for 100 min. Media were discarded and cells were used for RNA isolation.

3.3.5. Pharmacological cell line treatments

HMVEC/LEC- standard western blotting:

200,000 viable cells were seeded in each well of a 6 well plate and grown in 1600 µl EBM for 24 h. Afterwards the medium was replaced with EBM, which was supplemented with 2 µM C3 or 100 nM of Verubecestat. Equal volumes of DMSO were added to control wells. After 2 h of pre-dosing, media were replaced with fresh media, supplemented with respective inhibitors and incubated for another 24 h. Afterwards, lysates and media were collected for further analysis.

HMVEC/LEC- phospho western blotting:

Due to cell number limitations, 150,000 viable cells were seeded in each well of a 6 well plate and grown in 1600 µl EBM until high confluency of ~80% was achieved. Before treatment, cells were serum starved ovn. The next morning, medium was replaced with fresh EBM, supplemented with DMSO, 100 nM Verubecestat or 1.5µg/ml VEGF-C156S and incubated from 0 min for up to 100min. Lysates and media were collected at the indicated time points.

HMVEC/LEC- for qPCRs:

250,000 viable cells were seeded in each well of a 6 well plate and grown for 24 h in 1600 µl EBM. Before treatment, cells were serum starved ovn. The next morning, medium was replaced with fresh EBM, supplemented with DMSO, 100 nM Verubecestat or 1.5 µg/ml VEGF-C156S and incubated for 100 min. Media were discarded and cells were used for RNA isolation.

3.4. Protein Methods

3.4.1. Cell culture lysate and medium generation

Medium was collected, supplemented with 4 µl protease inhibitor cocktail (Pi) and centrifuged at 4 °C for 10 min and 15,300 g Afterwards, medium was transferred to a fresh tube and stored at -20 °C. Cells were washed with ice cold PBS and 150 µl (HEK) / 100 µl (HMVEC) of STET, freshly supplemented with 2 µl/ml Pi, was used for lysis. After adding the lysis buffer, cells were incubated on ice for 10 min, scraped off and transferred into a fresh Eppendorf tube. After another 20 min incubation on ice, lysates were centrifuged at 4 °C for 10 min and 15,300 g and transferred into a fresh tube. Lysates and media were stored at -20 °C. Deglycosylated samples were generated according to the manufacturer's protocol, using NEB's PNGaseF.

STET lysis buffer
50 mM Tris pH 7.5
150 mM NaCl
2 mM EDTA
1% TritonX-100

Lysate collection for phospho-blots in LECs were done with following alterations:

Media were discarded and cells were washed with ice cold TBS and lysed in RIPA lysis buffer, supplemented with 1:500 protease inhibitor cocktail (Pi), PhosStop, 1:100 NaF, 1:100 NA_3VO_4. Lysates were harvested immediately without incubation on ice and immediately centrifuged at 4°C for 10 min and 15,300 g. For phospo-stable storage, samples were mixed 4:1 with 4x Laemmli buffer.

RIPA lysis buffer
50 mM Tris pH 8.0
150 mM NaCl
2 mM EDTA
1% IGEPAL
0.1% SDS

3.4.2. Brain lysate generation and DEA fractionation

Collected frozen brains were weighted and combined with eight volumes of extraction buffer in MP BIO FastPrep tubes. After 20 min incubation on ice, brains were homogenized in a FastPrep instrument for 20 s, 6 m/s and lysates were spun down shortly at 4 °C. 900 µl of the supernatant were ultra-centrifuged for at 4 °C for 50 min and 221,000 g. 600 µl of the supernatant were collected into a fresh tube and neutralized with 66 µl 0.5 M Tris-HCl, pH 6.8. Until further usage, samples were stored at -80 °C. DEA lysates were diluted 1:10 in ELISA blocking solution and further used for Aß and sez6L ELISA.

Extraction buffer
50 mM NaCl
0.4% Diethylamine
2 µl/ml Roche inhibitor cocktail

3.4.3. Protein and peptide quantification

Proteins concentrations were estimated via the BC assay kit. Procedures were done according to the manufacturer's protocol. A serial dilution of bovine serum albumin was used to generate a calibration curve.

The concentration of digested peptides for mass spectrometric measurements were estimated via Nanodrop spectroscopy at 280 nm.

3.4.4. Glycoprotein enrichment via hydrazide beads

10 µl of plasma was combined with 90 µl GlycoLink Coupling buffer and 0.1 M sodium meta periodate was added to a final concentration of 25 mM to oxidize protein glycosylations. The mix was incubated at RT for 45 min in the dark. Meanwhile, zeba spin desalting columns were placed in 1.5 ml tubes and centrifuged at RT for 1min and 1,500 g. The flow trough was discarded and 300 µl GlycoLink Coupling buffer was added. The buffer was forced through the column by centrifuging at RT for 20 s and 1,500 g and discarded. The columns were washed two more times with GlycoLink Coupling buffer. Columns were placed in fresh 1.5 ml tubes and the glycoprotein solution was added. The glycoproteins were collected by centrifugation at RT for 2 min and 1,500 g to remove salts and amines. 50 µl Hydrazine resin was added to fresh snap cap columns and washed 6 times in the same manner as described above at RT for 10 s and centrifugation at 2,000 g. 100 µl 0.2 M Aniline catalyzer was added to protein mix and was vortexed for 10 s. Afterwards, samples were added to the hydrazine resin containing snap columns and mixed on an overhead rotator at RT for 4 h to couple oxidized proteins covalently to the hydrazide beads. After incubation, snap columns were centrifuged at RT for 10 s and 200 g and flow through was discarded. Columns were washed four times with 400 µl SDS buffer and six times with 500 µl 1 M NaCl in 100 mM Tris-HCl pH 8.5 and 500 µl UA buffer in an alternating manner to remove non-glycosylated proteins. The hydrazine resin was transferred into a fresh 1.5 ml tube, centrifuged for 10 s and 200 g and supernatants were discarded. Afterwards bound proteins were digested for mass spectrometric (MS) analysis.

3.4.5. Ig depletion and subsequent glycoprotein enrichment via Concanavalin A

Per sample, 50 µl of pierce protein A magnetic beads were mixed with pierce protein G magnetic beads and washed twice with 1ml binding/washing buffer. Additionally 50 µl of pierce protein L magnetic beads were washed in the same manner. 20 µl of plasma was combined with 480 µl of PBS, supplemented with 0.05% Tween 20, 2 µg/ml Pi cocktail and the mixture was added to the protein A/G mix. Samples were incubated at RT for 1 h on an overhead rotator and supernatants were transferred to the protein L beads. After another 1 h of incubation at RT with the overhead rotator, supernatants were collected for the glycoprotein enrichment.

The whole Ig depleted volume was used for glycoprotein enrichment via Concanavalin A agarose conjugate. Concanavalin A slurry was washed twice with PBS via an overhead rotator and was afterwards combined with the plasma. Binding buffer was added to a total volume of 1 ml and the mixture was incubated ovn at 4 °C on an overhead rotator. Beads were spun down for 30 s, at 2,000 g

and the supernatant was discarded. Beads were washed trice for 5 min with 1 ml binding buffer and eluted twice for 30 min with 250 µl elution buffer. Until further processing, the combined eluate was stored at -20 °C in lobind tubes.

Binding/Washing buffer
2 mM $MgCl_2$
2 mM $MnCl_2$
2 mM $CaCl_2$
0.5 M NaCl
20 mM Tris HCl, pH7.5

Elution buffer
500 mM methyl-alpha-D-mannopyranosidase
10 mM EDTA
20 mM Tris-HCl pH 7.5

3.4.6. Enzymatic and cellular BACE activity assays

BACE1 and BACE2 enzymatic activity was assessed via a FRET (Fluorescence Resonance Energy Transfer) assay[38]. Therein recombinant soluble BACE1 (Amino acids/AA 1-454) or recombinant soluble BACE2 (AA 21-466) were combined with an APP derived 13 amino acids containing peptide, which contains the "Swedish" Lys-Met/Asn-Leu mutation of the APP ß secretase cleavage site. This APP peptide substrate contains two fluorophores: On the one hand (7-methodxycoumarin-4-yl) acetic acid (Mca), which is a fluorescent donor with a excitation wavelength at 320 nm and an emission at 405 nm. On the other hand, 2,4.dinitrophenyl (Dnp), a Janssen pharmaceutica proprietary quencher acceptor. Proteolysis rates are linearly related to proteolysis via BACE1/BACE2. The BACE protease/substrate mix was incubated with different amounts of inhibitor for 120 min in a 384-well plate. Fluorescence was measured via a Flouroskan microplate fluorometer. No enzyme was present in the reaction mix for the low control.

Cellular BACE1 activity was determined, using the SK-N-BE(2) neuroblastoma cell line, expressing human WT APP. BACE inhibitors were added to the cells in indicated concentrations and incubated for 18h and media were collected for subsequent Aß42-MSD ELISA analysis[38,131,132].

Cellular BACE2 activity was determined using mouse insulinoma 6 (Min6) cells, expressing murine VEGFR3. BACE inhibitors were added to the cells in indicated concentrations and incubated for 18h and media were collected for subsequent VEGFR3-MSD ELISA analysis (see 3.4.7.1.).

3.4.7. ELISA

3.4.7.1. Murine VEGFR3

Empty MSD ELISA plates were pre-coated ovn. at 4 °C and 600 rpm with 30 µl of the coating antibody. Afterwards the plate was quickly washed five times with 200 µl washing buffer and blocked 2 h at RT and 600 rpm with 150 µl blocking buffer. The plate was washed another five times. Murine plasma samples were diluted 1:8 in blocking buffer. A standard serial dilution was generated for the protein of interest. Samples were heated for 10 min at 70 °C and 700 rpm and were cooled immediately on ice. 50 µl of sample and standard were added in duplicates and incubated ovn at 4 °C and 600 rpm. Plates were washed five times and 25 µl of secondary antibody was added at RT for 1.5 h and 600 rpm. After another five washing steps, 25 µl of 1 µg/ml MSD Streptavidin sulfo tag was added at RT for 20 min and 600 rpm. The five last washing steps were performed at RT for 20 min and 600 rpm.150 µl 2x

reading buffer was added directly before reading with the in-house MSD platform. Used antibody concentrations are indicated in the antibody table (table 05)

Blocking buffer
0.1% casein in PBS

Washing buffer
0.05% Tween-20 in PBS

Murine VEGFR3 antibodies
Coating: AFL4
Secondary: BAF743

Standard: Serial dilution of recombinant VEGFR3 of unknown starting concentration: 1, 0.3, 0.1, 0.03, 0.01, 0.003, 0.001 and 0 µl of standard/well. Purified and shared by collaboration partner.

3.4.7.2. Murine SEZ6L

Empty MSD ELISA plates were pre-coated ovn at 4 °C and 600 rpm with 30 µl of the coating antibody. Afterwards the plate was quickly washed five times with 200 µl washing buffer and blocked 2 h at RT and 600 rpm with 150 µl blocking buffer. The plate was washed another five times. 60 µl plasma were diluted in 60 µl blocking buffer (or 12 µl soluble brain fraction and 108 µl blocking buffer). A standard serial dilution was generated for the protein of interest. 50 µl of sample and standard were added in duplicates and incubated ovn. at 4 °C and 600 rpm. Plates were washed five times and 25 µl of secondary antibody was added at RT for 1.5 h and 600 rpm. After another five washing steps, 25 µl of 1 µg/ml MSD Streptavidin sulfo tag was added at RT for 20 min and 600 rpm. The five last washing steps were performed at RT for 20 min and 600 rpm.150 µl 2x reading buffer was added directly before reading with the in-house MSD platform. Used antibody concentrations are indicated in the antibody table (table 05)

Blocking buffer
0.1% casein in PBS

Washing buffer
0.05% Tween-20 in PBS

Murine SEZ6L antibodies
Coating: AF4808
Secondary: 21A11-1111/R2a

Standard: Serial dilution of recombinant murine SEZ6L with: 3000, 1000 300, 100, 30, 10, 3, 1, 0.3, 0.1, 0.03 and 0 pM of standard/well.

3.4.7.3. Human and non human primate VEGFR3

For the human ELISA, empty MSD ELISA plates were pre-coated ovn at 4 °C and 600 rpm with 30 µl of the coating antibody. Afterwards the plate was quickly washed five times with 200 µl washing buffer and blocked 2 h at RT and 600 rpm with 150 µl blocking buffer. The plate was washed another five times. 40 µl plasma were diluted 1:4 in blocking buffer. A standard serial dilution was generated for the protein of interest. Samples were heated for 10 min at 70 °C and 700 rpm and were cooled immediately on ice. Before loading, HBR-9 (Catalog No. 3KC564, Scantibodies Laboratory) was added to a final concentration of 0.225 mg/ml. 50 µl of sample and standard were added in duplicates and incubated ovn at 4 °C and 600 rpm. Plates were washed five times and 25 µl of secondary antibody was added at RT for 1.5 h and 600 rpm. After another five washing steps, 25 µl of 1 µg/ml MSD Streptavidin sulfo tag was added at RT for 20 min and 600 rpm. The five last washing steps were

performed at RT for 20 min and 600 rpm.150 µl 2x reading buffer was added directly before reading with the in-house MSD platform. Used antibody concentrations are identic to the murine setup.

Blocking buffer
0.1% casein in 1xPBS
0.0025% Tween-20

Washing buffer
0.05% Tween-20 in 1xPBS

Murine VEGFR3 antibodies
Coating: AFL4
Secondary: BAF743

Standard: Serial dilution of recombinant human VEGFR3 with: 300, 100, 30, 10, 3, 1, 0.3, 0.1, 0.03, 0.01, 0.003, 0.001 and 0 pM of standard/well.

NHP ELISA data were obtained using a commercial human ELISA kit (Immuno-Biological Laboratories 27779), according to the manufacturer's protocol.

3.4.8. Western blot analysis

Equal amounts of proteins were diluted in sample buffer, boiled for 5 min, at 95 °C and separated on 8% polyacrylamide gels. If not indicated otherwise, samples were run with reducing conditions. Gels were run in the electrophoresis chamber filled with SDS running buffer, at constant 80 V throughout the stacking gel and afterwards 130 V until the desired running distance. The separated proteins in the gels were transferred to nitrocellulose membranes using the BioRad Trans-Blot Turbo system according to the manufacturer's protocol. A constant 1 A/25V were applied for 40 min. Membranes were blocked ovn in blocking buffer, while shacking. Afterwards, membranes were incubated with the primary antibody (see table 05) diluted in washing buffer, 0.05% BSA (v/v), 0.0005% NaAzide ovn., shaking at 4°C. Membranes were washed three times with washing buffer, while shaking for 5 min and incubated with the secondary antibody- diluted in washing buffer and 0.05% BSA (v/v) - for 45 min at RT, while shaking. After incubation, membranes were again washed three times, 5 min, while shaking and developed using ECL Western Blotting Reagents. Images were generated, using the ImageQuant LAS 4000 platform. Displayed images were cropped, using the software Photoshop 12.1 and densiometric quantifications were done, using the software Fiji ImageJ (2.0.0-rc-67/1.52c).

Blocking buffer
0.1% casein in PBS

Washing buffer
0.05% Tween-20 in PBS

SDS-Running buffer
25 mM Tris
240 mM Glycin
0.1% (w/v) SDS

Sample buffer (4x)
8% SDS
0. 025% Bromophenol blue
10% ß-Mercaptoethanol (omitted in non-reducing conditions)
125 mM Tris pH 6.8

For phospho-blotting, following alterations were done: Casein was replaced with 5% BSA and TBS-T was used instead of PBS-T.

3.4.9. Sample preparation for mass spectrometric (MS) measurements of murine samples

3.4.9.1. Hydrazine-on bead digestion

50 µl of 10 mM dithiothreitol (DTT) in 100 mM ammonium bicarbonate (ABC) was added to the hydrazine-glycoprotein slurry and mixed at 37 °C for 30 min and 1,500 rpm. Supernatants were removed via centrifugation and 50 µl of 55 mM iodoacetamide (IAA) in 100 mM ABC was added and mixed in the dark at 20°C for 30 min and 1,500 rpm. Supernatants were again removed and beads were washed twice with 200 µl 100 mM AB, before adding 3 µg LysC in a total volume of 50 µl 100 mM ABC. Samples were mixed at 37 °C for 3 h and 1,500 rpm and 3 µg Trypsin in a total volume of 10 µl 100 mM ABC was added. Samples were incubated ovn. at 37 °C and 1,500 rpm and the supernatants were transferred into fresh tubes. Beads were washed twice with 100 µl 0.1% formic acid (FA) and supernatants were combined. Samples were acidified by adding 15 µl of 8% FA, before performing C18 stop and go extraction

3.4.9.2. Sodium deoxycolate (SDC) in solution digest

Non-enriched plasma was diluted 1:10 in 50 mM ABC and 10 µl of the dilution were combined with 10 µl denaturation buffer. Alternatively, 20 µg ConA enriched plasma was used and all buffer volumes were adjusted according to the following ratios of the non-enriched samples: 1 µl of 10 mM DTT was added and the mixture incubated at RT for 20 min. 1µl of 55 mM IAA was added for alkylation and incubated at RT for 30 min. After another 20 min incubation step with 1 µl of 10 mM DTT at RT, 3 µg of LysC in 50 mM ABC was added and incubated at RT for 3 h. Next, 3 µg trypsin in 50 mM ABC was added and incubated at RT ovn. Digested peptides were acidified with 150 µl 0.1% FA and 10 µl 8% FA and SDC precipitated at 4°C for 20 min. Precipitate was removed by centrifuging at 4°C for 10 min and 20,000 g. Samples were stage tipped before MS measurements.

Denaturation buffer
0.5% SDC in 250 mM ABC

3.4.9.3. Stop and go extraction

Stage tips were prepared by stacking four disks of C18 empore material into 200 µl pipette tips. Tips were conditioned with 100 µl MeOH and washed twice with 100 µl 0.1% FA. Solvents were forced through the tips by centrifugation at 2,00 g in a STAGE Tip centrifuge. After loading the digested protein samples, tips were washed four times with 0.1% FA and peptides were eluted with 40 µl of 60% ACN in 0.1% FA into protein LoBind tubes. Samples were dried in a SpeedVac and resuspended in 20 µl of 0.1% FA. Protein concentration was determined via Nanodrop spectroscopy.

3.4.10. Sample preparation for murine VEGFR3 ectodomain sequencing

3.4.10.1. Ectodomain purification

Supernatant of 11 T75 flasks of stably VEGFR3 transfected Min6 cells was collected after 24-48 h of cell growth and cell debris was removed via 5 min centrifugation at 4 °C and 1,000 rpm. Supernatants were thereafter concentrated in 30 kDa Vivaspin Turbo 15 columns via 10 min centrifugation at RT and 4,000 g. Next, VEGFR3 was immunoprecipitated using the Dynabead Protein IP kit and 20 µl AFL4 antibody per 50 µl beads. Non-denaturing conditions were used for the elution process and the whole eluted protein amount was deglycosylated, using the NEB deglycosylation kit. The final protein concentration was estimated via densiometric western blot quantification against a recombinant VEGFR3 standard curve of known concentration (743-R3).

3.4.10.2. Ectodomain sequencing

Identity of VEGFR3 bands: In gel digestion

20 µg of sample were separated on a 12% polyacrylamide gel and proteins were stained, using InstaBlue in order to simplify the cutting of appropriate gel fractions. Molecular weight ranges of interest were cut into 6 gel fractions and processed as follows:

Gel slices, cut into 1 mm^2 pieces were placed in individual tubes and washed four times with 500 µl washing solution, via shaking at RT,15 min, 1,400 rpm on a Thermomixer. After one wash with 500 µl ACN at RT, 15 min, 1,400 rpm, samples were denatured with 150 µl 50 mM ABC, supplemented with 150 µl 10 mM DTT and likewise incubated at 37 °C, 30 min, 1,400 rpm. For alkylation, the DTT solution was replaced with 150 µl 50 mM ABC, supplemented with 100 mM IAA and samples were incubated in the dark at RT, 30 min, 1,400 rpm. The IAA solution was discarded and replaced with 500 µl ACN and incubated at RT, 5 min, 1,400 rpm. Gel pieces were washed successively with 500 µl 50 mM ABC and 500 µl ACN and afterwards incubated with digestion buffer, supplemented with 0,0015 µg/µl trypsin at 37 °C, ovn. The next day, 8 µl 8%FA were added to stop the digest and the supernatants were transferred to fresh tubes. Remaining peptides were extracted twice by adding 150 µl extraction solution and incubating at RT, 15 min, 1,400 rpm. Supernatants of individual gel slices were combined and concentrated via vacuum centrifugation. Finally, samples were re-suspended in 30 µl 0.1%FA. Prior MS analysis, samples were purified via STAGE tipping (3.4.9.3.).

Washing solution
50 mM ABC in 40% ACN

Digestion buffer
10 mM ABC + 5%ACN

Extraction buffer
40%ACN + 0.1%FA

Cleavage site determination: SP3 digest

Magnetic SeraMag A and SeraMag B beads were mixed 1:1 and a fourfold volume of H_2O was added. Tubes were then placed in a magnetic rack and the supernatant discarded. Beads were rinsed two times with 500 µl H_2O and re-suspended in water to a concentration of 4 µg beads/µl. 5 µg of purified protein and 50 mM ABC were combined to a volume of 40 µl and 2.5 µl 200 mM DTT were added. Samples were mixed at 45 °C for 30 min and 1,200 rpm and subsequently 5 µl 400 mM IAA were added at 24

°C for 30 min and 1,200 rpm in the dark. Another 2.5 µl 200 mM DTT was added and 10 µl of mixed beads was combined with the protein mixture. 240 µl of 100% EtOH was mixed with the sample, followed by a 30 min incubation step at RT and 1000 rpm. For supernatant removal, beads were placed in a magnetic rack and the supernatant was discarded. Beads were then washed four times with 80% EtOH in the same manner. One third of the beads were resupsended in 20 µl 0.025 µg/µl LysC and incubated at 37 °C for 3 h and 1,000 rpm. Afterwards, another 20 µl of trypsin were added and beads were incubated ovn at RT without shacking. Equally, the other sample aliquots were resuspended in either LysN or AspN, without pre-digestion via LysC. The next day, 2 µl of 8% FA were added and the bead mix supernatant was loaded on 0.2 µm filter columns, which were washed once, using 200 µl 0.1% FA and by centrifuging 2 min for 2,000 g. The flow through was dried in a SpeedVac and resuspended in 20 µl of 0.1% FA. Protein concentration was determined via Nanodrop spectroscopy.

3.4.11. Sample preparation for mass spectrometric measurements of NHP samples

3.4.11.1. Single tube, solid phase sample preparation (SP3)

Before digestion, NHP plasma samples were depleted via Pierce Top12 depletion columns and 20 µg of eluted material were used for subsequent SP3 digestion. Samples were processed according to 3.4.10.2. However, only a LysC/trypsin double digest was used for the plasma samples.

3.5. LC-MS/MS analysis

3.5.1. Murine plasma sample analysis

Murine plasma samples were analyzed on an Easy nLC-1000 nano UHPLC coupled online via a Nanospray Flex electrospray ion source equipped with a column oven (Sonation, Germany) to a Q-Exactive HF mass spectrometer. An amount of 1-1.3 µg of peptides were separated on self-packed C18 columns (500 mm × 75 µm, ReproSil-Pur 120 C18-AQ, 1.9 µm; Dr. Maisch, Germany) using a binary 120 or 180 min gradient of water (A) and 100% acetonitrile (B) supplemented with 0.1% FA (0 min, 2% B; 5 min 5% B; 185 min, 25% B; 230 min, 35% B; 250 min , 60% B).

Glycoprotein enriched plasma samples were analyzed in data depended acquisition mode with a 180min gradient. Full MS spectra were acquired at a resolution of 60,000 (AGC target: 3E+6). The 10 most intense peptide ions were chosen for fragmentation by higher-energy collisional dissociation (resolution: 30,000, maximum ion trapping time: 100 ms, isolation width: 2 mass to charge (m/z), AGC target: 1E+5, NCE: 26%). A dynamic exclusion of 120 s was applied for fragment ion spectra acquisition.

Spectra for data independent acquisition (DIA) library generation were acquired at a resolution of 120,000 (AGC target 5E+6) on a Q-Exactive HF mass spectrometer. The 20 most intense peptide ions were chosen for fragmentation by higher energy collisional dissociation (resolution 15,000, maximum ion trapping time: 50 ms, isolation width: 1.6 m/z, AGC target 1e+5, NCE:26%). A dynamic exclusion of 120 s was applied for fragment ion spectra acquisition.

All non-enriched plasma samples were measured with a 120min gradient in data independent acquisition mode. Full MS spectra were acquired at a resolution of 120,000 (AGC target 5E+6). DIA fragmentation spectra were acquired by higher-energy collisional dissociation of all ions in 20 windows of variable size (Table 09; resolution: 30,000, AGC target: 3E+6, stepped NCE 23.4%, 26%, 28.6%).

Table 09. Used DIA windows for murine plasma. Optimized m/z window distribution for Sequential Window Acquisition of All Theoretical Mass Spectra (Swath-MS) based data independent acquisition.

Window	m/z start	m/z end	Center	Isolation width [m/z]
1	300	385	342.5	85
2	384	424	404	40
3	423	453	438	30
4	452	480	466	28
5	479	505	492	26
6	504	529	516.5	25
7	528	552	540	24
8	551	575	563	24
9	574	598	586	24
10	597	621	609	24
11	620	645	632.5	25
12	644	671	657.5	27
13	670	698	684	28
14	697	726	711.5	29
15	725	759	742	34
16	258	796	777	38
17	795	841	818	46
18	840	901	870.5	61
19	900	1051	975.5	151
20	150	1402	1226	352

3.5.2. Murine VEGFR3 ectodomain sequencing

All sequencing samples were analyzed on an Easy nLC-1000 nano UHPLC coupled online via a Nanospray Flex electrospray ion source equipped with a column oven (Sonation, Germany) to a Q-Exactive mass spectrometer.

Identity of VEGFR3 bands

A volume of 8 µl of the final protein digestions were separated on self-packed C18 columns (500 mm × 75 µm, ReproSil-Pur 120 C18-AQ, 1.9 µm; Dr. Maisch, Germany) using a binary 120 min gradient of water (A) and 100% acetonitrile (B) supplemented with 0.1% FA (0 min, 2% B; 5 min 5% B; 185 min, 25% B; 230 min, 35% B; 250 min , 60% B).

Gel samples were analyzed in data depended acquisition mode. Full MS spectra were acquired at a resolution of 70,000 (AGC target: 3E+6). The 15 most intense peptide ions were chosen for fragmentation by higher-energy collisional dissociation (resolution: 17,500, maximum ion trapping time: 50 ms, isolation width: 2 m/z, AGC target: 1E+5, NCE: 25%). A dynamic exclusion of 120 s was applied for fragment ion spectra acquisition.

Cleavage site determination

1500 fmol of the SP3 digested samples were separated on self-packed C18 columns (500 mm × 75 µm, ReproSil-Pur 120 C18-AQ, 1.9 µm; Dr. Maisch, Germany) using a binary 60 min gradient of water (A) and 100% acetonitrile (B) supplemented with 0.1% FA (0 min, 2% B; 3.5 min 5% B; 45.5 min, 35% B; 50.5 min, 60% B; 51.5 min , 95% B; 60.5 min , 95% B).

Samples were analyzed in data depended acquisition mode. Full MS spectra were acquired at a resolution of 70,000 (AGC target: 3E+6). The 10 most intense peptide ions were chosen for fragmentation by higher-energy collisional dissociation (resolution: 17,500, maximum ion trapping time: 100 ms, isolation width: 2 m/z, AGC target: 1E+5, NCE: 25%). A dynamic exclusion of 60s was applied for fragment ion spectra acquisition.

3.5.3. NHP plasma sample analysis

NHP plasma samples were analyzed on an Easy nLC-1200 nano UHPLC coupled online via a Nanospray Flex electrospray ion source equipped with a column oven (Sonation, Germany) to a Q-Exactive HF mass spectrometer. An amount of 1.0 µg of peptides were separated on self-packed C18 columns (500 mm × 75 µm, ReproSil-Pur 120 C18-AQ, 1.9 µm; Dr. Maisch, Germany) using a binary 180 min gradient of water (A) and 80% acetonitrile (B) supplemented with 0.1% FA (0 min, 3% B; 3.5 min, 6% B; 137.5 min, 30% B; 168.5 min, 44% B; 182.5 min, 75% B; 185 min, 99% B; 200 min, 99% B)

Samples were measured in data independent acquisition mode. Full MS spectra were acquired at s resolution of 120,000 (AGC target 5E+6). DIA fragmentation spectra were acquired by higher-energy collisional dissociation of all ions in 30 windows of variable size (Table 10; resolution: 30,000, AGC target: 3E+6, stepped NCE 23.4%, 26%, 28.6%).

Table 10. Used DIA windows for NHP plasma. Optimized m/z window distribution for Swath-MS based data independent acquisition.

Window	m/z start	m/z end	Center	Isolation width [m/z]
1	300	352	326	52
2	351	383	367	32
3	382	409	395.5	27
4	408	430	419	22
5	429	449	439	20
6	448	467	457.5	19
7	466	484	475	18
8	483	501	492	18
9	500	518	509	18
10	517	535	526	18
11	534	552	543	18
12	551	569	560	18
13	568	586	577	18
14	585	603	594	18
15	602	620	611	18
16	619	637	628	18
17	636	655	645.5	19
18	654	674	664	20
19	673	695	684	22
20	694	716	705	22
21	715	739	727	24

22	738	765	751.5	27
23	764	791	777.5	27
24	790	820	805	30
25	819	851	835	32
26	850	887	868.5	37
27	886	928	907	42
28	927	1029	978	102
29	1028	1180	1104	152
30	1179	1401	1290	222

3.6. LC-MS/MS data analysis and statistical evaluation

All DDA data were analyzed via the Maxquant (1.5.5.1.) -software[133], using the default setting with slight modifications as follows. Trypsin/P was defined as protease and the minimal peptide length was set to six amino acids. Two missed cleavages were allowed. The option first search was used to recalibrate the peptide masses within a search window of 20 ppm. For the main search, the peptide mass tolerance was set to 4.5 ppm. Tolerances for peptide fragment ions were set to 20 ppm for HCD. Carbamidomethylation of cysteine was defined as static modification. Acetylation of N-termini as well as oxidation of methionines were set as variable modifications. The false discovery rate for both peptides and proteins was adjusted to less than 1% using a target and decoy approach (concatenated forward and reversed database). Label free quantification (LFQ) of proteins required at least two ratio counts of razor peptides. Only unique peptides were used for quantification. The option "match between runs" was enabled with a matching time of 1.5 min.

Individual alterations are indicated in the following subchapters.

3.6.1. Murine plasma sample analyses

For the glycoprotein enrichment samples, spectra were searched against a reviewed canonical database of *Mus Musculus* from uniprot (download: 2017-01-11, entries: 16,843 proteins).

For the DDA library generation, eight of the B2KO mouse plasma samples, supplemented with the Biognosys iRT kit, were searched against a reviewed isoform database of *Mus Musculus* from uniprot (download: 2017-04-11, entries: 24,992 proteins). Match between runs, label free quantification and contaminant inclusion were disabled. Generated results were loaded into the Biognosys software Spectronaut (11.0.15038.22.23735)[134] and a library was generated using the default settings.

Using Spectronaut, the non-enriched DIA plasma samples, supplemented with the Biognosys iRT kit, were matched against the self-generated library, using the default settings. Briefly, a 1% FDR was applied to peptide and protein identifications and LFQ was performed on the MS1 level. LFQ of proteins required at least one identified peptide and was done with up to three peptides.

Generated LFQ outputs were log2 transformed and an average log2 fold change was calculated for each protein. No additional filters were applied. Changes in protein abundance were evaluated using a Student's t-test between the log2 LFQ intensities of the two experimental groups. A permutation based FDR estimation was used to account for multiple hypotheses (p=5%; s_0=0.1) using the software Perseus [135,136]. Volcanos only display proteins, which were identified often enough to apply statistical tests.

3.6.2. Murine VEGFR3 ectodomain sequencing

Identity of VEGFR3 bands

No protein LFQ was performed and the option "match between runs" was disabled. Spectra were searched against a reviewed canonical database of *Mus Musculus* from uniprot (download: 2018-07-23, entries: 16,989 proteins). All protein groups and identified VEGFR3 peptides were filtered for hits with a score >20 and the 10 peptides with the highest intensity were picked for manual mapping against the ectodomain.

Cleavage site determination

The digestion mode was set as unspecific and no protein LFQ was performed. The option "match between runs" was disabled. Additionally to already indicated modifications, Asn -> Asp was set as a variable modification in order to consider the deglycosylation step by PNGaseF. The false discovery rate for both peptides and proteins was adjusted to less than 95%. Spectra were searched only against the whole uniprot VEGFR3 sequence. Peptides from all digestion mixes with a score >20 were used as an input for the Qarip mapping tool[137]. The C-terminus of the semi-specific peptide with closest localization to the transmembrane domain was identified via LysN digestion and chosen as the likely cleavage site.

As a quality control for the peptide's identity, a synthetic peptide with the same sequence and sample preparation dependent modifications (cysteine carbamidomethylation, free COOH group) was measured in an identical manner. The software Skyline[138] (v.20.2.0.343) was subsequently used to compare the synthetic isotopic MS1 spectrum and associated fragmentation MS2 spectra with the corresponding spectra from the LysN measurement. The VEGFR3 ectodomain sequence (AA01-AA775) was used to generate the peptide and transition list. Following Skyline settings were changed from the default:

For peptide settings, LysN was set as the digestion enzyme and no missing cleavages were allowed. A 5min retention time window was used for inter sample comparison and peptides were filtered for a length between 6-25 AA. The spectral information from the LysN associated Maxquant results (see above) was used to generate a Skyline spectral library, using the default library settings. Peptide matching was picked via this library.

For the transitions, y, b and precursor ions were considered. All precursor ions with charges from 1-3 and all fragment ions with charges from 1-2 were considered for analysis. First, all product ions (from ion 1 to last ion) were displayed and filtered for the 3 most intense product ions, based on the generated spectral library. The library ion matching tolerance was set to 0.055 m/z. The instrument range was defined as 140-2,000 m/z Full scan MS1 filtering was based on the number (count) of 3 isotope peaks and the mass analyzer was set to the Orbitrap system, with a resolving power of 140,000 at 200 m/z. Only scans within 5 min of the spectral library were considered.

The raw file of the synthetic peptide was subsequently imported, filtered by described settings and compared to the LysN derived library. The dotp value histograms were exported to visualize precursor and fragmentation pattern similarities.

3.6.3. NHP plasma sample analyses

DIA files from iRT supplemented NHP plasma samples were processed without the use of a generated library, using the default direct DIA workflow in Spectronaut (14.10.201222.47784). Settings beyond direct DIA were the same as in murine samples and quantifications were also performed on the MS1 level. Due to the paired nature of processed samples and the lack of concurrent vehicle controls, no permutation based FDR could be performed. Instead a paired t-test without subsequent multiple hypothesis testing was performed.

3.6.4. Miscellaneous data processing software

The software Graphpad Prism 7.02 was used to generate displayed graphs and for any statistical testing except for the volcano scatter plot statistics, which was generated in Perseus. Any displayed normalized data is normalized on the mean value of the respective control condition.

3.7. Animal Work

Mouse lines used in this thesis were the following: wild type (WT) C57BL/6NCrl and C57BL/6J (Charles River), *Bace1*-/- (B1KO[71]) *Bace1/2* -/- (BDKO[73]) and *Bace2*-/- (Riken BRC, strain C57BL/6-Bace2<tm1.2>). Any *in vivo* material (e.g. plasma or tissue samples) were kindly provided by collaborating research- and pharma collaborators: Samples were send to the DZNE for processing and analysis. In short, mice had access to water and food ad libitum and were maintained on a 12/12h light dark cycle. All murine animal procedures were carried out in accordance with the European Communities Council Directive (86/609/EEC). All NHP experiments and sampling were conducted by Shionogi & Co., Ltd and performed according to the applicable Japanese ethical guidelines.

Plasma and brain tissue collection times are indicated in the individual experimental results. All samples were stored at -80°C.

4. Results

4.1. Identification of VEGFR3 as a putative BACE2 specific substrate

Currently, the only *in vivo* assessment of BACE2 inhibition is the monitoring of the fur pigmentation status of drug treated mice, due to the altered shedding of the pigmentation associated BACE2 substrate PMEL[79-81]. Since drug distribution in different tissues is highly dependent on the physico-chemical nature of the individual compound[139], obtained results may however vary between different BACE inhibitors of similar BACE2 potency. Additionally, the screening procedure is rather tedious und stressful for laboratory animals and is not well transferable to humans as a read out of BACE2 inhibition in clinical trials. Thus, the aim was to identify an alternative BACE2 activity biomarker with higher reliability, easier accessibility with the potential for translation to human studies.

To these ends, the plasma of 15-20 weeks old WT mice and BACE1/2 KO mice was analyzed via mass spectrometry. To assess BACE2 specific alterations, following mice were used for plasma proteomics: *Bace1* tm $KO^{+/+}$, *Bace1* tm $KO^{-/-}$, *Bace2* tm $KO^{-/-}$, *Bace1* tm $KO^{-/-}$ x *Bace2* tm $KO^{-/-}$, C57BL/6J. As the high protein complexity of plasma masked any meaningful changes and potential BACE2 substrates are glycosylated transmembrane type 1 proteins, glycoprotein enrichment was performed prior to the proteomic analysis. Most transmembrane proteins are highly glycosylated[58] , while many highly abundant plasma proteins like albumin are devoid of, or show only little glycosylation. Consequently, this workflow allowed a strong reduction of plasma protein complexity.

Following the glycoprotein enrichment, several proteins were identified, which were significantly downregulated in B2KO and BACE double knockout mice (BDKO) and stayed unchanged in B1KO mice (Fig. 05A-C). These included Alpha-1B-glycoprotein (*A1bg*), Desmoglein-2 (*Dsg2*), FMS-like tyrosine kinase 4 (*Flt4*=VEGFR3), Lysosomal alpha-mannosidase (*Man2b*) and Mannose-binding protein C (*Mbl2*). Of these, only *DSG2* and *FLT4* are transmembrane type one proteins, which could potentially be cleaved by BACE2. *Flt4*/VEGFR3 was the strongest and most significantly decreased plasma transmembrane type 1 protein with a reduction down to ~40% in BDKO and down to ~20% in B2KO mice, while staying unchanged in B1KO (Fig. 05A-D). Therefore, VEGFR3 was further analyzed as a potential BACE2 substrate.

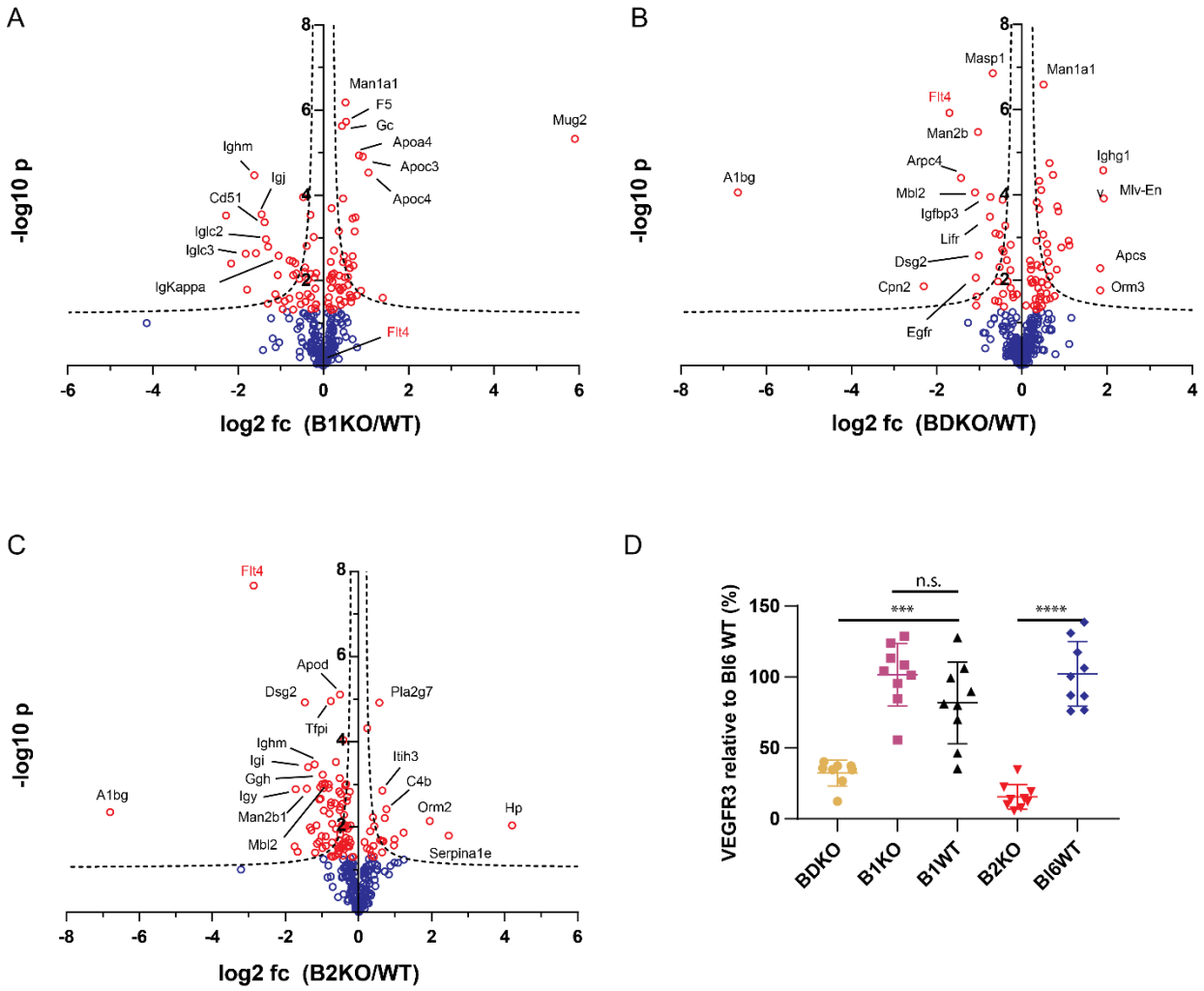

Figure 05. Discovery of VEGFR3 as a putative BACE2 substrate. (A-C) Volcano plots of proteomic analysis of B1KO, B2KO and BDKO mouse plasma. The minus log10 transformed t-test p-values are plotted against the log2 transformed label free quantification intensity ratios of KO against WT plasma for every relatively quantified protein. Proteins with a t-test p-value < 0.05 are shown in red circles. Proteins that remain significant after permutation based FDR correction (FDR <0.05, s_0= 0.1) are located above the dotted lines. Pronounced hits were labelled with their respective gene names. *Flt4* is highlighted in red for easier visibility. **(D)** Extracted LFQ ratios of plasma *FLT4*/VEGFR3 of KO mice and their respective WT littermates (B1WT, Bl6WT, one-way ANOVA with p< 0.0001, followed by Bonferroni's multiple comparison test, n= 8-9 n.s. non significant, *** p= 0.0001, **** p< 0.0001,)

4.2. Validation of *FLT4*/VEGFR3 as a BACE2 specific substrate

Subsequently, FLT4, which is also called VEGFR3, was validated as a true positive hit in independent mouse lines, using genetic and pharmacological approaches. First plasma from an independent BACE2 KO mouse line was investigated to validate the results (4.2.1.). Afterwards, VEGFR3 and BACE2 were co-overexpressed in HEK293T cells to further investigate BACE2 dependent shedding of VEGFR3 (4.2.2). Next, to avoid overexpression artifacts, endogenous shedding in human lymphatic endothelial cells was monitored upon altered BACE activity (4.2.3.). Furthermore, enzymatic and cellular BACE cleavage activity assays were performed under the administration of several BACE inhibitors with differential BACE selectivity (4.2.4.). Finally, individual VEGFR3 products, visible in the Western Blot analysis, were sequenced in order to identify the likely cleavage site of murine VEGFR3 by BACE2 (4.2.5.).

4.2.1. VEGFR3 processing in independent mouse lines

To ensure, that the observed decrease of plasma VEGFR3 is not unique to the performed experiment or mouse line, but BACE2 dependent, 4-5month old mice of an independently maintained *Bace2* tm $KO^{-/-}$ knockout line[73] was used for further proteomic analysis of plasma (Fig. 06A). Unlike the samples from 4.1. ,these samples were not enriched for glycoprotein, as recent advances in the data independent acquisition method[140-142] improved the sensitivity of mass spectrometric (MS) measurements and allowed for detection of VEGFR3 without further sample fractionation or glycoprotein enrichment. The analysis confirmed the initial data and reproduced the reduction of VEGFR3 down to 20% in comparison to WT levels (Fig. 06A, Fig. 06D). The same reduction was also detected via ELISA (Fig. 06D).

Additionally, 3-4 month old C57Bl/6 WT wild type mice were sub-chronically treated with either a vehicle control (VEH), 30 mg/kg of a BACE1/2 unspecific inhibitor MT070 (MTS)[143] or 100 mg/kg of a BACE1 preferring inhibitor LY2811376 (LY)[144] for 14 days. The plasma was analyzed via MS after trypsin digestion. Consistently with the previous data, the unspecific BACE inhibitor (Fig 06B), but not the BACE1 preferring inhibitor (Fig. 06C) led to a significant decrease of plasma VEGFR3 by 50% (Fig 06B-D). Administration of the BACE1 preferring compound lead to a slight, but significant increase of plasma VEGFR3 due to unknown reasons. Taking into consideration that none of the other BACE inhibitors throughout this thesis led to increased plasma VEGFR3, the effect is most likely specific to the LY inhibitor and does not directly derive from BACE inhibition.

The measured decrease of the plasma VEGFR3 was also visible, using western blotting analysis of the same plasma samples after ConcanavalinA glycoprotein enrichment (Fig. 06E-F). As tested loading controls did not properly work on the enriched samples, an independent whole protein staining of a nitrocellulose membrane was performed on equally separated and blotted samples from the same enrichment (not shown). Nevertheless, due to the lack of proper loading controls no densiometric quantification was performed on WB samples. However, the immunoblot was clearly able to show the genotypic decrease in the B2KO mice, which mirrored the results from corresponding MS and ELISA measurements. While a non-reducing loading buffer yielded a single ectodomain band at 120kDa, the usage of a reducing agent split the ectodomain into two smaller parts at 70kDa and 50kDa by reducing its sulfur bridge. A comprehensive characterization of VEGFR3 and its bands can be found in Figure 07.

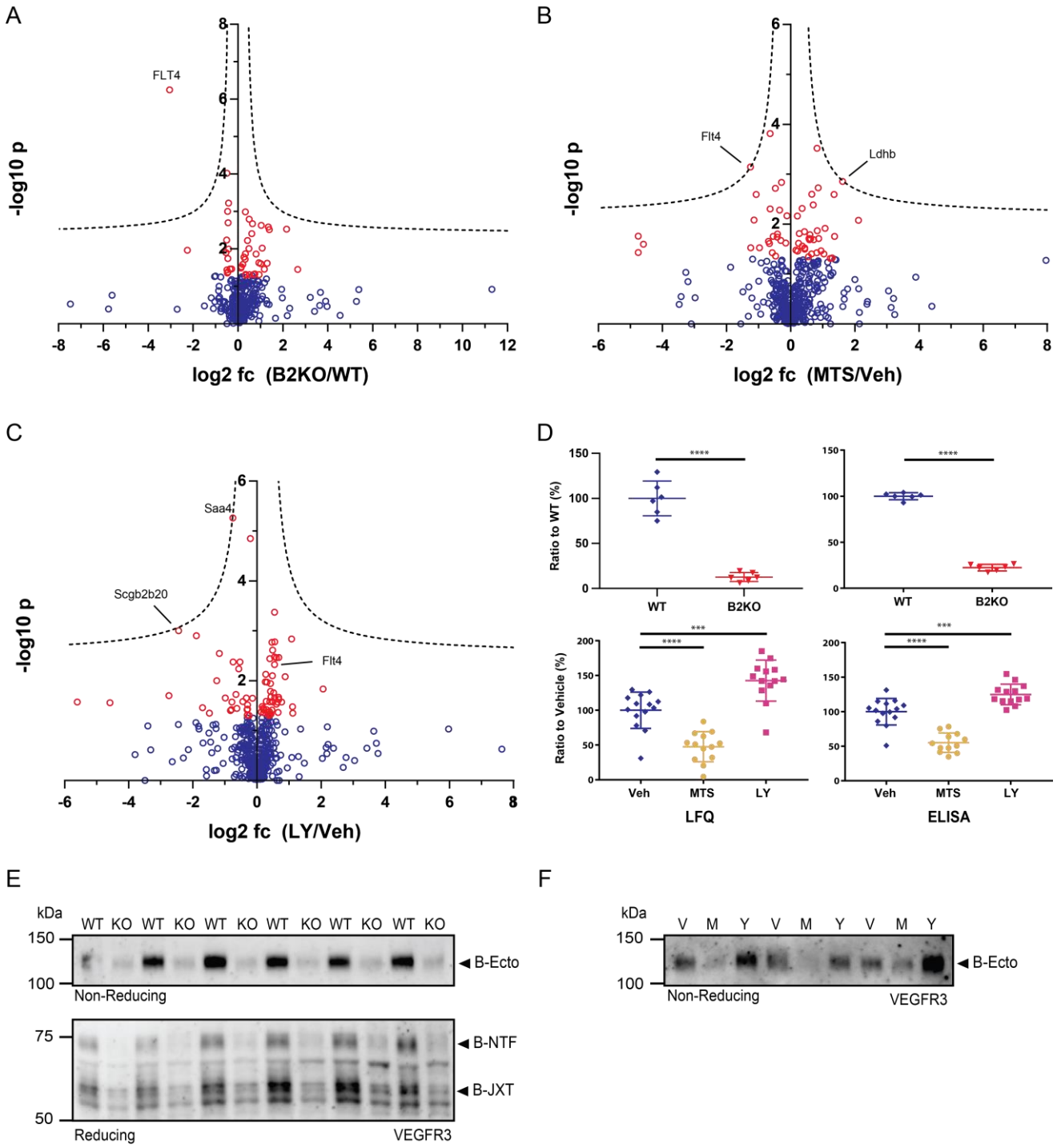

Figure 06. Validation of VEGFR3 as a putative BACE2 substrate in independent mouse lines. (A) Volcano plots of the proteomic analysis of B2KO mouse plasma. **(B-C)** Volcano plots of proteomic analyses of plasma from WT mice, treated with Vehicle, or BACE inhibitors MTS and LY. The minus log10 transformed t-test p-values are plotted against the log2 transformed label free quantification intensity ratios of plasma proteins comparing KO against WT or inhibitor against vehicle treated mice. Proteins with a t-test p-value < 0.05 are shown as red circles. Proteins that remain significant after permutation based FDR correction (FDR <0.05, s_0= 0.1) are located above the dotted lines. Hits above or close the dotted line were labeled with their respective gene names. *Flt4* was always indicated for better comparison. **(D)** Extracted protein LFQ intensity ratios (graphs on the left) and ELISA data (graphs on the right) on the same samples (n.s. non significant, *** p= 0.0001, **** p< 0.0001, for single comparisons: Welch's t-test, n=6. For multiple comparisons: one-way ANOVA with p< 0.0001, followed by Bonferroni's multiple comparison test, n= 13-14). **(E)** Immunological detection of the VEGFR3 ectodomain of ConA enriched B2KO (KO) and WT mouse plasma. Band pattern shown for non-reducing and reducing conditions. **(F)** Representative immunological detection of the VEGFR3 ectodomain of ConcanavalinA (ConA) enriched Vehicle of plasma from WT mice treated with Vehicle (V), or BACE inhibitors MTS (M) and LY (Y).

4.2.2. VEGFR3 shedding in the HEK293-T overexpression system

Next, HEK293-T cells were transfected with murine VEGFR3 and BACE2. Immunoblotting was used to further demonstrate the ability of BACE2 to cleave VEGFR3. Figure 07 shows a general overview to comprehend possible cleavage products, which can be obtained via western blotting. Note, that depicted molecular weights are estimations, which derive from already published human VEGFR3 band descriptions[145] and logical deductions, which are based on the theoretical masses of fragments and their corresponding detected western blot bands. Therefore, the actual detected sizes can be variable due to differences in posttranslational modifications (PTM), depending on the organism, the cell type[146] and on the artificial alterations like overexpression[147], which was partly performed in serum free conditions, which can additionally alter PTM patterns[148]. Noteworthy, additional bands were detected upon overexpression, which did not appear in the other experimental setups due to following reasons:

1) The murine overexpressed form was detected, using a polyclonal antibody with presumably several epitopes along the ectodomain, while the human form was visualized, using a monoclonal antibody, which presumably binds at the extracellular part below the sulfur bridge (both logically deducted from detectable bands). 2) The strong overexpression appears to result in the additional artificial cleavage products of the immature VEGFR3. Furthermore, serum free conditions may notably alter protein modifications and therefore yields additional bands for affected fragments. 3) As further explained below, use of reducing or non-reducing agents additionally yields alternative fragments, depending on the maturation status of VEGFR3.

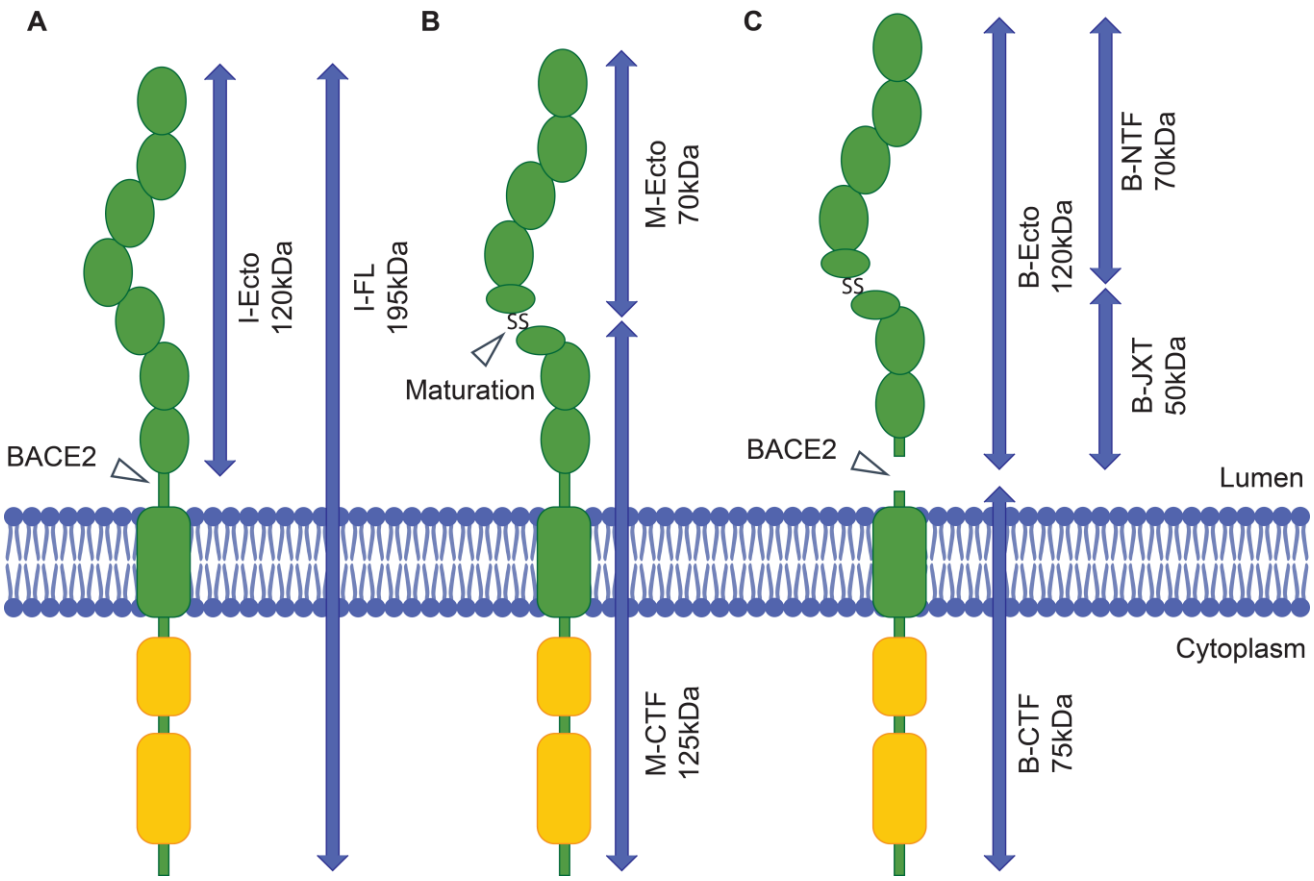

Figure 07. Overview of VEGFR3 and its possible products during maturation and shedding. From left to right: **(A)** The immature full length (I-FL) VEGFR3 protein is indicated with a size of 195 kDa and BACE2 cleavage can release the 120 kDa immature Ectodomain (I-Ecto), which was only observed upon artificial overexpression. **(B)** Endogenously, the I-FL is further processed during its

maturation process by cleavage between Arg472 // Ser473 and reconnection via a disulfide bond in the Ig like domain 5[149]. As a consequence, non reducing conditions can still yield a 195 kDa band, while reducing conditions cleave the disulfide bond, which produces the ectodomain product (M-Ecto) at 70 kDa and the corresponding mature C-terminal fragment (M-CTF) at 125 kDa. **(C)** Mature full length VEGFR3 can be further cleaved by BACE2, presumably in the juxtamembrane region. This shedding process yields the BACE2 processed C-terminal fragment (B-CTF) at 75 kDa and the corresponding BACE2 processed ectodomain (B-Ecto). Under non-reducing conditions, the shed ectodomain B-Ecto stays intact and appears at 120 kDa, while it is cleaved into two fragments under reducing conditions. The N-terminal fragment (B-NTF) at 70 kDa and the juxtamembrane region (B-JXT) at 50 kDa.

In the following, western blots of VEGFR3 and BACE2 transfected HEK293-T are shown (Fig. 08A-B). Smeary or several bands at expected heights can be attributed to differential glycosylation (Fig. 08C), which are most likely artifacts due to the abnormal high expression levels and/or the serum free cell culture conditions, during the transient transfection process. As a lot of the expressed VEGFR3 was still in the immature form, the use of reducing conditions resulted in a mixed band pattern, deriving from immature and mature VEGFR3. N-terminal HA and C-terminal FLAG tags were used for additional visualization with independent antibodies to distinguish between N- and C-terminal cleavage products.

Control (Ctrl) and BACE2 (B2)

As expected due to low endogenous levels, no VEGFR3 and BACE2 was detectable in the control transfected cell lysates or medium (Fig. 08A-B), while respective bands were visible in the lysates of VEGFR3 and BACE2 transfected cells (Fig 08A). Note, that BACE2 bands are not overexposed but in general blurry, in HEK overexpression. The BACE2 size shift upon co-expression with VEGFR3 is not BACE2 specific and can also be seen when co-expressing other BACE substrates (data not shown).

VEGFR3

As already mentioned, strong I-FL bands at 195 kDa were detectable in the VEGFR3 transfected cells via both, the tag antibodies and the ectodomain specific VEGFR3 antibody (Fig. 08A). Additionally, these samples also contain the mature and non-shed form, which can be visualized with the VEGFR3 antibody, yielding the M-Ecto (70 kDa) and M-CTF (125 kDa). The N-terminal HA tag was used to independently detect the M-Ecto fragment, while the C-terminal FLAG tag was used to independently detect the M-CTF fragment. Taken together, the used polyclonal VEGFR3 antibody appears to be specific for the protein of interest and is recognizing sequences on both sides of the disulfide bridge.

Some BACE2 dependent VEGFR3 bands are already visible in the medium without co-overexpression of BACE2 (Fig. 08B), showing that some degree of cleavage by other proteases or secretion of excess protein may occur in VEGFR3 overexpression conditions. Using the VEGFR3 antibody, detectable bands include the shed immature ectodomain (I-Ecto), which was detected at a higher than expected height of ~140 kDa and the B-NTF (70 kDa) and the B-JXT (50 kDa) fragments. Consistently, with the N-terminal location of the HA tags, the HA antibody does not detect the B-JXT (50 kDa) fragment.

VEGFR3 + BACE2

With additional co-expression of BACE2, the band pattern changes in a consistent manner (Fig. 08A-B). Due to the processing by BACE2, the I-FL lysate band and its products are notably weaker than in the VEGFR3 only condition and instead bands for B-Ecto and B-CTF become visible. The lack of M-CTF and M-Ecto bands under these conditions suggest very low levels of remaining mature VEGFR3 in the lysates, indicating extensive processing by BACE2. Complementary to the lysates, the shedding

products I-Ecto and also the mature form derived B-NTF and B-JXT are notably stronger in the cell culture medium than without BACE2 co-transfection (Fig. 08B). Again, the B-JXT fragment is not detected with the HA-tag antibody.

Glycosylation

Most of the fragment sizes like M-Ecto and B-CTF differ notably from expected weights according to the amino acid sequence and/or show multiple bands (Fig. 08A). After additional processing with the de-glycosylating enzyme PNGaseF (Fig. 08C), these bands are shifting and merging to the expected theoretical weights of the amino acid sequences. For example, the M-CTF is yielding two bands in the VEGFR3 transfected lysates (Fig. 08A), one of which is running at a molecular weight of 140 kDa, instead of the expected 125 kDa. After de-glycosylation (Fig. 08C) only one band is remaining at the height of 125 kDa, suggesting a glycosylation dependent effect. Accordingly, all size shifts and multiple bands can be attributed to differential glycosylation except for the B-CTF FLAG double band in VEGFR3/BACE2 co-expression. For the B-CTF double band, it is therefore possible that BACE2 is able to cleave VEGFR3 at several closely located positions in the juxtamembrane, similarly to the generation of two C-terminal APP fragments after BACE1 and BACE2 cleavage[70].

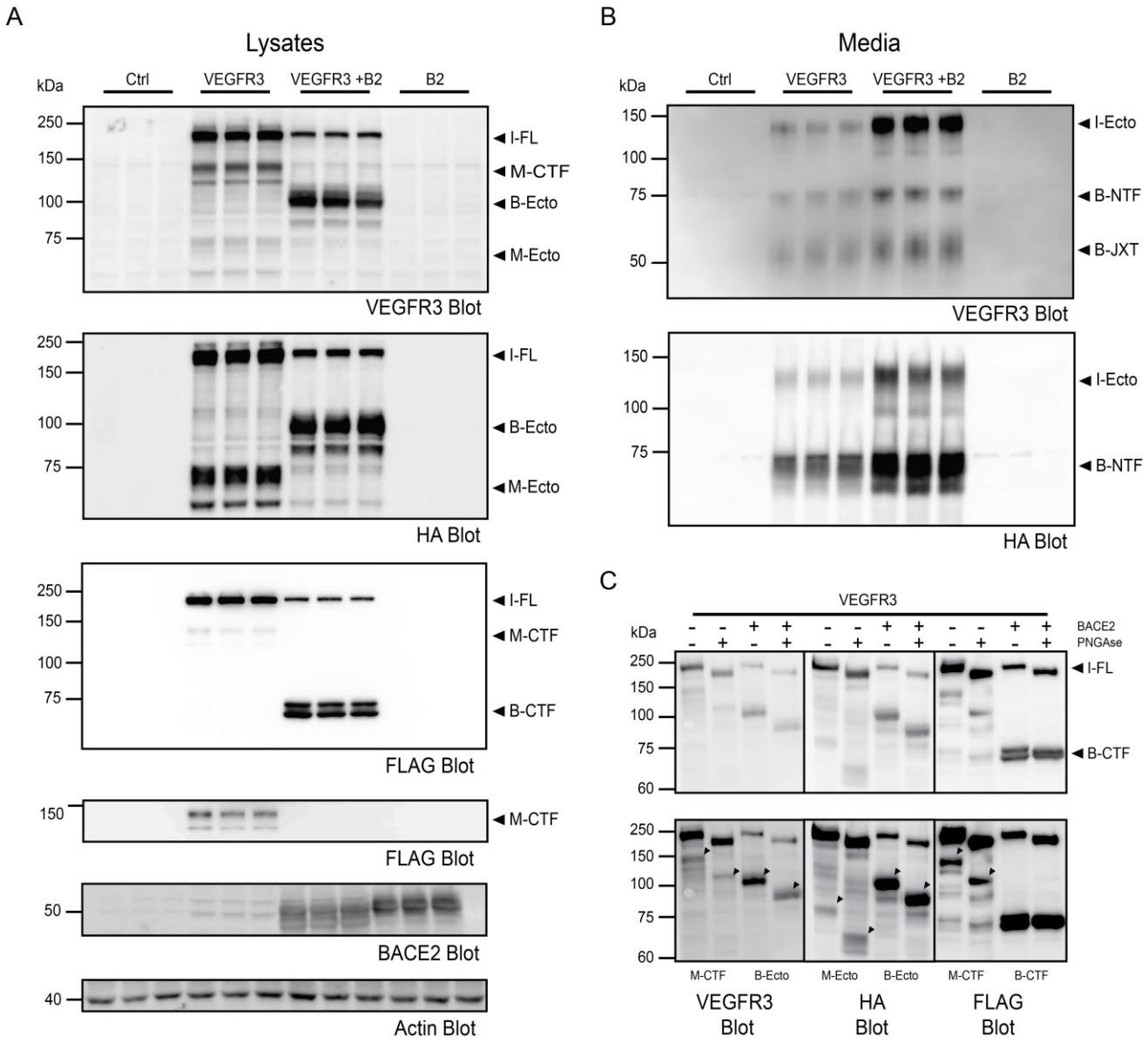

Figure 08. Shedding of VEGFR3 in a HEK293-T overexpression system. Blots of HEK293-T cells, transfected with empty control plasmids (Ctrl), *Bace2* (B2), *Flt4* (VEGFR3) and *Flt4* + *Bace2* (VEGFR3 + B2). **(A)** Lysate blots for VEGFR3, HA tag, FLAG tag, BACE2 and Actin. The FLAG blot for M-CTF is additionally shown with a stronger exposure to visualize the bands. **(B)** Cell culture media blots for VEGFR3 and HA tag. **(C)** Cell lysate blots with -VEGFR3, HA and FLAG antibodies with (+) and without (-) BACE2/PNGase. Upper panel: Best exposure for visualization of I-FL and B-CTF. Lower panel: Higher exposure to visualize M-CTF, M-Ecto and B-Ecto. Arrows indicate the relevant bands before and after size shift. For fragment nomenclature, see figure 07.

4.2.3. Endogenous VEGFR3 processing in lymphatic endothelial cells

While the overexpression in HEK cells showed logically consistent cleavage of VEGFR3 by BACE2, it cannot be excluded, that the cleavage occurs artificially as a result of overexpression conditions. E.g. SEZ6L was validated as a BACE2 specific substrate in pancreatic beta cells[56], but a BACE1 specific substrate in neurons[38]. Consequently, BACE2 may be able to also process physiological non-substrates upon co-overexpression.

Consequently, the human lymphatic endothelial cell (LEC) line HMVECdLYAd, which endogenously expresses both, VEGFR3 and BACE2 was included, to confirm BACE2 cleavage in endogenous

conditions. First, the specificity of detected VEGFR3 bands was demonstrated via siRNA mediated knockdown of VEGFR3.

Afterwards, the two independent unselective BACE inhibitors C3 (ß secretase inhibitor IV) and Verubecestat were used to confirm BACE dependency (Fig. 09A-B). In this thesis, mostly Verubecestat was administered across various experiments, as Verubecestat is the most potent commercially available BACE2 inhibitor (1.5.). siRNA mediated knockdown of BACE1 or BACE2 was further applied to confirm BACE2 specificity (Fig. 09C-D). Hereafter, all medium samples were diluted in non-reducing loading buffer, since reduction of VEGFR3 rendered the ectodomain undetectable (Fig. 09B).

In contrast to HEK293-T (Fig. 09A-B), LECs allowed for detection of endogenous levels of VEGFR3 in lysates and media (Fig. 09). As already described[145], the glycosylated and unglycosylated form of the immature full-length protein (195 kDa and 175 kDa) and the M-CTF band of the mature protein at ~125 kDa are detected in lysates. On the other hand, blots of cell culture media represent the B-Ecto fragment. As expected, the knockdown of VEGFR3 almost abolished all of the mentioned VEGFR3 specific bands.

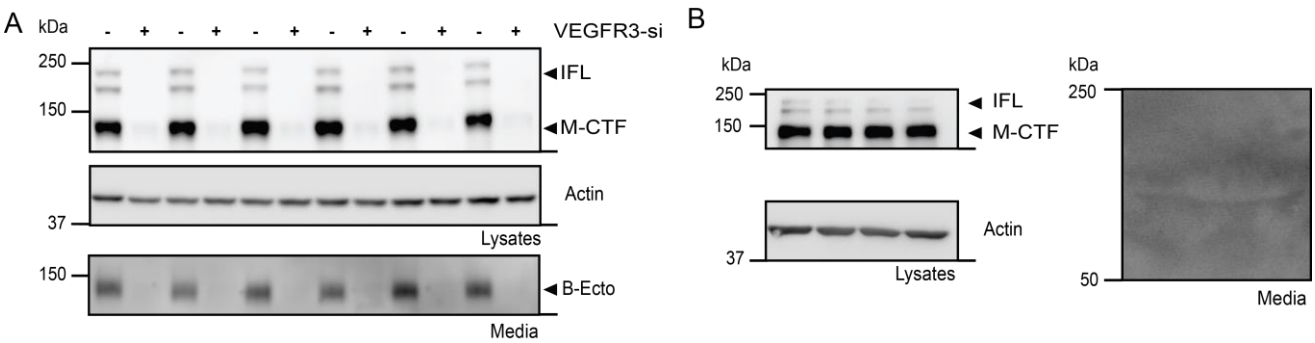

Figure 09. Detection of endogenous VEGFR3 in LECs. (A) *Flt4* silenced LEC lysates and media (n=6). **(B)** Example for detectable bands in lysates and media when only using reducing conditions. Untreated lysates were blotted for VEGFR3 (M-CTF), BACE1/2 and Actin. Untreated cell culture media were blotted for VEGFR3 (B-Ecto) (n=4).

Additionally to VEGFR3, LECs also allowed for detection of endogenous levels BACE2 and BACE1 (Fig. 10A-D), which were also not be immunologically detectable in HEK293-T cells. Consequently, LECs are a valid cell culture system to observe VEGFR3 cleavage in regards to BACE proteases. Application of both BACE inhibitors confirmed the dependency of VEGFR3 cleavage by BACE (Fig. 10A-B) and resulted in an accumulation of ~125% of full-length VEGFR3 in the lysates, compared to DMSO treated control lysates. Complementary, VEGFR3 in cell culture supernatants decreased to ~50%. Silencing of BACE proteases showed specific dependency of VEGFR3 on *BACE2*, as *BACE1* silencing did not influence VEGFR3 levels in lysates or media (Fig. 10C), while *BACE2* silencing reproduced the effect of pharmacological BACE inhibition and led to an accumulation of lysate VEGFR3 to ~125% and to a reduction of medium VEGFR3 to ~50% (Fig. 10D).

Despite their similar size, it is unlikely, that M-CTF contaminations in the medium are falsely assumed as B-Ecto fragments, since reducing conditions do not allow the detection of the B-Ecto in the medium, while the lysate M-CTF band remains unaffected. Additionally, described bands changed consistently

as expected for the fragments when impairing BACE cleavage, i.e. increasing abundance in lysates and decreasing abundance in media. This effect would not be observable in M-CTF contaminated media samples.

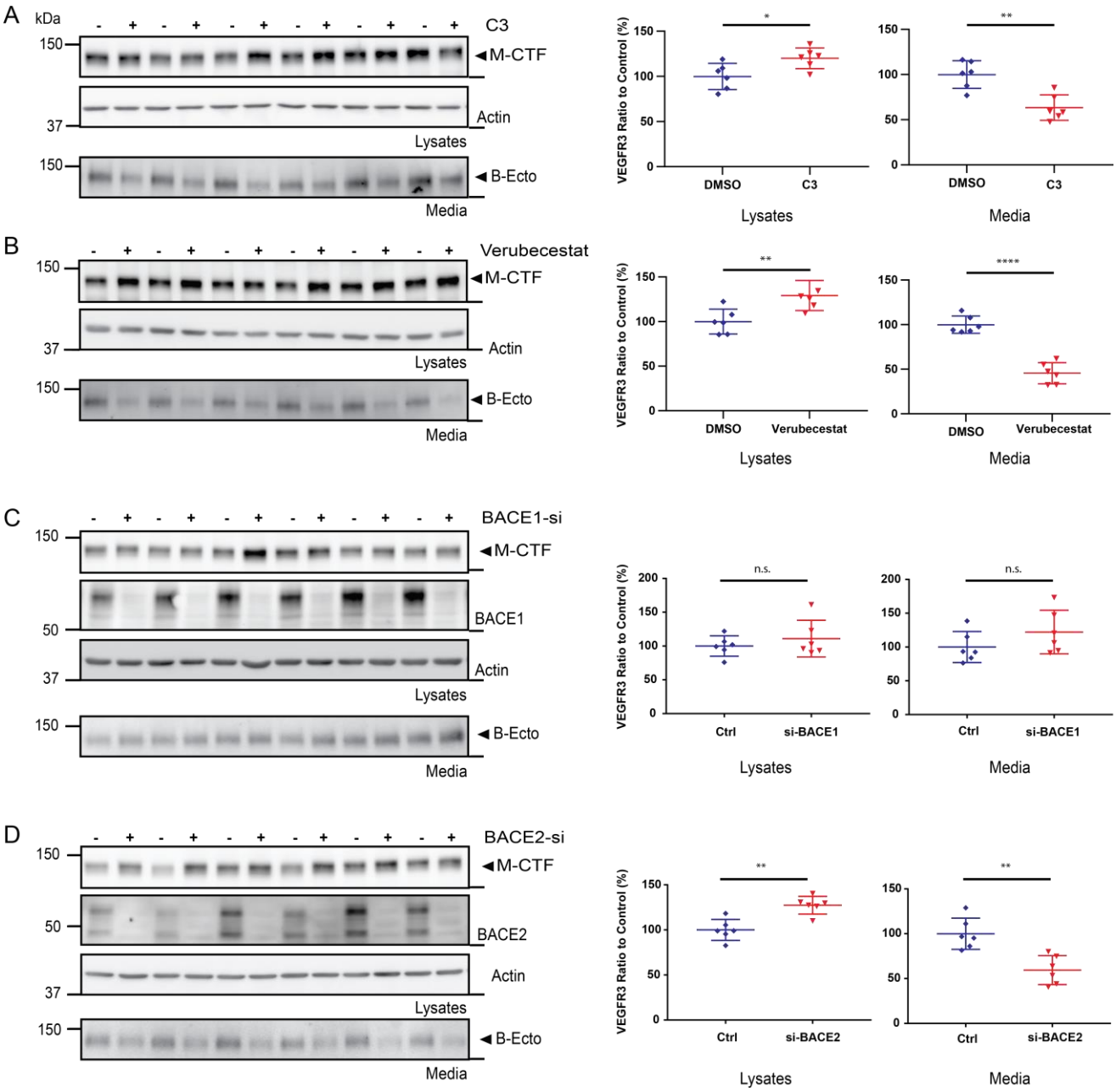

Figure 10. Endogenous processing of VEGFR3 in LECs. Left column: Blots of **(A)** C3 treated **(B)** Verubecestat treated, **(C)** *BACE1* silenced and **(D)** *BACE2* silenced HMVEC lysates and media. Lysates were blotted for VEGFR3 (M-CTF), BACE1/2 and Actin. Media were blotted for VEGFR3 (B-Ecto). For fragment nomenclature, see Figure 07. Right column: Corresponding densiometric quantifications were performed on M-CTF and B-Ecto. (n.s. non significant, * p< 0.05, ** p= 0.01, **** p< 0.0001, Welch's t-test, n=6).

4.2.4. Enzymatic cleavage behavior of VEGFR3 by BACE2

To further validate the specificity of VEGFR3 cleavage by BACE2, additional *in vitro* assays were conducted by our collaborators Janssen Pharmaceutica. Experimental workflows and used compounds are the same as described for the analysis of SEZ6[38]. On the one hand recombinant BACE1 and BACE2 were incubated with synthetic peptides for human WT APP and VEGFR3, respectively, which release a fluorescent signal after cleavage. The results show decreasing fluorescence signal intensity upon BACE inhibition related to reduced enzymatic activity (Fig. 11A-C, continuous lines). For the cellular assays, media supernatants from SK-N-BE cells, expressing APP and Min6 cells expressing VEGFR3 were analyzed via ELISA, which detect the BACE dependent cleavage products Aß42 or VEGFR3. Respective substrate levels were monitored upon BACE inhibition (Fig. 11A-C, dotted lines).

As expected, the application of an unselective BACE inhibitor (Pfizer, JNJ-63605776/Compound 4[150]) led to a similarly decreased turnover of both, the BACE1 preferred APP substrate and the supposedly BACE2 specific VEGFR3 substrate (Fig. 11A). Consistently, the complete activity loss for both substrate cleavages was achieved at similar drug concentrations for all the assays. When applying a marginally BACE1 selective inhibitor (Wyeth, JNJ-63916905/S-38[151]), the activity curves for VEGFR3 cleavage already shifted to higher concentrations in contrast to the BACE1 dependent Aß42 generation activity curve (Fig. 11B). Last, the application of a rather BACE1 selective compound (Janssen/Shionogi, JNJ-64489737[152]) led again to a complete abolition of BACE1 cleavage, while VEGFR3 cleavage by BACE2 remains unaffected until very high concentrations of the inhibitor, which are able to block BACE2. This effect was only observable in the *in vitro* cleavage assay, as the excessive required inhibitor concentration for cellular BACE2 inactivation was not feasible (Fig. 11C). Taken together, BACE1 selective inhibitors do not alter VEGFR3 turnover at concentrations, which sufficiently inhibit BACE1, while decreasing BACE1 selectivity increases the turnover of VEGFR3. These observations further support the assumption of BACE2 specificity for VEGFR3 cleavage using a different experimental approach.

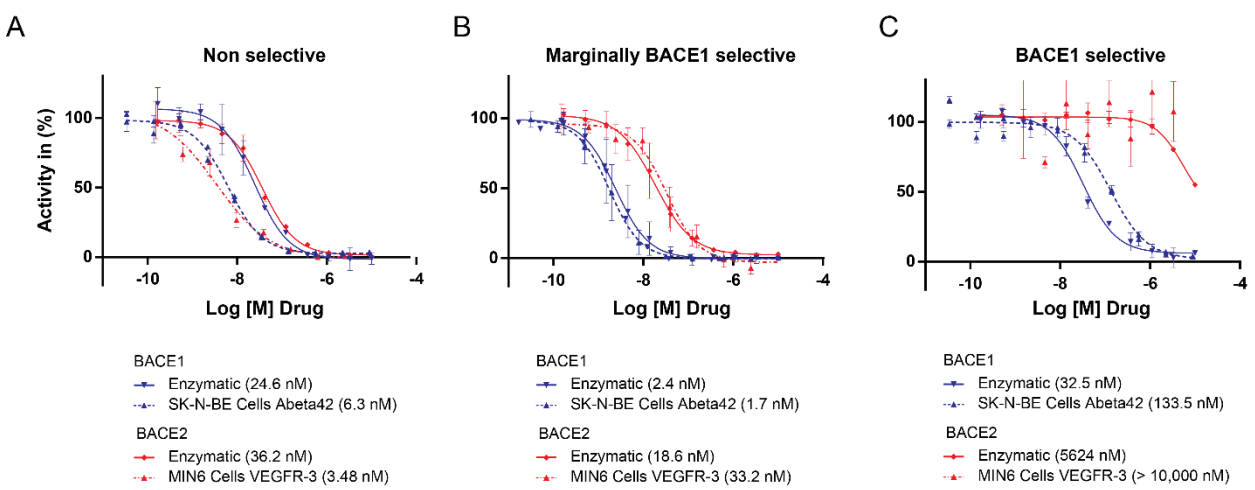

Figure 11. BACE activity curves for Aß42 and VEGFR3 cleavage upon application of inhibitors with different selectivity. Application of **(A)** an unselective **(B)** a marginally BACE1 selective and **(C)** a BACE1 selective compound. Blue lines indicate turnover of the BACE1 specific Aß42 substrate and red lines the turnover of the suggested BACE2 specific VEGFR3. Continuous lines represent the enzymatic fluorescent assays and pointed lines the cell culture ELISA assays. Data represents biological duplicates with two technical replicates. Brackets indicate the deriving IC50 values for given inhibitors in these assays.

4.2.5. VEGFR3 ectodomain sequencing and BACE2 cleavage site determination

Only a few BACE2 substrates are known and bioinformatic analysis of the BACE2 cleavage site on its respective substrates may help to identify additional putative substrates via screening of databases for transmembrane type 1 or GPI anchored proteins with similar amino acid sequences or with similar biochemical behavior, like e.g. hydrophobicity and the related structural features. In order to contribute to available BACE2 cleavage site sequences, a cellular cleavage assay was conducted for murine VEGFR3 and the shed ectodomain was sequenced via mass spectrometry. Briefly, Min6 cells were stably transfected with murine VEGFR3 and the shed ectodomain containing supernatant was collected, concentrated and immuno-precipitated for VEGFR3. Due to the high homology to BACE1, BACE2 is expected to cleave near the plasma membrane within the juxtamembrane region[38,58]. In analogy to BACE1, BACE2 might preferably cleave C-terminal of leucine or other hydrophobic amino acids[153] Therefore, the cleavage site was expected to be located within the KGCVNSSASVAVEGSEDKGSME juxtamembrane sequence, with the highest probability for the hydrophobic VAV area. Since uniprot reports a N-glycosylation site at Asn758 of this sequence based on the consensus sequence NXS/T (X all amino acids except for proline), which may interfere with the downstream proteolytic digestion for mass spectrometric sequencing, the shed ectodomain was additionally de-glycosylated prior to mass spectrometric sample preparation. Additionally, the individual bands from immunoprecipitation were sequenced in order to further confirm the in 4.2.2. described band pattern of VEGFR3 cleavage products. To these ends purified protein was either separated by SDS-PAGE, followed by in gel digestion using trypsin (cleavage product identification), or the immunoprecipitated ectodomain was subjected to SP3 digestion using the enzymes LysC, Trypsin and LysN (cleavage site determination).

Various amounts of eluted and deglycosylated samples were separated on a polyacrylamide gel and MS analysis after in gel digestion confirmed successful sample processing (Fig. 12A). Note, that the monoclonal AFL4 antibody was used for detection, which epitope was mapped within the region from E491-D525[154] and therefore binds below the sulfur bridge. Consequently, AFL4 is only able to detect the I-Ecto (95kDa) and B-JXT (34kDa) bands, while B-Ecto (53KDa) is not detectable. After gel fractionation and in-gel digestion with indicated fractions, only VEGFR3 was detectable in any of the fractions, considering peptides with scores > 20 and notable raw intensities above 1.0^9 (not shown). Due to the high sensitivity of current mass spectrometers, traces of any observed peptide can be found in almost all of the fractions. This can also be due to minimal sample carry-over between individual LC-MS/MS analyses. When however analyzing peptide intensity distribution of the 10 peptides with the highest intensity and a score > 20 across the fractions, peptides are mapped onto the expected fractions (Fig. 12B). While e.g. the B-JXT located YLSVQALEAPR peptide was identified with the highest intensity in the predicted B-JXT fraction F05, the B-Ecto located GPVLEATAGDELVKLPVK peptide displayed the highest abundance in the predicted B-Ecto fraction F04. In contrast, the predicted I-FL fraction F03 contained peptides with similar ion intensities from all over the ectodomain, thereby supporting the presence of a non-reducible fragment (Fig. 12C).

Taken together, the shed VEGFR3 ectodomain was successfully purified and processed from Min6 medium. While no absolute quantification was performed, the mass spectrometric sequencing of detected and expected VEGFR3 bands still further supported the identity of in 4.2.2. described medium fragments, which display a similar pattern behavior (i.e. three bands, consisting of I-Ecto, B-Ecto and B-JXT).

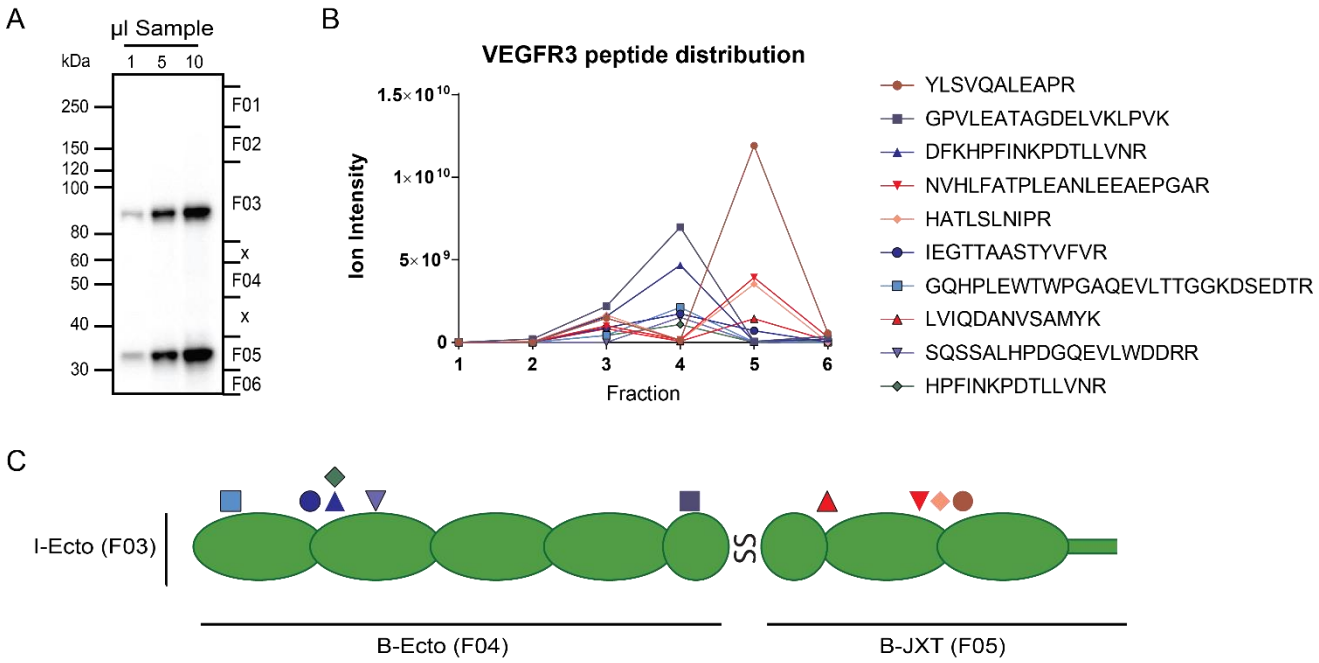

Figure 12. VEGFR3 Ectodomain sequencing. (A) Control blot including standard dilution of recombinant VEGFR3 (left side) and VEGFR3 sample after IP and deglycosylation (right side). Approximate depiction of the digested gel fractionations Fraction 01 (F01) - Fraction 06 (F06) and omitted parts (x) is included. **(B)** Distribution of the 10 VEGFR3 peptides with the highest raw intensity among indicated fractions. The peptide list is ordered dependent on their respective intensities (highest to lowest). **(C)** Theoretical location of the 10 depicted peptides, based on the AA sequence of the VEGFR3 ectodomain. Peptides with highest intensity in the B-Ecto fraction F04 are depicted in the blue color spectrum and peptides with highest intensity in the B-JXT fraction are depicted in the red color spectrum.

To identify the potential cleavage site of VEGFR3 by BACE2, a database search of the MS data was performed, which allows for semi-specifically cleaved peptides. The semi-specific peptide bears one terminus, derived from the cleavage of the applied protease such as trypsin, LysN, or LysC, whereas the other terminus derives from another cleavage event, such as the cleavage via BACE2. Sequencing with different proteases, revealed KGCVDSSASVA (N to D conversion due to deglycosylation with PNGaseF) as the last semi-specific identifiable peptide using LysN (cleavage N-terminal of lysine/K) digestion (Fig. 13A, marked in yellow), suggesting the cleavage site between Alanine764 and Valine765 (Fig. 13A, indicated via | |). As expected for a BACE substrate, the proposed cleavage site is located close to the transmembrane region (Fig. 13A, marked in grey). This peptide could only be identified with LysN, as the other used proteases cleave C-terminally of Lysine, thereby resulting in a peptide without a basic amino acid, which has a poor ionization efficiency and therefore was not detectable. Fragmentation of the KGCVDSSASVA peptide leads to a partially complete series of y and b fragment ions (Fig. 13B), which was used for its identification. To exclude KGCDNSSASVA as a false positive identification, a synthetic peptide with the same sequence and sample preparation dependent modifications (cysteine carbamidomethylation, free COOH group) was generated and fragmented in the mass spectrometer. In comparison to the biological sample, the synthetic peptide ran at similar retention times (not shown) and the dot product (dotp, similarity score: product peak area and spectral library peak area distributions) determined with the software Skyline, confirmed a very high similarity of the respective fragmentation pattern (dotp=0.98, Fig. 13C), which strongly supports the correct identity of the semi-specific peptide. Furthermore, the high sequence coverage of the shed and purified ectodomain indicates the high sensitivity of the performed sequencing experiment (Fig. 13D) and almost exclusive mapping of detectable peptides to the ectodomain again confirmed the successful

purification without major cellular contaminations. Taken together, KGCVDSSASVA was identified as the last detectable semi specific peptide and its identity was confirmed via spectra comparison against an identical synthetic peptide. Therefore, the BACE2 cleavage site is likely localized between Alanine764 and Valine765.

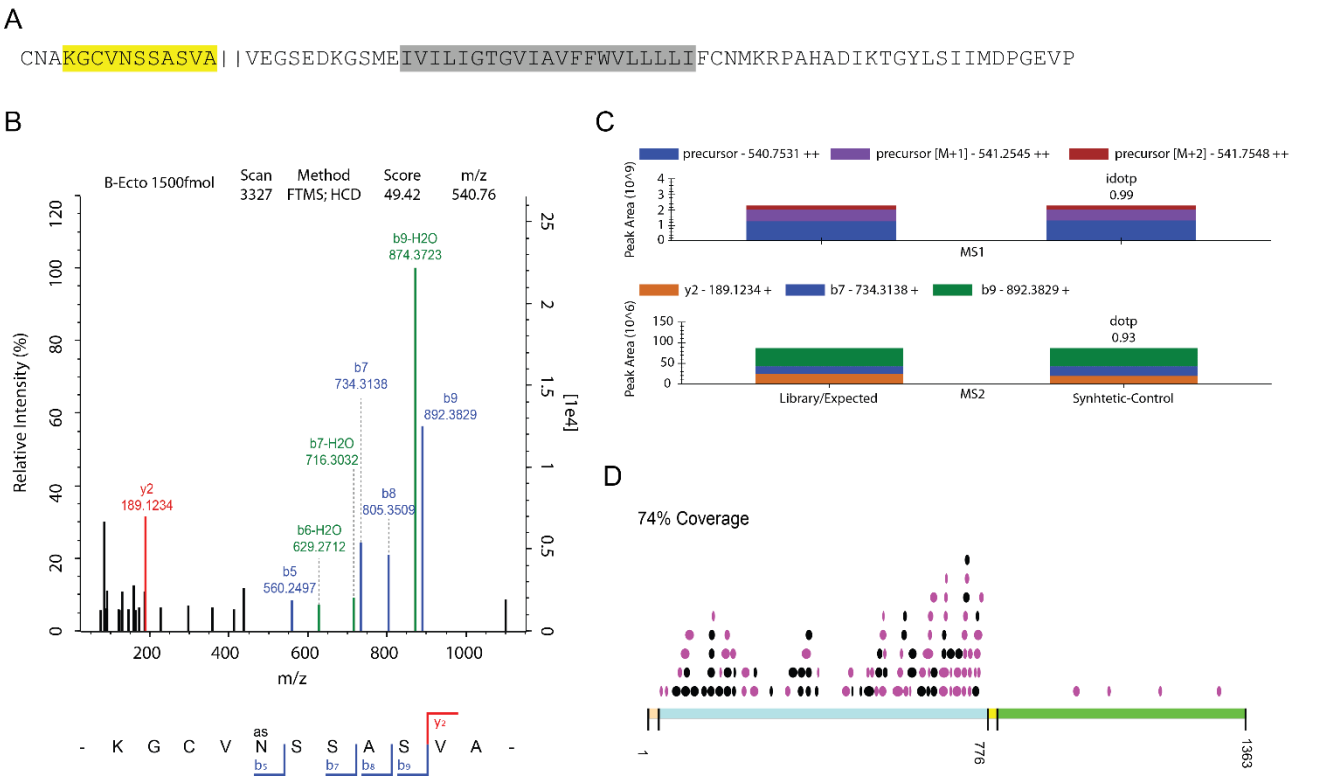

Figure 13. BACE2 cleavage site on murine VEGFR3. (A) Segment of the murine VEGFR3 sequence, close to the plasmamembrane. The identified semi specific peptide after LysN digestion was marked in yellow, the proposed cleavage site with || and the transmembrane region in grey. The sequence is depicted from N- to C-terminus. **(B)** MS2 fragment ion spectrum of the identified KGCVDSSASVA peptide. y- ions are indicated in red, b-ions in blue and neutral losses in green. Background signals are shown in black. The two y-axes depict the ion intensity in % (left) and absolute (right), while the x-axis depicts m/z values. The fragment ions are indicated in the peptide sequence below. **(C)** Comparison of the identified peptide (library/expected peptide and fragments) with a synthetic peptide of the same sequence and modifications (synthetic control). Colors indicate the distribution of different precursor isotopes and fragment ions. Distribution similarities are indicated via (i)dotp values. **(D)** Localization of identified individual peptides (black and purple dots) on the VEGFR3 sequence. The ectodomain is indicated in blue, the intracellular domain in green and the signal-peptide and transmembrane domain are indicated in yellow. All identified peptides are depicted in black and purple (additionally predicted as luminal localization) dots, which sizes reflect the lengths of identified peptides. For better distinction, dots are depicted in several rows.

4.3. SEZ6L and VEGFR3 as *in vivo* blood plasma biomarker for BACE activity

After the successful *in vitro* validation of VEGFR3 as a BACE2 dependent substrate, it was essential to further evaluate its applicability as a BACE2 activity biomarker under *in vivo* conditions. Therefore, WT, BACE1KO and BACE2KO mice were treated for different durations with the unselective inhibitor Verubecestat and plasma VEGFR3 levels were monitored (Fig. 14A-C). Additionally, the already validated BACE1 specific substrate SEZ6L[38] was included as a marker for BACE1. At last, the sensitivity and variance of plasma VEGFR3 levels were compared to the current method of choice for the monitoring of BACE2 activity (Fig. 15A-C): The depigmentation status of compound treated mice.

4.3.1. Validation of murine SEZ6L and VEGFR3 in mice

B1KO (8-12 months old), B2KO (3-6 months old) and respective C57Bl/6 WT wild type mice were dosed for 3 days with 50 mpk of Verubecestat and plasma VEGFR3 and SEZ6L levels were determined via MSD ELISA (Fig. 14A-C). An additional 7-day time course study using a 0.1% w/w Verubecestat diet on 6-week-old C57Bl/6 WT mice was performed in order to monitor time dependent biomarker decline towards basal levels.

Plasma VEGFR3

Here, a Verubecestat treatment of BACE1 and BACE2 KO mice and their related WT control mice was performed for 3 days. Note, that plasma VEGFR3 levels of BACE2 KO compared to WT mice were slightly higher than in the initial discovery experiment (4.1. ,25% vs. 20%) which might result from a different mouse facility housing of the animals. In WT and BACE1 KO mice treated with Verubecestat, plasma VEGFR3 levels were significantly reduced to ~60% of vehicle treated control mice. (Fig. 14A). This dependency of Verubecestat decrease on the genotype is additionally shown by the statistical interaction parameter for B2KO (i.e. dosing dependent significance is dependent on the presence of BACE2), which is absent when analyzing the B1KO data (i.e. significance is not dependent on the presence BACE1). As VEGFR3 levels of Verubecestat treated mice were notably higher than those of B2KO mice (Fig. 14A), an additional dosing experiment with 7 days of daily dosing with a 0.1% w/w diet of Verubecestat using WT mice was performed, to ensure that the in BACE2 KO observed decrease of ~25% can also be achieved via BACE2 inhibition (Fig. 14C). This time series experiment already showed significant plasma VEGFR3 reduction to ~75% after 1 day of treatment, ~50% after 3 days and finally 25% after 7 days, which is similar to the levels of B2KO mice.

Plasma SEZ6L

SEZ6L is almost exclusively cleaved by BACE1 in the CNS, whereas it can also be cleaved by BACE2 in other organs, such as the pancreas[38,56]. In contrast to VEGFR3, plasma SEZ6L reduction was not visible in the plasma of B2KO mice and only decreased in B1KO compared to WT (~20- 25%) (Fig. 14B). In line with this, Verubecestat treatment did not lead to a further plasma SEZ6L decrease in B1KO mice, while significantly decreasing plasma SEZ6L levels in B2KO mice and the wild type controls to ~50% in comparison to control levels. Accordingly, the statistical interaction parameter is only significant for B1KO (dosing dependent significance is dependent on the presence of BACE1), but not dependent on the *Bace2* KO (dosing dependent significance is not dependent on the presence of BACE2). Observation of plasma SEZ6L during the 7 days of dosing (Fig. 14C) confirmed observed SEZ6L levels after 3 days of dosing and revealed a similar time dependent decrease like plasma VEGFR3, with SEZ6L appearing to be slightly more responsive. Therefore, plasma SEZ6L is an indicator for BACE1 activity.

Brain Aß1-40 and SEZ6L

Since SEZ6L was chosen as a putative BACE1 activity plasma biomarker, its soluble brain levels were also monitored in the time course experiments. Therefore, brains were homogenized using DEA fractionation and membranes containing cellular SEZ6Lwere removed by centrifugation. The timeline data for sSEZ6L levels in brain (Fig. 14D) confirmed successful inhibition of BACE1, by displaying strong and significant reductions of Aß1-40, already 1 day after Verubecestat dosing. SEZ6L, which was already validated as a BACE1 specific substrate in the CNS, also displayed a significant reduction, although it reacted less sensitive than Aß1-40 and reached its maximal reduction only after 3 days of treatment. The weaker observed reduction of SEZ6L might be a technical artifact due to insufficient removal of full length SEZ6L during the fractionation process or the result of a longer half-life.

Taken together, plasma VEGFR3 was confirmed as a promising *in vivo* biomarker for BACE2 activity in mice, while BACE1 may be monitored *in vivo* via plasma SEZ6L levels. Both biomarker show a similar sensitivity and similar reductions in the performed experiment with Verubecestat.

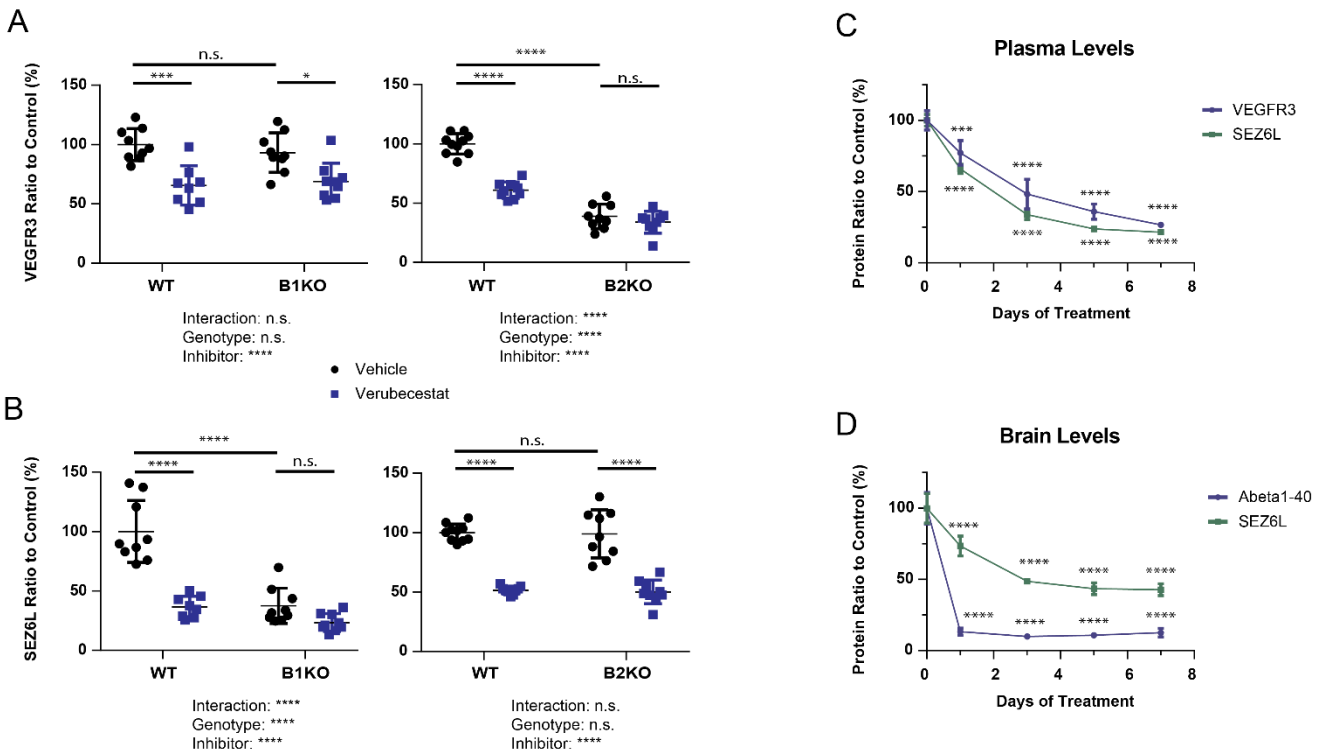

Figure 14. *In vivo* monitoring of BACE activity via ELISA. (A-B) Plasma VEGFR3 **(A)** and plasma SEZ6L **(B)** levels in B1KO, B2KO and respective WT mice with (blue) and without (black) 3 days of Verubecestat dosing. (two-way ANOVA, followed by Bonferroni's multiple comparison test, n=9-10) **(C)** Plasma levels of VEGFR3 and SEZ6L and **(D)** brain levels of Aß1-40 and SEZ6L during 7 days of daily Verubecestat dosing in WT mice. One way ANOVA with p< 0.0001, followed by Bonferroni's multiple comparison test against control baseline levels, n=5-6).- (n.s. non significant, * p< 0.05, *** p= 0.0001, **** p=0.0001).

4.3.2. Comparison of plasma VEGFR3 to the established fur pigmentation assay for BACE2 activity

Next, plasma VEGFR3 levels were measured in C57Bl/6 WT mice, which were treated for 21 days with a vehicle diet, or a diet, containing 0.002 or 0.1% (w/w) Verubecestat (Fig. 15A-B). Obtained results were further compared to the currently established BACE2 activity assay, based on fur pigmentation (Fig. 15C). To assess changes in fur pigmentation, mice were depilated using Veet facial wax on the first day of dosing onset and the pigmentation of newly grown hair was assessed. To control for successful on target BACE1 inhibition, Aß1-40 and SEZ6L were monitored in the soluble fraction of the brain.

Soluble Aß1-40 and SEZ6L brain levels both confirmed successful BACE1 inhibition due to strong decreases at 0.1% Verubecestat dosing. While Aß1-40 showed more prominent decreases than SEZ6L, only the latter one was able to reflect BACE activity changes at the lower 0.002 % dosing concentrations. Furthermore, plasma SEZ6L showed an even stronger sensitivity towards BACE inhibition with a strong reduction at already 0.002% Verubecestat diet (Fig. 15B). Consequently, plasma SEZ6L appeared to be a more sensitive and better accessible readout for BACE1 inhibition. When monitoring for BACE2 activity via plasma VEGFR3 level, a strong reduction was already detected at 0.002% Verubecestat diet, which decreased to basal levels at 0.1% Verubecestat diet (Fig. 15B), further demonstrating the high sensitivity of the VEGFR3 readout.

Analysis of the current BACE2 activity biomarker (i.e. fur pigmentation) on the same mice, showed a clear reduction of pigmentation at 0.1% Verubecestat diet (Fig. 15C), but variable results were obtained with 0.002% Verubecestat diet. At theses doses, plasma VEGFR3 is already strongly decreased and showed less variance (Fig. 15B), indicating superior performance of plasma VEGFR3 over fur pigmentation. While the pigmentation status may be quantified vie the extraction of melanin[80], corresponding samples were not available.

Taken together, the data indicated successful inhibition of both BACE proteases and validate plasma SEZ6L and plasma VEGFR3 as promising BACE1 and BACE2 biomarkers. The VEGFR3 plasma biomarker has the advantage to avoid the painful waxing of laboratory animals. Additionally, VEGFR3 might also be suitable to monitor BACE2 inhibition in the plasma of human clinical trial participants. Complementary for BACE1, the application of plasma SEZ6L as a biomarker for BACE1 activity might also avoid invasive CSF sampling.

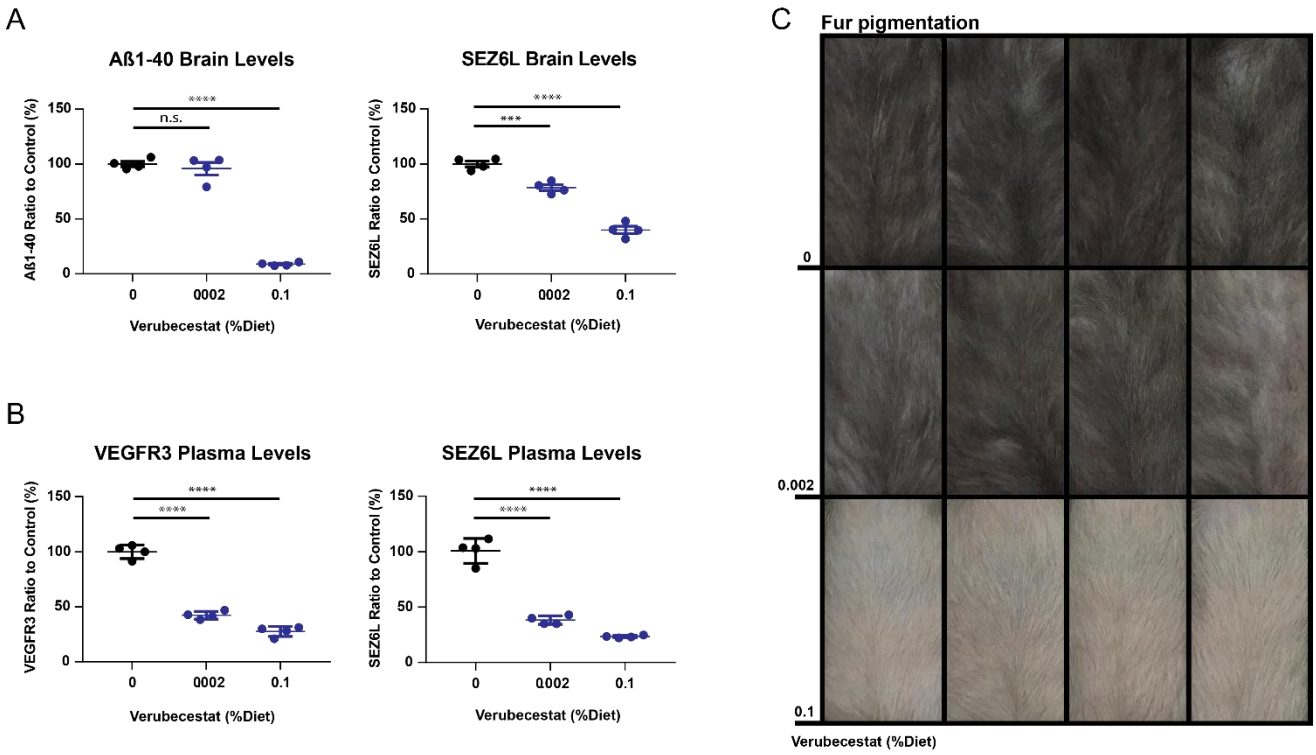

Figure 15. ***In vivo*** **monitoring of BACE activity via ELISA. (A)** Brain Aß1-40 and SEZ6L levels **(B)** Plasma VEGFR3 and SEZ6L levels in mice, fed with diet, supplemented with 0 (black), 0.002 and 0.1 % of Verubecestat (blue) (one-way ANOVA with p< 0.0001, followed by Bonferroni's multiple comparison test, n=4, n.s. non significant, *** p= 0.0001, **** p< 0.0001). **(C)** Pictures of the fur pigmentation of the same mice.

4.4. Processing of VEGFR3 in non-human primates and human patients

Results, obtained in experiments with mice are not always transferable to humans. Therefore, blood plasma samples from non human primates (NHP) and human study participants were collected before and after dosing with unspecific BACE inhibitors and subjected to proteomics. Herein, NHP received daily doses of 10 mpk Verubecestat for 7 days, while the human plasma samples derive from a 28 days, 50mg Atabecestat trial.[122] Plasma VEGFR3 levels were determined on the last day of dosing and compared to pre- dosing levels. Due to chronological and logistical reasons, NHP values derive from mass spectrometric measurements, while human levels of VEGFR3 were obtained via ELISA.

A significant reduction of plasma VEGFR3 was observed in both experiments, with an average reduction of NHP plasma VEGFR3 to 60 % (Fig. 16A-B) and human plasma VEGFR3 to 75% in comparison to pre dosing levels (Fig. 16C). Furthermore, the used mass spectrometric workflow, also allowed the straightforward detection of 406 plasma proteins and several already known BACE1 substrates, like *CHL1*, Podocalyxin-like protein 2 (*PODXL2*), Interleukin-6 receptor subunit beta (*IL6ST*) and CD166 antigen (*ALCAM*). Note however, that obtained identifications in plasma are still very shallow in comparison to e.g. CSF or lysate measurements, which negatively affects statistical significance in multiple hypothesis corrections. As a consequence all hits of interest are insignificant, when applying e.g. Bonferroni's multiple hypothesis correction and any result is in need of an independent validation method like ELISA.

While the validity of the results is limited by its small sample size, these results strongly indicate a transferability of BACE2 dependent plasma VEGFR3 levels to the NHP and human system. *SEZ6L* was not detectable by mass spectrometry and ELISAs were not sensitive enough to detect it in the plasma. Given the high transferability of human primate research to the human systems, it seems likely that detected alterations may also occur in humans[155,156]. A higher number of identifications and lower variance can be expected, when a higher number of biological replicates and corresponding vehicle controls for normalization were available.

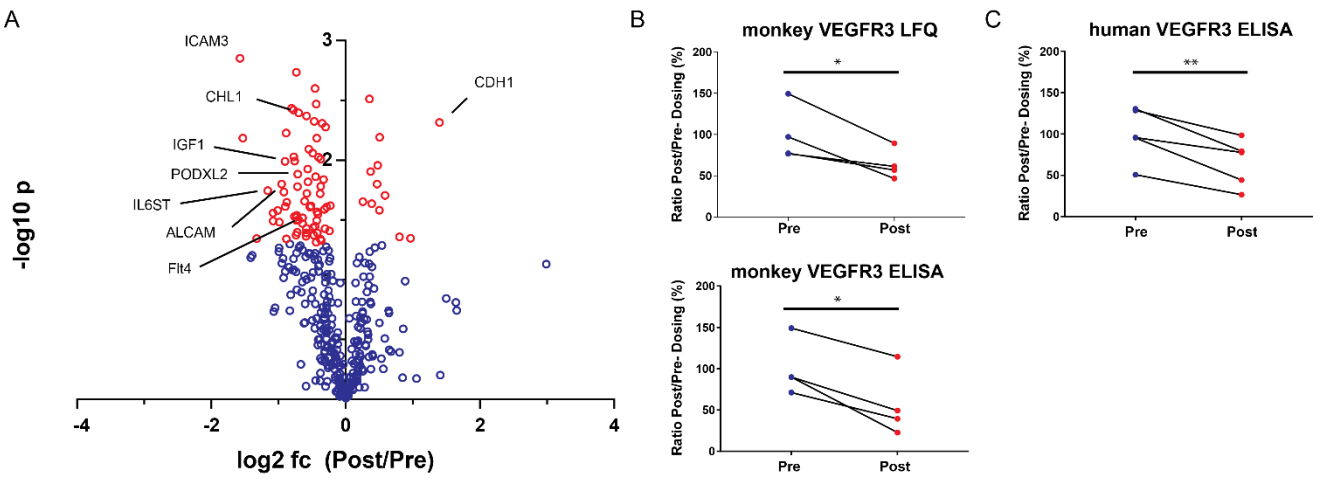

Figure 16. *In vivo* monitoring of NHP and human BACE2 activity via MS and ELISA based VEGFR3 quantification. (A) Volcano plots of proteomic analysis of Atabecestat dosed NHP plasma. The minus log10 transformed t-test p-values are plotted against the log2 transformed label free quantification intensity ratios between post- and pre- dose for each protein. Proteins with a t-test p-value < 0.05 are shown in red circles. Meaningful hits were labelled with their respective gene names. **(B)** Extracted LFQ plasma VEGFR3 (top) and ELISA determined VEGFR3 (bottom) levels in corresponding NHP samples. **(C)** ELISA derived plasma VEGFR3 levels in humans, before (pre) and after (post) application of an unspecific BACE inhibitor. (Paired t-test, * p< 0.05, ** p< 0.01, n=4-5).

4.5. Cellular consequences of decreased VEGFR3 processing

As described in (1.3.), shedding of different identified BACE1 substrates was associated with functional and physiological consequences and also the few identified BACE2 substrates were shown to serve physiological functions, like e.g. the pigmentation. Consequently, altered VEGFR3 processing by BACE2 may also be accompanied by yet unknown functional changes.

Primary lymphatic endothelial cells are one of the few cell types, which show an expression of both BACE2 and VEGFR3 and were chosen for functional analysis. In order to get a first impression about the possibility of functional consequences, cells were analyzed for changes in VEGFR3 associated downstream pathways (4.5.1.) and associated gene expression (4.5.2.) upon BACE2 impairment.

4.5.1. Phosphorylation of downstream pathways

VEGFR3 is a receptor tyrosine kinase, which is capable of auto-phosphorylation and cellular accumulation of VEGFR3 due to decreased BACE2 shedding may therefore result in increased activation and thus downstream signaling. In order to assess possible alterations in this activation, VEGFR3 associated downstream signaling of the AKT and ERK pathways was determined after applying either, Verubecestat, or the VEGFR3 exclusive ligand VEGF-C156S[157] positive control. Indicated mutated version of VEGF-C was used, as endogenous VEGF-C not only interacts with VEGFR3, but also with VEGFR2 or VEGFR2-VEGFR3 heterodimers[158]. For this purpose, LEC cells were treated with those compounds for different periods and Western blotting for total and phosphorylated AKT as well as ERK was performed in order to monitor the VEGFR3 downstream signaling.

AKT, as well as ERK were shown to be activated upon application of Verubecestat (Fig. 17A), wherein 40min of Verubecestat dosing induced the strongest overall phosphorylation, when monitoring both, AKT and ERK. This activation appeared similarly strong to the 20 min activation via VEGF-C156S, which was added in a concentration range that is described as half maximal activation in HUVEC cells (see manufacturers data sheet) and should lead to a strong activation. Note, that due to the direct application of VEGF-C, pathway activation was expected to occur at earlier time points, compared to the presumed indirect activation by Verubecestat application. Consequently, different time points were chosen for the screening experiment. Increased signaling did not alter total amounts of ERK and AKT, demonstrating the specificity of increased phosphorylation to monitor signaling activity. VEGFR3 levels in lysates appeared stable across observed dosing durations, however depleted when applying VEGF-C156S for a longer time period of 6 h (Fig. 17B). This replicates enhanced VEGFR3 turnover after strong VEGF-C activation, which is accompanied by receptor endocytosis[159]. Meanwhile, Verubecestat dosing did not lead to notable changes in VEGFR3 lysate levels after 6 h of incubation, but may also enhance VEGFR3 turnover in a less pronounced fashion. Note, that due to the lack of sufficient amounts of the primary LECs, only an initial screening experiment was performed, which could not be repeated with a larger n number and all appropriate controls.

Taken together, it is likely that a decrease of BACE2 dependent VEGFR3 processing may lead to the increased activation of the associated downstream pathways AKT and ERK, which was well visible 40 min after the application of Verubecestat. VEGFC-156S as well as Verubecestat treatment achieved a similar strong activation, while VEGFR3 lysate levels were only affected by VEGFC-156S treatment after 6 h of incubation.

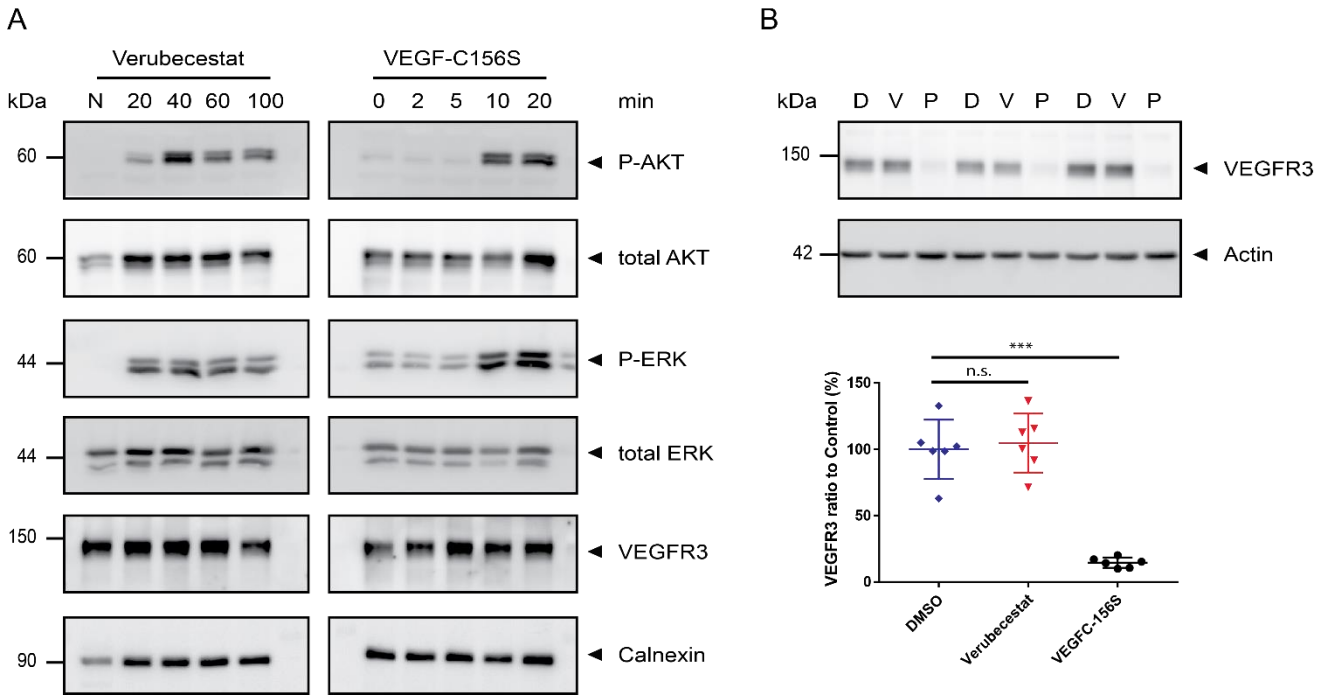

Figure 17. Downstream path activation in LECs. (A) Western blots of Verubecestat and VEGF-C156S treated LECs between 0 and 100 min. A negative control lysate without Phosphatase inhibitors (N) was included. Lysates were blotted for VEGFR3 (M-CTF), Calnexin and phosphorylated AKT/ERK (P-AKT/ERK) and their respective total levels (n=1). **(B)** VEGFR3 Western Blot after 6 h treatment of LECs with DMSO (D), Verubecestat (V) and VEGF-C156S positive control (P). Corresponding densiometric quantifications were performed on M-CTF (one-way ANOVA with $p< 0.0001$, followed by Bonferroni's multiple comparison test, n.s. non significant, ** $p= 0.01$, n=6).

4.5.2. Differential expression of downstream genes

Next, mRNA expression levels of Verubecestat and VEGF-C156S treated LECs were analyzed for the two genes Delta-like 4 (*DLL4*) and Forkhead box protein C2 (*FOXC2*) (Fig. 18), which were already established to be increased in LECs upon VEGF-C156S dependent VEGFR3 activation[160]. DLL4 is the ligand for NOTCH1 and NOTCH4[161], wherein ligand binding negatively regulates cell proliferation and branching during blood vessel formation[162,163]. FOXC2 is involved in lymphatic cellular identity[164] and plays a major role in lymphatic valve formation and therefore proper function of lymphatic vessels [165]. Expression of *FLT4* and the BACE proteases were additionally analyzed for possible effects. Furthermore, pharmacological treatment was performed on cells with a transient knockdown of *BACE1* or *BACE2* in order to exclude BACE independent secondary effects from Verubecestat dosing.

Both of the observed genes displayed a significantly increased expression after treatment with Verubecestat, when comparing to the DMSO control (Fig. 18- left column). The VEGF-C156S positive control was excluded from statistical analysis due to its extreme effects. *DLL4* and *FOXC2* expression more than doubled to 200-250%. While *FLT4* expression remained unaffected from even the VEGF-C156S treatment, *BACE1* expression significantly increased to 150% in respect to the DMSO control and *BACE2* expressions was significantly reduced to 70% after Verubecestat dosing.

When analyzing the combination of transient knockdown and pharmacological dosing, significantly enhanced *DLL4* and *FOXC2* expression was only observed in the siB1+V condition, where BACE2 is still present and can therefore be inhibited (Fig. 18- right column). In the absence of BACE2, no expression changes were inducible via Verubecestat dosing. Note, that the observed gene expression

changes are highly time dependent, as e.g. VEGF-C156S dependent effects have been shown to completely dissolve after 8h of incubation[160]. The transient knockdown for BACE proteases was performed over 24 h and cells were subsequently serum starved for an additional night, before compounds were added. The impairment for notably longer times than in the initially observed 100 min dosing experiment may also lead to other compensatory mechanisms in the siB2 condition, which might explain that no significant effects were detected.

While *FLT4* expression remained again unaffected in all of the conditions, *BACE* mRNA levels confirmed the successful knockdown of both proteases. Last, *BACE1* mRNA levels showed a similar increase to 140% due to Verubecestat treatment (Fig. 18- left column) as well as in response to the siB2 knockdown combined with Verubecestat treatment (Fig. 18- right column).The decrease of Verubecestat dependent *BACE2* expression could not be reproduced, when comparing siB1+ V with control samples.

Taken together, pharmacological impairment of BACE2 via Verubecestat mimicked the upregulation of VEGFR3 dependent gene expression. In combination with transient knockdowns, this phenotype was reproducible in conditions, where BACE2 was still present and presumably BACE2-VEGFR3 dependent changes were therefore still inducible.

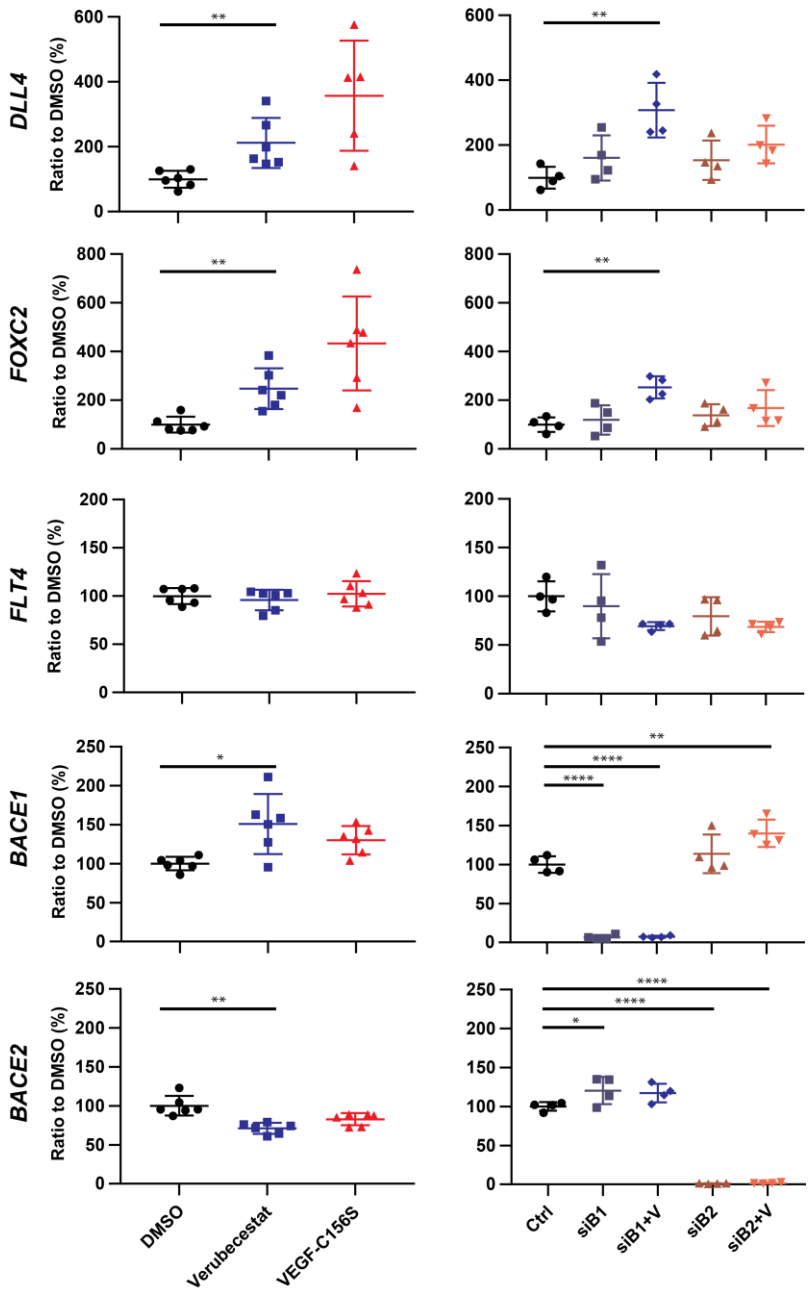

Figure 18. Alterations in gene expression in LECs. Gene expression levels of *DLL4*, *FOXC2*, *FLT4*, *BACE1* and *BACE2* were analyzed after the pharmacological application of DMSO, Verubecestat and VEGF-C (left column), or after transient knockdown of control siRNA (Ctrl), *BACE1* (siB1) and *BACE2* (siB2) and additional pharmacological application of Verubecestat (siB1+V, siB2 +V) (right column). For statistical analysis either the Welch's t-test under the exclusion of the VEGF-C156S positive control was performed (left column), or a one-way ANOVA, followed by Bonferroni's multiple comparison test was performed (* p< 0.05, ** p= 0.01, **** p< 0.0001, n=4-6).

5. Discussion

BACE1 catalyzes the first step in the generation of the aggregating Aß. Therefore, BACE1 is a major drug target in the effort to slow or delay onset and disease progression of AD. However, many of the associated clinical trials testing BACE inhibitors were recently terminated due to lack of efficacy and were often accompanied by undesired side effects, like cognitive decline. BACE1 has a plethora of physiological substrates, which can be logically associated to the observed side effects. Furthermore, barely any attention has been paid to the close homologue protease BACE2, which does not play a major role in the amyloid cascade, but is nevertheless expected to be impaired by most -or possibly all- clinical inhibitors due to lack of BACE selectivity. To the most part, BACE2 substrates and their functions have barely been established and no sophisticated *in vivo* BACE2 activity biomarker exists, which could be used to monitor BACE selectivity and to correlate it with observed side effects in clinical trials.

In this thesis, the major aims were successfully achieved. VEGFR3, a potential biomarker for BACE2 activity, was identified in murine plasma and validated for its application in the murine as well as the NHP system and human clinical trial participants. Given the physiological functions of the receptor VEGFR3, possible functional implications of altered VEGFR3 processing via BACE2 were elucidated in a primary lymphatic endothelial cell line with high endogenous levels of VEGFR3 and BACE2. Alterations in downstream signaling and gene expression changes hinted towards the possibility of cellular (e.g. proliferation) and possibly physiological consequences (e.g. altered lymph vessel morphology) due to increased signaling activity of cellular accumulated VEGFR3.

In the following chapters, the challenges of blood plasma proteomics, the benefits of plasma VEGFR3 as a BACE2 activity biomarker and the cellular and physiological implications, which may arise from enhanced VEGFR3 activity due to BACE2 inhibition, will be discussed. Furthermore, possible consequences for other pathologies are briefly considered and consequences for the BACE inhibitor field are presented.

5.1. Challenges of blood plasma proteomics in AD and beyond

BACE1 substrates and biomarkers were primarily identified and validated in neuronal cell cultures and the CSF from different organisms. Here, the extracellular space is in direct contact with the source tissue (i.e. the CNS) and deriving proteomic changes can be monitored easily[38,42,69]. However, CSF sampling is an invasive and uncomfortable procedure and obtainable volumes are very limited in smaller animals during pre-clinical phases (e.g. 5µl in mice).[38]. Furthermore, sampling procedures easily result into blood or cell contaminations of the CSF, thereby heavily impairing protein quantification results, from e.g. mass spectrometry[166]. As described, the most important BACE1 CSF biomarker have been, or are in the process of being successfully transferred into plasma as an alternative readout[108,114,115]. Given the easy accessibility and minimal invasiveness of plasma collection and considering the ever increasing capabilities of plasma proteomics, novel protein biomarkers should best be established –if applicable- in blood samples, like e.g. blood plasma.

For now, blood plasma remains one of the most challenging bio fluids for proteomic analyses, due to its high complexity and high dynamic concentration range of its proteins. 75% of the plasma proteome

only consists of albumin and immunoglobulins. Including 22 additional proteins, roughly 99% of the plasma protein concentration is covered , whereas only 1% of plasma proteins represent potential proteins of interest, like e.g. hormones[167]. Here, this problem was targeted via the enrichment for glycoproteins, or the immuno-depletion of the most abundant proteins, resulting in the identification of up to 508 protein groups in the glycoprotein enriched samples, which facilitated the successful identification of the putative BACE2 biomarker VEGFR3 in murine plasma. Recent advantages in the nature of spectral library based mass spectrometric data independent acquisition[140-142] also enabled the detection of murine plasma VEGFR3 without prior enrichment of glycoproteins, enabling a similar identification depth of up to 522 protein groups, while strongly decreasing sample processing workload and possible associated artificial variability, derived from the enrichment procedure.

In NHP samples however, only the combination of immunological depletion of redundant proteins with Spectronaut's library independent direct DIA[168,169] algorithm (based on DIA-Umpire[170]) allowed the quantification of plasma VEGFR3 and yielded a total of 406 protein identifications in NHP. Curiously, the described direct DIA approach outperformed any other approach to detect plasma VEGFR3 and other meaningful identifications in NHP samples. Among these, were attempts to enrich for glycoproteins, immunoprecipitation of VEGFR3 and the use of an extensive spectral library, which consisted of various fractionation approaches, like e.g. gel fractionation and strong cation exchange fractionation and contained 736 different protein groups, including several unique VEGFR3 peptides of satisfying quality (q-value < 0.01). Immuno-depleted NHP samples were also analyzed with this library, which either resulted in no meaningful or in poor matching of the spectra, thereby resulting in highly variable quantifications. These issues may derive from the fact, that the spectral library was generated at a much earlier time point and changes in the peptide elution, e.g. due to variability in self-packed LC columns or matrix effects, may have introduced more variability for the highly complex plasma samples. This may have negatively influenced the data analysis with the retention time indexed DIA spectral libraries. Furthermore, it is possible, that the high number of library spectra resulted into an inflated library, which may result into harsh FDR filtering and the loss of true VEGFR3 peptide identifications.

In contrast, the performed direct DIA analysis first creates a spectral library based on the DIA measurements by extracting and correlating precursor and fragment ion m/z signals, based on their elution profiles, in order to create pseudo-MS2 spectra for a database search. Conclusively, the spectral library generated for this experiment results in very narrow retention time matching windows, therby reducing the variability. Furthermore, this spectral library consist of fewer, but very high quality peptide fragmentation spectra, based on the limited number of analyzed NHP plasma samples, which potentially increase the data analysis performance[168]. Therefore, direct DIA has been described for strong precision and little missing values[169]. For plasma, also a small hybrid library, consisting of DDA and DIA runs may be a feasible approach to enhance meaningful identifications[171].

Another important matter, which is commonly ignored in discussions, but may play a major role for any plasma analysis, is the matter of sample handling and storage. The stability of any protein of interest may be heavily influenced by the care and speed of plasma preparation from blood samples. Additionally, repeated thaw-freeze cycles above -30°C further diminish plasma sample quality[172] and only two freeze-thaw cycle may already influence the mass spectrometric abundance of a given protein of interest[173]. As a consequence, good laboratory practice in regards to plasma handling is of high importance and should be documented more stringently. Additionally, plasma proteomics might require an easily accessible sample quality readout to evaluate the samples prior to MS analysis. One feasible

approach may be the quantification of the albumin proteoform Delta-S-Cys-Albumin[172], which is able to reflect the cumulative exposure of samples to temperatures above -30°C and could be used either as a pre-test before sample fractionation or concurrently with standard measurements of non-fractionated samples.

Today, the curated human plasma peptide atlas contains information on 4,395 canonical plasma proteins, which were combined from over 240 experiments, consistent of proteomic datasets and complementary expression data (http://www.peptideatlas.org/builds/human/plasma/, version 07/2021)[174]. In comparison, standard proteomic experiments recently yielded e.g. up to ~1639 plasma protein identifications via e.g. excessive sample fractionation or multiplexed labeling techniques[175,176]. These approaches however, while not required to detect VEGFR3, introduce increased sample processing complexity, enhanced measurement time and, in regards to labeling, require specific instrumental properties for proper measurements.

In the near future, plasma sample measurements may be significantly improved by the widespread use of micro-LC systems[177,178]. In contrast to nano-LC systems, micro-LC columns are more robust against the challenging complexity of plasma samples and allow the analysis of up to 10 µg of undepleted plasma per run, without overloading the column[178,179]. Coupling a micro-LC with the modern Q-Exactive HF mass spectrometer, this approach was able to analyze >14,000 samples without losses in chromatographic performance, while enabling routine measurements of 2600 proteins per sample, when fractionating the samples prior analysis[178]. In these setups, it is recommendable to omit any fractionation step like immune-depletion, which potentially introduce artificial alterations for proteins of interest and strongly increases sample processing efforts.

Furthermore, recent computational advances, could improve the analysis of DIA data, using predictions of peptide elution, fragmentation, or also collisional cross section in the case of ion mobility separation[180,181].

5.2. BACE2 cleaves VEGFR3 similarly to other substrates

Identifications in BACE cleavage sites may in the future further the identification of shared substrate motifs in regards to amino acid sequence, but also in consideration of associated steric and chemical properties. To date, several BACE1[38,58,153] and BACE2[70,74,182] substrate cleavage sites have been described (Table 09). According to available cleavage site data, BACE2 sites have been mostly described to occur between a Leu and an Ala/Asp/Asn residue, or between Phe and a random hydrophobic residue[74]. In my thesis, the likely BACE2 cleavage site in VEGFR3 was determined between Ala764 and Val765. While not exactly resembling this cleavage prediction rules, that are based on only a few validated substrates, Val and Ala closely resemble the prediction. Therein, only Val slightly deviates with a residue chain, which only differs from leucine by the lack of one methyl-group and is therefore slightly shorter.

Table 11. BACE2 substrates and their cleavage sites. Overview of BACE2 juxtamembrane sequences and their cleavage site localization. Cleavage sites are indicated with || and the start of the transmembrane domain is indicated with TM. Table was adapted from Yan, Riqiang[183].

Protein substrate	Substrate recognition site
APP	KMDAEFGHDSGFEVRHQKLVF || FAEDVGSNKGA-TM
JAG1	KEITDKIIDL || VSKRDGNSSLIA || AVAEVRVQRRPLKNRTD-TM
TMEM27	RMNKNRINNAF || FL || NDQTLEF || LKIPSTLAPPMDPSVP-TM
VEGFR3	KGCVNSSASVA || VEGSEDKGSME-TM

While murine VEGFR3 was used to identify the cleavage site, the identic human sequence of the juxtamembrane region supports the notion of an identical cleavage site in the human system. Using shotgun proteomic sequencing to identify the most C-terminal semi-specific peptide of the shed ectodomain, it cannot be excluded, that additional cleavage events occurs more N-terminally as it is the case for e.g. TMEM27. Therefore, MALDI-TOF generated spectra from immuno-precipitated VEGFR3 should be generated in order to assess for the occurrence of additional cleavage sites. Additional measurements may be performed on the supernatant of BACE2 impaired cells to ensure the BACE2 specificity of the obtained semi-specific peptide.

While the newly discovered cleavage site may be incorporated in future BACE2 substrate predictions, more BACE2 cleavage sites of other substrates need to be identified in order to gain enough information for a useful algorithm. As discussed below, obtained cleavage site information may also be useful in the generation of BACE2 cleavage site specific antibodies.

5.3. Blood biomarker in the context of BACE proteases

AD related biomarkers are in large parts focused on monitoring the onset and progression of AD via e.g. PET imaging and determination of the CSF concentrations of the AD hallmark proteins Aß and p-Tau[11]. During BACE inhibitor application however, the activity of BACE proteases needs to be monitored closely to put results into perspective in regards to the degree of BACE activity inhibition. Possible future treatments would also require this readout in order to adapt dosing regimens according to individual responsiveness[184]. Plenty of BACE1 substrates have been described for the CSF[38,42] and Aß42 and SEZ6L have been successfully used for the purpose of *in vivo* BACE1 activity monitoring[38]. For the clinically more desirable plasma specimen however, only Aß subspecies determination would currently be feasible as a BACE1 activity readout (see 1.4.), while other BACE1 substrates like e.g. SEZ6 remain unreported in plasma. Due to individual proteome variability, it is preferable to observe a panel of proteins, instead of only e.g. Aß42. Therefore, more plasma readouts for BACE1 activity are needed and one is provided here in the form of soluble SEZ6L. However, a direct comparison to the current standard of Aß42 plasma levels would be desirable in order to better asses its responsiveness towards BACE1 activity and furthermore its transferability towards the human system needs to be demonstrated.

Recent failures in BACE inhibitor research stress the importance of a higher BACE1 selectivity for future inhibitors[184]. Due to the long lasting lack of interest in BACE2, no fluid biomarker has however been described for BACE2, which could be used to monitor *in vivo* BACE2 activity. In the efforts to identify a BACE2 specific plasma detectable substrate, the transmembrane receptor tyrosine kinase[185] VEGFR3 was identified and validated as a promising BACE2 biomarker candidate in my thesis. VEGFR3 plays essential roles in the embryonic development of the blood[186]- and lymphvaculature[187]. In adult stages, VEGFR3 becomes mainly restricted to lymphatic vasculature, were it remains essential for lymph angiogenesis[188,189]. The source tissue of plasma VEGFR3 is speculative, but the lymphatic vasculature appears the most likely explanation due to VEGFR3's expression restriction to the lymphatic tissue in adult stages, which furthermore is in close contact with the blood circulatory system, thereby allowing easy protein exchange. Additionally, macrophages have been described to express VEGFR3 and may be an additional resource of plasma VEGFR3[190]. In direct comparison to fur pigmentation assays, plasma VEGFR3 appears to be a superior readout in the plasma of mice in regards to sensitivity and variability. Together with plasma SEZ6L, VEGFR3 provides a straightforward approach to easily monitor *in vivo* BACE1 and BACE2 activity in contrast to uncomfortably invasive CSF analysis for BACE1 and the cumbersome monitoring of the pigmentation status of re-grown hairs for BACE2. Another drawback for the fur pigmentation assay is the observation, that different pharmaceutical compounds may differ in their drug distribution across the body[139] and hair pigmentation status does not always correlate with an inhibitors potency against BACE2[93,116,118].

In contrast, in NHP and clinical trial participants subjected to strong unselective BACE inhibition, high levels of BACE2 independent baseline VEGFR3 and therefore low effect sizes complicate the applicability as a biomarker in the clinical context. Discrepancy between murine and NHP and human samples in general, may e.g. arrive from different protein turnover kinetics, which can differ strongly between various species[191] and may result into a different composition in NHP and human plasma. While BACE1 dependent VEGFR3 cleavage in regards to its plasma levels can be excluded, it may also be possible, that BACE2 is not an exclusive protease for VEGFR3. In APP processing for example, not only BACE cleavage occurs, but processing is also achieved via the A disintegrin and metalloprotease 10 (ADAM10), which processes APP into a neuroprotective product[192,193]. Likewise,

processing via another, yet unknown protease appears possible for VEGFR3. Furthermore, compensation mechanisms via another protease, which during normal BACE2 activity would not process VEGFR3 is possible. In the case of BACE1 impairment, unexpected compensation via the protease cathepsinD could be observed[194]. Alternatively, the presence of the secreted soluble isoform of VEGFR3 may be to blame[195]. As the shed ectodomain only differs in form of the BACE2 generated cleavage terminus from the secreted isoform, these fragments are indistinguishable via shotgun MS and non-specialized ELISAs. Meaningful changes of BACE2 dependent VEGFR3 levels may therefore be covered by high levels of the soluble isoform. As this is the first report of protease dependent shedding of the VEGFR3 ectodomain into the plasma, the plasma composition ratios of shed and secreted VEGFR3 have however not been described yet. The underlying issue resembles the initial challenges in specifically detecting BACE1 generated APP products (i.e. Aß42). Due to processing of APP by various proteases as e.g. ADAM10 and both BACE proteases, no BACE1 dependent fluid changes are visible upon the quantification of total soluble APP levels. Subsequent generation of cleavage site-recognizing antibodies enabled the meaningful monitoring of ADAM10 and BACE1 activity detection of the respective generated cleavage products[192]. Likewise, the generation of BACE2 cleavage site binding antibody against the shed VEGFR3 is required to distinguish BACE2 generated fragments from the soluble isoform and possible unknown protease products. To these ends, the herein described BACE2 cleavage site may be used in order to generate such antibodies.

Regardless of the underlying reason, the overall low plasma concentrations of VEGFR3 support the notion to use more sensitive approaches than the herein used methods. ELISA sensitivity limitations may be overcome via the combination of a BACE2 cleavage site specific antibody with the SIMOA technology, which has been described as 100 fold more sensitive in comparison to standard ELISA techniques[196]. For the mass spectrometric approach, the immunological capture of BACE2 generated plasma VEGFR3 in combination with matrix-assisted-laser-dissociation time-of-flight (Maldi-TOF) may be a feasible, as the technique was already successfully utilized for the streamlined detection of e.g. low abundant serum proteins and would therefore also be eligible for high throughput clinical applications[197-199].

While a first BACE2 *in vivo* activity biomarker was introduced in this thesis, establishing a whole panel of readouts for BACE2 activity (as well as for BACE1) is nevertheless a desirable aim in order to better account for individual proteome and medication response variability. This is especially important as VEGFR3 and BACE2 may also undergo unexpected alterations due to independent pathological processes.

5.4. Possible functional implications for altered VEGFR3 processing for lymphatic cells

Many BACE1 substrates were shown to serve physiological functions[200], which can be affected by altered processing via BACE1. Among these lines, functional implications for altered VEGFR3 processing appear likely. Given the receptor tyrosine kinase function of VEGFR3[185,201], increased cellular accumulation of VEGFR3 due to BACE2 impairment may result into increased VEGFR3 signaling. Enhanced activation of downstream regulation events, which are associated to VEGFR3 signaling, were indeed demonstrated in this thesis. In canonical signaling (Fig. 19), VEGFR3 is activated when homo- or heterodimers (with VEGFR2)[149] undergo conformational changes due to the binding of the ligand VEGF-C[202], thereby stimulating kinase domain phosphorylation[203] and positively

regulating cell survival, proliferation and cell migration via its downstream pathways AKT and ERK[202,204]. Besides canonical signaling, also ligand independent VEGFR activation has been described. Of note, VEGFR3 can be indirectly regulated via the interaction with integrin like kinase (ILK), which is sensitive towards mechanical stimulations, like e.g. pressure from adjacent blood flow[205]. Ligand independent signaling has furthermore been described for VEGFR3 in regards to cellular oxidative stress[206], or due to interactions with the extracellular matrix[207].

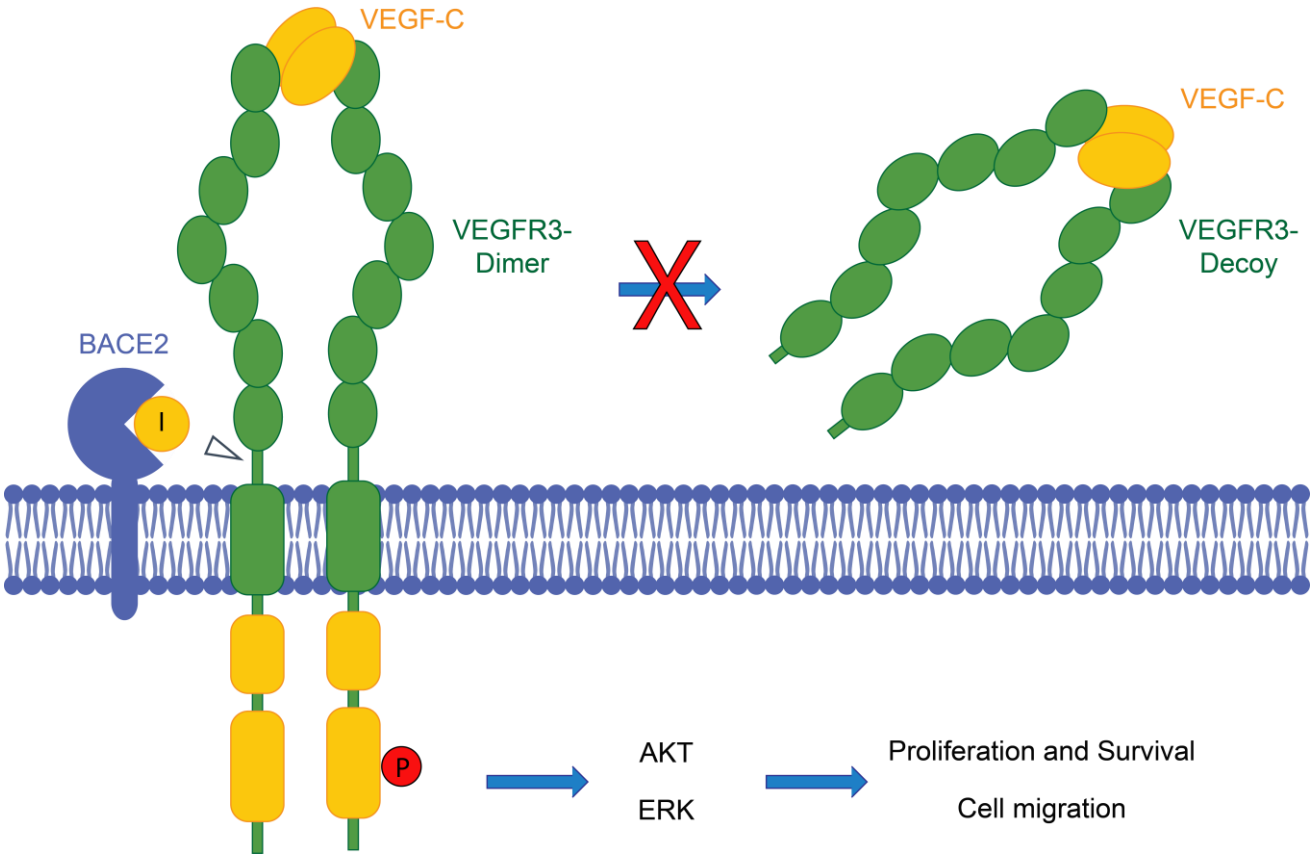

Figure 19. Canonical/ligand dependent VEGFR3 signaling and altered BACE2 processing. VEGFR3 can form homodimers or heterodimers with VEGFR2. Upon ligand-dimer binding, conformational shifts induce intracellular auto phosphorylation, which in turn activates the pathways AKT and ERK (and Jun-Kinase, not discussed here). Pathway activation results into increased cell proliferation, cell survival and cell migration. Under endogenous conditions, extracellular VEGFR3 is able to function as a decoy for VEGF-C thereby possibly affecting remote VEGFR3 signaling. Upon BACE2 inhibition, no decoy VEGFR3 is generated via shedding, while cellular VEGFR3 level increase and may result into enhanced signaling activities.

While embryonic VEGFR3 is expressed both, in blood- and lymphvasculature, in adult stages VEGFR3 remains restricted to the lymphatic tissue. Alongside podoplanin, lymphatic vessel endothelial hyaluronic acid receptor-1 (LYVE1) and prospero-related homeobox-1 (PROX1), VEGFR3 is even considered one of the major markers for lymphatic tissue[208] and is strongly co-expressed with BACE2 in lymphatic endothelia cells (https://www.proteinatlas.org)[85,209]. This raises the need to closely monitor lymphatic cell behaviour in the context of BACE2 processing. Due to the limited proliferation potential and comparatively slow growth of primary lymphatic endothelial cells, comprehensive cellular *in vitro* experiments were not feasible in the scope of this dissertation. Given VEGFR3's described functions, it would be of special interest to monitor LEC behaviour in regards to proliferation, migration and *in vitro* vessel formation capabilities in the context of BACE inhibition. Furthermore,

cellular accumulation of VEGFR3 was demonstrated and would be expected to accumulate at the cell surface. To further demonstrate this, VEGFR3 FACS analysis, or proteomic analysis of BACE inhibitor affected cell surface proteome, e.g. via the click sugar mediated SUSPECs[57] method may be feasible. Complementary to enhanced phosphorylation of AKT and ERK, increased phosphorylation of VEGFR3 would be an additional desirable readout in order to clearly demonstrate P-VEGFR3 involvement of downstream signals. As no P-VEGFR3 antibodies exist, this may be achieved by immunoprecipitation VEGFR3 and blotting against P-Tyrosine, or via fluorescence signal quantification of a proximity ligation assay, which is targeted against VEGFR3 and P-Tyr[205].

Besides canonical VEGFR3 signaling further mechanisms appear possible on the cellular level. First, VEGFR3 has been described as a γ secretase substrate[210]. While no dedicated functions for the VEGFR3 CTF has been described, γ secretase dependent CTFs from various kinases such as e.g. ERBB4 have been shown to play regulatory roles in the form of transcription factors, wherein the generated intracellular part of ERBB4 promoted e.g. breast cancer cell growth [211]. The γ secretase cleaves at the intramembrane site of their substrates and often require a pre-processing step via e.g. BACE proteases[212]. Therefore, the resulting lack of CTF generation upon BACE impairment may result into additional unforeseeable consequences on the cellular level. As soluble VEGFR3, including the shed VEGFR3 was demonstrated to act as a VEGF-C decoy[195,213,214], decreased extracellular/fluid concentrations may influence neighboring and remote cells, which may consequently be exposed to an abnormal amount of free VEGF-C.

5.5. Possible functional implications of altered VEGFR3 processing for peripheral and meningeal lymphatic vasculature

In mice, VEGFR3 mediated vascularization was shown to be highly dependent on its activation via VEGF-C[215-217] and VEGF-C deficiency is embryonically lethal, between E15.5. and E. 17.5., due to an impaired formation of the lymphatic vasculature[187]. Heterozygous VEGF-C mice are viable, but similar to VEGFR3 deficient mice develop lymphedema[187]. The axis of VEGF-C and VEGFR3 are closely connected and often monitored together for their biological functions. Furthermore, the VEGF-C/VEGFR3 axis is involved in the plasticity of lymphatic vessels[218,219] and support migration and survival of endothelial cells[204]. Concurrently to the essential vasculature functions, VEGFR3 KO mice are not viable and die at E10, however in contrast to VEGF-C KO mice, due to defects in cardiovascular formation[186]. Furthermore, functional impairment of VEGFR3 signaling is associated to lymphedema in humans[220] and mice[221]. In connection to the essential function of VEGFR3 signaling for lymph angiogenesis, important issues arise in regards to lymphatic vascularization and lymphatic drainage efficiency. Given the considerations for cellular consequences of altered BACE2 dependent VEGFR3 activity, it is of interest to validate the in vivo lymphatic vasculature and its draining functionality via trace clearance e.g. in the ear skins and corneas[205], of BACE2 impaired mice. As no lymphatic abnormalities like lymphedema have been described for BACE2 KO mice, possible alterations, if present, should however be of minor strength[71].

In regards to the BACE inhibitor field, special attention should be paid to the meningeal lymphatics. Despite the initial description of meningeal lymphatic vasculature in 1787, the presence and role of meningeal lymphatic vessels have been forgotten for many years[222]. Clearance of the CSF and its waste products were thereafter largely reviewed under the aspect of the glymphatic system, wherein waste

product are transferred across the blood brain barrier into the meningeal blood vessels via astrocyte located aquaporin channels[223]. Lately, meningeal lymphatics were "re-discovered" by the scientific community and recent works highlight their importance for clearance of the CSF and their close connection to cognitive capabilities [224-227]. This drainage appears to mainly occur on the basal meninges and has been shown to be transported into the superficial and deep cervical lymph nodes[228-231].

Several independent studies demonstrated that meningeal lymphatic vasculature is also dependent on VEGFR3-VEGF-C signaling and that its impairment resulted into decreased CSF clearance and cognitive worsening. When monitoring the clearance of injected Tau into the brain parenchyma of VEGFR3 impaired mice, clearance was slowed and presence of Tau in the plasma was delayed[232]. Equally, lymphatic impairment in mice was able to enhance Aß deposition[230]. Interestingly, MCI and aged patients both display enhanced VEGFR3 gene expression in their prefrontal cortex, wherein VEGFR3 expression correlated with worse cognitive trajectories[233]. Whether this shift in expression itself is pathological, or a neuroprotective response against already present pathogenicity of e.g. Tau, remains to be seen. In general however, integrity of meningeal vasculature and its CSF clearance efficiency decreases during aging[229-231]. In contrast to impairment, stimulation of lymph angiogenesis using VEGF-C, enhanced lymphatic vascularization, improved CSF clearance and improved the cognitive capabilities of aged mice[189,230]. Therein, lymphatic vasculature proofed to be highly plastic and its VEGFR3 dependent alterations via pharmacological intervention where reversible[189].

Here, it was shown that BACE2 inhibition may indirectly activate VEGFR3 dependent pathways in similar strength like VEGF-C activation and may therefore influence lymph angiogenesis. If and how possible effects may actually materialize still needs to be determined. While the intuitive approach would suggest increased lymph vascularization and enhanced CSF clearance, the actual phenotype may ultimately differ. A direct comparison with VEGF-C stimulation may not be appropriate, since BACE2 dependent lymph angiogenesis would be a secondary effect, which operates on a different mechanism. While VEGF-C application can only activate endogenously available VEGFR3, BACE2 inhibition may lead to global cellular VEGFR3 increases across different cells and cell types. As shown here, BACE dependent VEGFR3 activation not only induces transcription of pro-lymphangiogenic genes like *FOXC2*, but also the anti-proliferative NOTCH ligand *DLL4*. DLL4/NOTCH signaling is regulated in a sophisticated manner and different ratios between receptor and ligands may lead to opposite result in regards to their VEGFR associated fine-tuning of angiogenic sprouting[234]. Therefore, it is unclear if ectopic lymph vascularization might occur and if resulting new vessels would clear the CSF in a useful manner. Instead, ectopic vessels might be nonsensical and only act as a sink/source tissue for accumulated waste products, or transport towards the periphery may be impaired due to alterations in the AKT/FOXC2 dependent valve formation. While many meningeal lymphatic vessels are devoid of valves, their presence has been described to be prominent at the basal site of the skull, which appears to be the major route for CSF drainaige[229]. As mentioned before, VEGFR3 has been identified as a γ secretase substrate and alterations in CTF generation may also contribute to function changes in vascularization. Furthermore, VEGFR3 dependent sprouting of new blood vessels requires locally increased VEGFR3 levels in the tips of newly forming vessels[235], which is accompanied by locally increased DLL4 levels, which prohibits sprouting in adjacent cells[163,236]. A mosaic type deletion of VEGFR3 in lymphatic vasculature was demonstrated to induce hyperplasia and hyperbranching in neighboring lymphatic cells[235]. These concentration dependent mechanisms may be disrupted among BACE2 inhibition induced uniform VEGFR3 accumulation and may therefore not necessarily lead to increased vessel formation.

Another layer of complexity is added by the ambivalent role for VEGFR3 signaling and lymphatic vasculatures for inflammatory events. Beneficial roles for recovery of cognition and motor function have been described in response to traumatic brain injury in mice and rats[237]. In stroke however, VEGFR3 signaling has been associated with pro-inflammatory activation and invasion of peripheral macrophages and increased brain infarction[228]. In line, ablation of meningeal lymph vasculature also decreases pathology and invasion of inflammation dependent T-cells in multiple sclerosis[227]. Therefore, the role of lymphatic vasculature appears context dependent and it remains unclear if hypothetical induced lymph vascularization would be beneficial or disadvantageous in the context of the inflammatory situation of AD.

BACE2 dependent lymph vascularization may also not play any notable role, as compensatory mechanisms might prevent lasting effects on the highly plastic lymph vasculature. Possible effects may also only appear in aged organisms, where efficiency and morphology of lymphatic vasculature are changed[229,230], or may even only play a role when inflammatory conditions are present, as it was the case for BACE2 dependent VCAM1 shedding[73]. Increased VEGFR3 accumulation could require complementation with secreted VEGF-C from macrophages[238,239] or potentially from microglia[237].In the cornea for example, VEGFR3 dependent vessel formation directly requires the presence of macrophages[239,240]. Finally yet importantly, shifts in the activation state of macrophages[228] have been observed, wherein VEGFR3 activation in LECs induced pro-inflammatory behavior in adjacent macrophages, raising the possibility of indirectly influencing macrophage and possibly microglia behavior.

Taken together, it is yet unclear if and how altered VEGFR3 processing can influence lymphatic vasculature. Due to the complex nature of lymph vascularization and the lack of a comparable model, a plethora of different hypothetical outcomes and phenotypes are possible.

5.6. BACE2 and VEGFR3 in disease

Besides the context of BACE inhibitors, monitoring of plasma VEGFR3 levels may also be interesting for different pathological processes, wherein BACE2 and/or VEGR3 are altered or targeted. Due to its role in glucose tolerance and insulin signaling, BACE2 is an ongoing target for diabetic research, wherein BACE2 inhibition is currently discussed and where first BACE2 selective inhibitors have been designed[78,241]. The current feasibility of this approach is however yet unclear. BACE2 KO mice were associated with higher glucose tolerance and increased insulin levels[74], but a prolonged high fat diet resulted into aggravated weight gain, hyperinsulinemia and insulin resistance in BACE2 KO mice[242]. If the BACE2 inhibition approach should turn out as a feasible approach for the treatment of diabetes and should not otherwise lead to non-tolerable off target effects, plasma VEGFR3 levels may be useful in order to indirectly account for the strength of BACE2 impairment.

More importantly, BACE2 and especially VEGFR3 have been described for their negative roles in cancer. BACE2, but mostly not BACE1 gene expression has been demonstrated to be upregulated in various cancer types, such as pancreatic cancer[243], glioblastoma[244,245] and melanoma[246], wherein BACE2 expression correlates with worse prognosis in survival. BACE2 impairment was able to decrease tumor proliferation[247,248] and may therefore become an interesting target in the therapy of various cancer types[249]. While effects of BACE inhibition on tumor growth were often attributed to the pro-proliferative function of processed APP[248,250], important involvements of VEGFR3 seem likely,

given the ameliorating influence of BACE impairment on vascularization, cell proliferation and survival in tumor cells[247].

Additionally to the already described pro-proliferative and pro-survival functions, VEGFR3 plays important roles in wound healing[251] and vascular remodeling of e.g. expanding tissue[252]. In line with this, enhanced VEGFR3 activation is also associated with cancer related tumor vascularization and metastasis and correlates with a poor prognosis of survival[253-255]. Poor prognosis from VEGFR3 level probably derives from the vascularization of tumor tissue and is together with its VEGF-C ligand already monitored in the plasma of respective patients[253-255].

Due to the novelty of VEGFR3 as a BACE2 substrate, its interconnection in cancer has not yet been elucidated. It will be of interest to see, how BACE2 inhibition may affect VEGFR3 signaling and resulting physiological effects in cancer types, which co-express both proteins. As discussed, it remains difficult for now to make any predictions on the effects of BACE2 dependent cellular VEGFR3 accumulation. Additional complexity is added by the unique tumor microenvironments, which are generated around tumors[256]. Besides other types of immune cells these often harbor plenty of macrophages, which as mentioned express VEGFR3 as well as VEGF-C[190] and play major roles in vascularization[190,240]. Therefore, it remains to be seen whether BACE2 would have additional beneficial effects via the disruption of the prevailing VEGFR3 -VEGF-C interactions in tumors and their microenvironment, or whether the amelioration of tumor proliferation due to other substrates like APP would be cut short by boosting inflammatory macrophages and the pro-proliferative/pro-(lymph)angiogenic activation of the VEGFR3-VEGF-C axis.

5.7. Implications for BACE inhibitor research and future of BACE inhibitors

After the recent negative outcomes, no BACE inhibitors are currently in clinical trials. While the focus for treatment of AD currently lies on other issues like the controversial FDA approval of the anti-amyloidogenic antibody aducanumab[257,258], the search for the underlying reasons for BACE dependent side effects is still ongoing. As described, clinical trial participants from failed inhibitor studies were all in advanced age groups and suffered mostly already from MCI, which is generally accompanied by CNS inflammation. Considering the here described BACE2 dependent effects on VEGFR3, more attention should be paid to effects on the lymph vascularization in clinical research. As mentioned, lymphatic vasculature in the context of brain inflammation may play disadvantageous or beneficial roles. If present, possible effects from BACE2 dependent lymph vascularization should nevertheless be of minor strength, as no lymph-associated phenotypes have been prominent enough to be described for B2KO mice[71]. Note however, that also cognitive effects of clinical trial participants showed only a minor effect size and were reversible. To shed further light into the importance of BACE2, it would be necessary to monitor for functional consequences in lymph vasculature in BACE2 impaired mice.

Inhibitor dependent effects in clinical trials are also highly likely to be dependent on BACE1 activity. To elucidate the dependency of BACE selectivity, a comparison of the two inhibitors, which did not display cognitive decline against cognitive decline enhancing inhibitors, would be highly desirable. Proteomic comparison of e.g. inhibitor treated primate CSF samples, might highlight, which BACE1 substrates contribute strongest to cognitive decline. Together with the results of this thesis, it would also be advisable to also determine plasma VEGFR3 levels of these cohorts in order to put the role of BACE2 activity in perspective. As mentioned before, a strong BACE1 inhibition might also be

accompanied with moderate BACE2 inhibition, even when applying marginally selective inhibitors. Note also, that plasma VEGFR3 levels is an indirect readout for BACE2 shedding and is supposedly limited by the half life time of plasma VEGFR3 and the generation of the soluble isoform. In contrast, local effect sizes and possible effects from altered BACE2 processing in the tissue of origin (i.e. lymphatic endothelial cells) may be stronger than observed in the plasma.

Independent of the exact underlying reason for failed BACE inhibitors, highly BACE1 selective compounds, which are administered in more moderate doses and at earlier time points (i.e. before onset of notable pathogenesis) are still a promising approach to prevent or delay the onset of AD. Given the long time span of ~20 years between initial Aß deposition and the onset of symptoms, a widespread acceptance of preventive BACE inhibitor treatment for the broad public appears unlikely. Instead, more targeted approaches, like e.g. anti Aß antigen therapy[259] will be needed against the rising numbers of sporadic AD. BACE inhibitors may however still be promising in the context of the genetically determined familiar AD, in which disease onset can be exactly predicted. Therein, mild BACE inhibitor treatment may be started in a chronic manner, or in short termed more stringent treatment rounds. Even, if the minor inhibitor side effects, cannot be resolved, effective BACE inhibitors with mild cognitive worsening should still be considered preferable in comparison to the early onset of familial AD.

In the end, plasma VEGFR3 as a BACE2 activity biomarker should also be explored across a larger variety of BACE inhibitors, in order to stress its clinical applicability. Furthermore, the generation of absolute quantification assays will allow comparing the responsiveness of plasma VEGFR3 with e.g. Aß42 and therefore the *in vivo* determination of inhibitor selectivity. Therein, it will be of interest to assess, how well the broadly used selectivity information from *in vitro* assays correlate with the *in vivo* data and if advertised selectivity information indeed reflect physiological reality.

6. Outlook

In conclusion, VEGFR3 was identified as a BACE2 specific substrate, which is processed into the plasma and is therefore easily accessible. VEGFR3 was subsequently thoroughly validated as a BACE2 specific substrate and in principle demonstrated to be transferable to the NHP and human systems. While highly promising as an *in vivo* BACE2 activity readout, quantification of VEGFR3 needs to be improved for proper use in NHP and human plasma samples. In order to overcome the discussed interfering plasma VEGFR3 background levels, the design of immunological assays, which are specifically targeted against the BACE2 generated nascent C-terminus of the cleaved ectodomain, is required. Furthermore, the comparably difficult detectability of any VEGFR3 fragments in NHP and human plasma suggests the combination of a cleavage site specific antibody with highly sensitive immunological methods like SIMOA and preferably a high throughput technique like immuno-MALDI for clinical applications.

Initial data on the VEGFR3 regulated downstream regulatory pathways AKT and ERK and gene expression data for FOXC2 and DLL4 indicate the possibility of functional implications for lymphatic cells upon cellular BACE2 impairment derived VEGFR3 accumulation. In order to confirm dependency on VEGFR3 signaling, monitoring of downstream pathway/gene regulatory events upon both BACE2 and VEGFR3 impairment appears feasible. For cellular functional readouts, this approach may be combined with assays for cell proliferation and migration. More importantly, BACE2 dependent VEGFR3 functions need to be assessed in the much more complex context of *in vivo* studies. Effects of BACE2 impairment should therefore be monitored in e.g. BACE2 KO mice or zebrafish, which are two already well described models in the field of BACE inhibitors. No severe lymphatic phenotypes like lymphedema have been noticed for these models, but lymphatic vessel morphology has not been closely assessed. Therein it will be of interest to analyze e.g. the ear skin lymphatics of mice for their number of sprouts, interconnections and diameter and if differences can be seen, for their capabilities to drain tracer fluids. Furthermore, positive results would clearly indicate the need for assessing the consequences of BACE inhibitors for meningeal lymphatics and associated CSF drainage.

Regardless of the presence of physiological differences in lymphatics, plasma VEGFR3 levels from clinical trial participants should be determined across studies with BACE inhibitors of differing BACE selectivity. This will help to determine the actual *in vivo* BACE selectivity of the inhibitors and will help to put the role of BACE2 silencing into perspective in regards to the sides effects, which arose in clinical trials.

Considering the established role of VEGFR3 and the increasingly indicated role of BACE2 in various types of cancer, highlights the possible importance of BACE2 dependent VEGFR3 processing in the field of cancer therapeutics. If BACE2 dependent VEGFR3 processing should notably contribute to tumor growth and metastasis, this might ultimately result into the meaningful anti tumoral use of BACE2 affecting BACE inhibitors, which have already been assessed as save for patient use, but are currently considered redundant due to their failure to treat AD symptoms.

7. References

1. Berchtold NC, Cotman CW. Evolution in the conceptualization of dementia and Alzheimer's disease: Greco-Roman period to the 1960s. Neurobiology of aging 1998;19:173-89.
2. Halpert BP. Development of the term" senility" as a medical diagnosis. Minnesota medicine 1983;66:421-4.
3. Yang HD, Kim DH, Lee SB, Young LD. History of Alzheimer's Disease. Dementia and neurocognitive disorders 2016;15:115-21.
4. Alzheimer A. Uber eine eigenartige Erkrankung der Hirnrinde. Zentralbl Nervenh Psych 1907;18:177-9.
5. Strassnig M, Ganguli M. About a peculiar disease of the cerebral cortex: Alzheimer's original case revisited. Psychiatry (Edgmont (Pa : Township)) 2005;2:30-3.
6. Brookmeyer R, Johnson E, Ziegler-Graham K, Arrighi HM. Forecasting the global burden of Alzheimer's disease. Alzheimer's & dementia : the journal of the Alzheimer's Association 2007;3:186-91.
7. Querfurth HW, LaFerla FM. Alzheimer's disease. The New England journal of medicine 2010;362:329-44.
8. 2020 Alzheimer's disease facts and figures. Alzheimer's & Dementia 2020;16:391-460.
9. Fink HA, Linskens EJ, MacDonald R, et al. Benefits and Harms of Prescription Drugs and Supplements for Treatment of Clinical Alzheimer-Type Dementia. Ann Intern Med 2020;172:656-68.
10. Loera-Valencia R, Cedazo-Minguez A, Kenigsberg PA, et al. Current and emerging avenues for Alzheimer's disease drug targets. Journal of internal medicine 2019;286:398-437.
11. Zetterberg H, Bendlin BB. Biomarkers for Alzheimer's disease-preparing for a new era of disease-modifying therapies. Molecular psychiatry 2021;26:296-308.
12. Jack CR, Jr., Bennett DA, Blennow K, et al. NIA-AA Research Framework: Toward a biological definition of Alzheimer's disease. Alzheimer's & dementia : the journal of the Alzheimer's Association 2018;14:535-62.
13. Selkoe DJ, Hardy J. The amyloid hypothesis of Alzheimer's disease at 25 years. EMBO molecular medicine 2016;8:595-608.
14. De Strooper B, Karran E. The Cellular Phase of Alzheimer's Disease. Cell 2016;164:603-15.
15. Haass C, Selkoe DJ. Soluble protein oligomers in neurodegeneration: lessons from the Alzheimer's amyloid beta-peptide. Nature reviews Molecular cell biology 2007;8:101-12.
16. Mullan M, Crawford F, Axelman K, et al. A pathogenic mutation for probable Alzheimer's disease in the APP gene at the N-terminus of beta-amyloid. Nature genetics 1992;1:345-7.
17. Di Fede G, Catania M, Morbin M, et al. A recessive mutation in the APP gene with dominant-negative effect on amyloidogenesis. Science (New York, NY) 2009;323:1473-7.
18. Oakley H, Cole SL, Logan S, et al. Intraneuronal beta-amyloid aggregates, neurodegeneration, and neuron loss in transgenic mice with five familial Alzheimer's disease mutations: potential factors in amyloid plaque formation. The Journal of neuroscience : the official journal of the Society for Neuroscience 2006;26:10129-40.
19. Eckman CB, Mehta ND, Crook R, et al. A new pathogenic mutation in the APP gene (I716V) increases the relative proportion of A beta 42(43). Human molecular genetics 1997;6:2087-9.
20. Jonsson T, Atwal JK, Steinberg S, et al. A mutation in APP protects against Alzheimer's disease and age-related cognitive decline. Nature 2012;488:96-9.
21. Hamley IW. The amyloid beta peptide: a chemist's perspective. Role in Alzheimer's and fibrillization. Chemical reviews 2012;112:5147-92.
22. Nelson PT, Jicha GA, Schmitt FA, et al. Clinicopathologic correlations in a large Alzheimer disease center autopsy cohort: neuritic plaques and neurofibrillary tangles "do count" when staging disease severity. Journal of neuropathology and experimental neurology 2007;66:1136-46.
23. Congdon EE, Sigurdsson EM. Tau-targeting therapies for Alzheimer disease. Nature reviews Neurology 2018;14:399-415.

24. Irwin DJ. Tauopathies as clinicopathological entities. Parkinsonism & related disorders 2016;22 Suppl 1:S29-33.
25. Choi SH, Kim YH, Hebisch M, et al. A three-dimensional human neural cell culture model of Alzheimer's disease. Nature 2014;515:274-8.
26. Israel MA, Yuan SH, Bardy C, et al. Probing sporadic and familial Alzheimer's disease using induced pluripotent stem cells. Nature 2012;482:216-20.
27. Maia LF, Kaeser SA, Reichwald J, et al. Changes in amyloid-β and Tau in the cerebrospinal fluid of transgenic mice overexpressing amyloid precursor protein. Science translational medicine 2013;5:194re2.
28. Schelle J, Häsler LM, Göpfert JC, et al. Prevention of tau increase in cerebrospinal fluid of APP transgenic mice suggests downstream effect of BACE1 inhibition. Alzheimer's & dementia : the journal of the Alzheimer's Association 2017;13:701-9.
29. Hyman BT. Amyloid-dependent and amyloid-independent stages of Alzheimer disease. Archives of neurology 2011;68:1062-4.
30. Golde TE, Koo EH, Felsenstein KM, Osborne BA, Miele L. γ-Secretase inhibitors and modulators. Biochimica et biophysica acta 2013;1828:2898-907.
31. Doody RS, Raman R, Farlow M, et al. A phase 3 trial of semagacestat for treatment of Alzheimer's disease. The New England journal of medicine 2013;369:341-50.
32. Coric V, van Dyck CH, Salloway S, et al. Safety and tolerability of the γ-secretase inhibitor avagacestat in a phase 2 study of mild to moderate Alzheimer disease. Archives of neurology 2012;69:1430-40.
33. De Strooper B. Lessons from a failed γ-secretase Alzheimer trial. Cell 2014;159:721-6.
34. Woo HN, Park JS, Gwon AR, Arumugam TV, Jo DG. Alzheimer's disease and Notch signaling. Biochemical and biophysical research communications 2009;390:1093-7.
35. Vassar R, Bennett BD, Babu-Khan S, et al. Beta-secretase cleavage of Alzheimer's amyloid precursor protein by the transmembrane aspartic protease BACE. Science (New York, NY) 1999;286:735-41.
36. Zhao J, Fu Y, Yasvoina M, et al. Beta-site amyloid precursor protein cleaving enzyme 1 levels become elevated in neurons around amyloid plaques: implications for Alzheimer's disease pathogenesis. The Journal of neuroscience : the official journal of the Society for Neuroscience 2007;27:3639-49.
37. Kandalepas PC, Sadleir KR, Eimer WA, Zhao J, Nicholson DA, Vassar R. The Alzheimer's β-secretase BACE1 localizes to normal presynaptic terminals and to dystrophic presynaptic terminals surrounding amyloid plaques. Acta neuropathologica 2013;126:329-52.
38. Pigoni M, Wanngren J, Kuhn PH, et al. Seizure protein 6 and its homolog seizure 6-like protein are physiological substrates of BACE1 in neurons. Molecular neurodegeneration 2016;11:67.
39. Fleck D, Garratt AN, Haass C, Willem M. BACE1 dependent neuregulin processing: review. Current Alzheimer research 2012;9:178-83.
40. Lichtenthaler SF, Lemberg MK, Fluhrer R. Proteolytic ectodomain shedding of membrane proteins in mammals-hardware, concepts, and recent developments. The EMBO journal 2018;37.
41. Huse JT, Doms RW. Closing in on the amyloid cascade: recent insights into the cell biology of Alzheimer's disease. Molecular neurobiology 2000;22:81-98.
42. Dislich B, Wohlrab F, Bachhuber T, et al. Label-free Quantitative Proteomics of Mouse Cerebrospinal Fluid Detects β-Site APP Cleaving Enzyme (BACE1) Protease Substrates In Vivo. Molecular & cellular proteomics : MCP 2015;14:2550-63.
43. Olsson B, Lautner R, Andreasson U, et al. CSF and blood biomarkers for the diagnosis of Alzheimer's disease: a systematic review and meta-analysis. The Lancet Neurology 2016;15:673-84.
44. Rasmussen MK, Mestre H, Nedergaard M. The glymphatic pathway in neurological disorders. The Lancet Neurology 2018;17:1016-24.
45. Tamura R, Yoshida K, Toda M. Current understanding of lymphatic vessels in the central nervous system. Neurosurgical review 2019.
46. Luo Y, Bolon B, Kahn S, et al. Mice deficient in BACE1, the Alzheimer's beta-secretase, have normal phenotype and abolished beta-amyloid generation. Nature neuroscience 2001;4:231-2.

47. Filser S, Ovsepian SV, Masana M, et al. Pharmacological inhibition of BACE1 impairs synaptic plasticity and cognitive functions. Biological psychiatry 2015;77:729-39.
48. Laird FM, Cai H, Savonenko AV, et al. BACE1, a major determinant of selective vulnerability of the brain to amyloid-beta amyloidogenesis, is essential for cognitive, emotional, and synaptic functions. The Journal of neuroscience : the official journal of the Society for Neuroscience 2005;25:11693-709.
49. Savonenko AV, Melnikova T, Laird FM, Stewart KA, Price DL, Wong PC. Alteration of BACE1-dependent NRG1/ErbB4 signaling and schizophrenia-like phenotypes in BACE1-null mice. Proceedings of the National Academy of Sciences of the United States of America 2008;105:5585-90.
50. Hu X, Zhou X, He W, et al. BACE1 deficiency causes altered neuronal activity and neurodegeneration. The Journal of neuroscience : the official journal of the Society for Neuroscience 2010;30:8819-29.
51. Hitt BD, Jaramillo TC, Chetkovich DM, Vassar R. BACE1-/- mice exhibit seizure activity that does not correlate with sodium channel level or axonal localization. Molecular neurodegeneration 2010;5:31.
52. Willem M, Garratt AN, Novak B, et al. Control of peripheral nerve myelination by the beta-secretase BACE1. Science (New York, NY) 2006;314:664-6.
53. Hu X, Hicks CW, He W, et al. Bace1 modulates myelination in the central and peripheral nervous system. Nature neuroscience 2006;9:1520-5.
54. Kobayashi D, Zeller M, Cole T, et al. BACE1 gene deletion: impact on behavioral function in a model of Alzheimer's disease. Neurobiology of aging 2008;29:861-73.
55. Hemming ML, Elias JE, Gygi SP, Selkoe DJ. Identification of beta-secretase (BACE1) substrates using quantitative proteomics. PloS one 2009;4:e8477.
56. Stützer I, Selevsek N, Esterházy D, Schmidt A, Aebersold R, Stoffel M. Systematic proteomic analysis identifies β-site amyloid precursor protein cleaving enzyme 2 and 1 (BACE2 and BACE1) substrates in pancreatic β-cells. The Journal of biological chemistry 2013;288:10536-47.
57. Herber J, Njavro J, Feederle R, et al. Click Chemistry-mediated Biotinylation Reveals a Function for the Protease BACE1 in Modulating the Neuronal Surface Glycoproteome. Molecular & cellular proteomics : MCP 2018;17:1487-501.
58. Kuhn PH, Koroniak K, Hogl S, et al. Secretome protein enrichment identifies physiological BACE1 protease substrates in neurons. The EMBO journal 2012;31:3157-68.
59. Zhou L, Barão S, Laga M, et al. The neural cell adhesion molecules L1 and CHL1 are cleaved by BACE1 protease in vivo. The Journal of biological chemistry 2012;287:25927-40.
60. Wong HK, Sakurai T, Oyama F, et al. beta Subunits of voltage-gated sodium channels are novel substrates of beta-site amyloid precursor protein-cleaving enzyme (BACE1) and gamma-secretase. The Journal of biological chemistry 2005;280:23009-17.
61. Kim DY, Carey BW, Wang H, et al. BACE1 regulates voltage-gated sodium channels and neuronal activity. Nature cell biology 2007;9:755-64.
62. Meziane H, Dodart JC, Mathis C, et al. Memory-enhancing effects of secreted forms of the beta-amyloid precursor protein in normal and amnestic mice. Proceedings of the National Academy of Sciences of the United States of America 1998;95:12683-8.
63. Roch JM, Masliah E, Roch-Levecq AC, et al. Increase of synaptic density and memory retention by a peptide representing the trophic domain of the amyloid beta/A4 protein precursor. Proceedings of the National Academy of Sciences of the United States of America 1994;91:7450-4.
64. Abramov E, Dolev I, Fogel H, Ciccotosto GD, Ruff E, Slutsky I. Amyloid-beta as a positive endogenous regulator of release probability at hippocampal synapses. Nature neuroscience 2009;12:1567-76.
65. Kamenetz F, Tomita T, Hsieh H, et al. APP processing and synaptic function. Neuron 2003;37:925-37.
66. Barão S, Gärtner A, Leyva-Díaz E, et al. Antagonistic Effects of BACE1 and APH1B-γ-Secretase Control Axonal Guidance by Regulating Growth Cone Collapse. Cell reports 2015;12:1367-76.

67. De Strooper B, Annaert W, Cupers P, et al. A presenilin-1-dependent gamma-secretase-like protease mediates release of Notch intracellular domain. Nature 1999;398:518-22.
68. Güner G, Lichtenthaler SF. The substrate repertoire of γ-secretase/presenilin. Seminars in cell & developmental biology 2020;105:27-42.
69. Tüshaus J, Müller SA, Kataka ES, et al. An optimized quantitative proteomics method establishes the cell type-resolved mouse brain secretome. The EMBO journal 2020;39:e105693.
70. Farzan M, Schnitzler CE, Vasilieva N, Leung D, Choe H. BACE2, a beta -secretase homolog, cleaves at the beta site and within the amyloid-beta region of the amyloid-beta precursor protein. Proceedings of the National Academy of Sciences of the United States of America 2000;97:9712-7.
71. Dominguez D, Tournoy J, Hartmann D, et al. Phenotypic and biochemical analyses of BACE1- and BACE2-deficient mice. The Journal of biological chemistry 2005;280:30797-806.
72. Bennett BD, Babu-Khan S, Loeloff R, et al. Expression analysis of BACE2 in brain and peripheral tissues. The Journal of biological chemistry 2000;275:20647-51.
73. Voytyuk I, Mueller SA, Herber J, et al. BACE2 distribution in major brain cell types and identification of novel substrates. Life science alliance 2018;1:e201800026.
74. Esterházy D, Stützer I, Wang H, et al. Bace2 is a β cell-enriched protease that regulates pancreatic β cell function and mass. Cell metabolism 2011;14:365-77.
75. Alcarraz-Vizán G, Castaño C, Visa M, Montane J, Servitja JM, Novials A. BACE2 suppression promotes β-cell survival and function in a model of type 2 diabetes induced by human islet amyloid polypeptide overexpression. Cellular and molecular life sciences : CMLS 2017;74:2827-38.
76. Rulifson IC, Cao P, Miao L, et al. Identification of Human Islet Amyloid Polypeptide as a BACE2 Substrate. PloS one 2016;11:e0147254.
77. Zhang YM, Zimmer MA, Guardia T, et al. Distant Insulin Signaling Regulates Vertebrate Pigmentation through the Sheddase Bace2. Developmental cell 2018;45:580-94.e7.
78. Ghosh AK, Brindisi M, Yen YC, et al. Highly Selective and Potent Human β-Secretase 2 (BACE2) Inhibitors against Type 2 Diabetes: Design, Synthesis, X-ray Structure and Structure-Activity Relationship Studies. ChemMedChem 2019;14:545-60.
79. Rochin L, Hurbain I, Serneels L, et al. BACE2 processes PMEL to form the melanosome amyloid matrix in pigment cells. Proceedings of the National Academy of Sciences of the United States of America 2013;110:10658-63.
80. Shimshek DR, Jacobson LH, Kolly C, et al. Pharmacological BACE1 and BACE2 inhibition induces hair depigmentation by inhibiting PMEL17 processing in mice. Scientific reports 2016;6:21917.
81. Cebers G, Lejeune T, Attalla B, et al. Reversible and Species-Specific Depigmentation Effects of AZD3293, a BACE Inhibitor for the Treatment of Alzheimer's Disease, Are Related to BACE2 Inhibition and Confined to Epidermis and Hair. The journal of prevention of Alzheimer's disease 2016;3:202-18.
82. Benzel I, Bansal A, Browning BL, et al. Interactions among genes in the ErbB-Neuregulin signalling network are associated with increased susceptibility to schizophrenia. Behavioral and brain functions : BBF 2007;3:31.
83. Yan L, Shamir A, Skirzewski M, et al. Neuregulin-2 ablation results in dopamine dysregulation and severe behavioral phenotypes relevant to psychiatric disorders. Molecular psychiatry 2018;23:1233-43.
84. Czarnek M, Bereta J. Proteolytic Processing of Neuregulin 2. Molecular neurobiology 2019.
85. Uhlén M, Fagerberg L, Hallström BM, et al. Proteomics. Tissue-based map of the human proteome. Science (New York, NY) 2015;347:1260419.
86. Liu F, Zhang Y, Liang Z, et al. Cleavage of potassium channel Kv2.1 by BACE2 reduces neuronal apoptosis. Molecular psychiatry 2018;23:1542-54.
87. Terry RD, Masliah E, Salmon DP, et al. Physical basis of cognitive alterations in Alzheimer's disease: synapse loss is the major correlate of cognitive impairment. Annals of neurology 1991;30:572-80.

88. Heneka MT, Carson MJ, El Khoury J, et al. Neuroinflammation in Alzheimer's disease. The Lancet Neurology 2015;14:388-405.
89. Frisoni GB, Fox NC, Jack CR, Jr., Scheltens P, Thompson PM. The clinical use of structural MRI in Alzheimer disease. Nature reviews Neurology 2010;6:67-77.
90. Tabatabaei-Jafari H, Shaw ME, Cherbuin N. Cerebral atrophy in mild cognitive impairment: A systematic review with meta-analysis. Alzheimer's & dementia (Amsterdam, Netherlands) 2015;1:487-504.
91. Cohen AD, Landau SM, Snitz BE, Klunk WE, Blennow K, Zetterberg H. Fluid and PET biomarkers for amyloid pathology in Alzheimer's disease. Molecular and cellular neurosciences 2019;97:3-17.
92. Itoh N, Arai H, Urakami K, et al. Large-scale, multicenter study of cerebrospinal fluid tau protein phosphorylated at serine 199 for the antemortem diagnosis of Alzheimer's disease. Annals of neurology 2001;50:150-6.
93. Egan MF, Kost J, Voss T, et al. Randomized Trial of Verubecestat for Prodromal Alzheimer's Disease. The New England journal of medicine 2019;380:1408-20.
94. Sperling R, Henley D, Aisen PS, et al. Findings of Efficacy, Safety, and Biomarker Outcomes of Atabecestat in Preclinical Alzheimer Disease: A Truncated Randomized Phase 2b/3 Clinical Trial. JAMA neurology 2021.
95. Wessels AM, Tariot PN, Zimmer JA, et al. Efficacy and Safety of Lanabecestat for Treatment of Early and Mild Alzheimer Disease: The AMARANTH and DAYBREAK-ALZ Randomized Clinical Trials. JAMA neurology 2020;77:199-209.
96. Molinuevo JL, Ayton S, Batrla R, et al. Current state of Alzheimer's fluid biomarkers. Acta neuropathologica 2018;136:821-53.
97. Suárez-Calvet M, Kleinberger G, Araque Caballero M, et al. sTREM2 cerebrospinal fluid levels are a potential biomarker for microglia activity in early-stage Alzheimer's disease and associate with neuronal injury markers. EMBO molecular medicine 2016;8:466-76.
98. Kvartsberg H, Duits FH, Ingelsson M, et al. Cerebrospinal fluid levels of the synaptic protein neurogranin correlates with cognitive decline in prodromal Alzheimer's disease. Alzheimer's & dementia : the journal of the Alzheimer's Association 2015;11:1180-90.
99. Casaletto KB, Elahi FM, Bettcher BM, et al. Neurogranin, a synaptic protein, is associated with memory independent of Alzheimer biomarkers. Neurology 2017;89:1782-8.
100. Saint-Aubert L, Lemoine L, Chiotis K, Leuzy A, Rodriguez-Vieitez E, Nordberg A. Tau PET imaging: present and future directions. Molecular neurodegeneration 2017;12:19.
101. Alexander GE, Chen K, Pietrini P, Rapoport SI, Reiman EM. Longitudinal PET Evaluation of Cerebral Metabolic Decline in Dementia: A Potential Outcome Measure in Alzheimer's Disease Treatment Studies. The American journal of psychiatry 2002;159:738-45.
102. Reiman EM. Fluorodeoxyglucose positron emission tomography: emerging roles in the evaluation of putative Alzheimer's disease-modifying treatments. Neurobiology of aging 2011;32 Suppl 1:S44-7.
103. Chen MK, Mecca AP, Naganawa M, et al. Assessing Synaptic Density in Alzheimer Disease With Synaptic Vesicle Glycoprotein 2A Positron Emission Tomographic Imaging. JAMA neurology 2018;75:1215-24.
104. Jack CR, Jr., Petersen RC, O'Brien PC, Tangalos EG. MR-based hippocampal volumetry in the diagnosis of Alzheimer's disease. Neurology 1992;42:183-8.
105. Khalil M, Teunissen CE, Otto M, et al. Neurofilaments as biomarkers in neurological disorders. Nature reviews Neurology 2018;14:577-89.
106. Elahi FM, Casaletto KB, La Joie R, et al. Plasma biomarkers of astrocytic and neuronal dysfunction in early- and late-onset Alzheimer's disease. Alzheimer's & dementia : the journal of the Alzheimer's Association 2020;16:681-95.
107. Janelidze S, Stomrud E, Palmqvist S, et al. Plasma β-amyloid in Alzheimer's disease and vascular disease. Scientific reports 2016;6:26801.
108. Nakamura A, Kaneko N, Villemagne VL, et al. High performance plasma amyloid-β biomarkers for Alzheimer's disease. Nature 2018;554:249-54.

109. Palmqvist S, Janelidze S, Stomrud E, et al. Performance of Fully Automated Plasma Assays as Screening Tests for Alzheimer Disease-Related β-Amyloid Status. JAMA neurology 2019;76:1060-9.
110. Zetterberg H. Review: Tau in biofluids - relation to pathology, imaging and clinical features. Neuropathology and applied neurobiology 2017;43:194-9.
111. Pereira JB, Westman E, Hansson O. Association between cerebrospinal fluid and plasma neurodegeneration biomarkers with brain atrophy in Alzheimer's disease. Neurobiology of aging 2017;58:14-29.
112. Sato C, Barthélemy NR, Mawuenyega KG, et al. Tau Kinetics in Neurons and the Human Central Nervous System. Neuron 2018;98:861-4.
113. Randall J, Mörtberg E, Provuncher GK, et al. Tau proteins in serum predict neurological outcome after hypoxic brain injury from cardiac arrest: results of a pilot study. Resuscitation 2013;84:351-6.
114. Mielke MM, Hagen CE, Xu J, et al. Plasma phospho-tau181 increases with Alzheimer's disease clinical severity and is associated with tau- and amyloid-positron emission tomography. Alzheimer's & dementia : the journal of the Alzheimer's Association 2018;14:989-97.
115. Janelidze S, Mattsson N, Palmqvist S, et al. Plasma P-tau181 in Alzheimer's disease: relationship to other biomarkers, differential diagnosis, neuropathology and longitudinal progression to Alzheimer's dementia. Nature medicine 2020;26:379-86.
116. Neumann U, Ufer M, Jacobson LH, et al. The BACE-1 inhibitor CNP520 for prevention trials in Alzheimer's disease. EMBO molecular medicine 2018;10.
117. Kennedy ME, Stamford AW, Chen X, et al. The BACE1 inhibitor verubecestat (MK-8931) reduces CNS β-amyloid in animal models and in Alzheimer's disease patients. Science translational medicine 2016;8:363ra150.
118. Egan MF, Kost J, Tariot PN, et al. Randomized Trial of Verubecestat for Mild-to-Moderate Alzheimer's Disease. The New England journal of medicine 2018;378:1691-703.
119. Eketjäll S, Janson J, Kaspersson K, et al. AZD3293: A Novel, Orally Active BACE1 Inhibitor with High Potency and Permeability and Markedly Slow Off-Rate Kinetics. Journal of Alzheimer's disease : JAD 2016;50:1109-23.
120. Hsiao CC, Rombouts F, Gijsen HJM. New evolutions in the BACE1 inhibitor field from 2014 to 2018. Bioorganic & medicinal chemistry letters 2019;29:761-77.
121. McKinzie DL, May PC, Boggs LN, et al. P1-080: Nonclinical Pharmacological Characterization of the Bace1 Inhibitor LY3202626. Alzheimer's & Dementia 2016;12:P432-P3.
122. Timmers M, Streffer JR, Russu A, et al. Pharmacodynamics of atabecestat (JNJ-54861911), an oral BACE1 inhibitor in patients with early Alzheimer's disease: randomized, double-blind, placebo-controlled study. Alzheimer's research & therapy 2018;10:85.
123. Willis BA, Lowe SL, Daugherty LL, et al. P1-044: Pharmacokinetics, Pharmacodynamics, Safety, and Tolerability of LY3202626, a Novel Bace1 Inhibitor, in Healthy Subjects and Patients with Alzheimer’s Disease. Alzheimer's & Dementia 2016;12:P418-P.
124. Eric McDade IV, Paul Aisen, Randall J. Bateman ,Maria C. Carrillo , Bart De Strooper, Christian Haass, Eric M. Reiman ,Reisa Sperling, Pierre N. Tariot , Riqiang Yan, Colin L. Masters, Robert Vassar and Stefan F. Lichtenthaler. The case for low-level BACE1 inhibition for the prevention of Alzheimer disease. Nature Reviews Neurology, submitted 2021.
125. Cheret C, Willem M, Fricker FR, et al. Bace1 and Neuregulin-1 cooperate to control formation and maintenance of muscle spindles. The EMBO journal 2013;32:2015-28.
126. Zhu K, Xiang X, Filser S, et al. Beta-Site Amyloid Precursor Protein Cleaving Enzyme 1 Inhibition Impairs Synaptic Plasticity via Seizure Protein 6. Biological psychiatry 2018;83:428-37.
127. Willem M, Tahirovic S, Busche MA, et al. eta-Secretase processing of APP inhibits neuronal activity in the hippocampus. Nature 2015;526:443-7.
128. McConlogue L, Buttini M, Anderson JP, et al. Partial reduction of BACE1 has dramatic effects on Alzheimer plaque and synaptic pathology in APP Transgenic Mice. The Journal of biological chemistry 2007;282:26326-34.

129. Maloney JA, Bainbridge T, Gustafson A, et al. Molecular mechanisms of Alzheimer disease protection by the A673T allele of amyloid precursor protein. The Journal of biological chemistry 2014;289:30990-1000.
130. Martiskainen H, Herukka SK, Stančáková A, et al. Decreased plasma β-amyloid in the Alzheimer's disease APP A673T variant carriers. Annals of neurology 2017;82:128-32.
131. Struyfs H, Van Broeck B, Timmers M, et al. Diagnostic Accuracy of Cerebrospinal Fluid Amyloid-β Isoforms for Early and Differential Dementia Diagnosis. Journal of Alzheimer's disease : JAD 2015;45:813-22.
132. Van Broeck B, Timmers M, Ramael S, et al. Impact of frequent cerebrospinal fluid sampling on Aβ levels: systematic approach to elucidate influencing factors. Alzheimer's research & therapy 2016;8:21.
133. Cox J, Hein MY, Luber CA, Paron I, Nagaraj N, Mann M. Accurate proteome-wide label-free quantification by delayed normalization and maximal peptide ratio extraction, termed MaxLFQ. Molecular & cellular proteomics : MCP 2014;13:2513-26.
134. Bruderer R, Bernhardt OM, Gandhi T, et al. Extending the limits of quantitative proteome profiling with data-independent acquisition and application to acetaminophen-treated three-dimensional liver microtissues. Molecular & cellular proteomics : MCP 2015;14:1400-10.
135. Tusher VG, Tibshirani R, Chu G. Significance analysis of microarrays applied to the ionizing radiation response. Proceedings of the National Academy of Sciences of the United States of America 2001;98:5116-21.
136. Tyanova S, Temu T, Sinitcyn P, et al. The Perseus computational platform for comprehensive analysis of (prote)omics data. Nature methods 2016;13:731-40.
137. Ivankov DN, Bogatyreva NS, Hönigschmid P, et al. QARIP: a web server for quantitative proteomic analysis of regulated intramembrane proteolysis. Nucleic acids research 2013;41:W459-64.
138. MacLean B, Tomazela DM, Shulman N, et al. Skyline: an open source document editor for creating and analyzing targeted proteomics experiments. Bioinformatics (Oxford, England) 2010;26:966-8.
139. Paul A. Drug Distribution. In: Raj GM, Raveendran R, eds. Introduction to Basics of Pharmacology and Toxicology: Volume 1: General and Molecular Pharmacology: Principles of Drug Action. Singapore: Springer Singapore; 2019:89-98.
140. Ludwig C, Gillet L, Rosenberger G, Amon S, Collins BC, Aebersold R. Data-independent acquisition-based SWATH-MS for quantitative proteomics: a tutorial. Molecular systems biology 2018;14:e8126.
141. Gillet LC, Navarro P, Tate S, et al. Targeted data extraction of the MS/MS spectra generated by data-independent acquisition: a new concept for consistent and accurate proteome analysis. Molecular & cellular proteomics : MCP 2012;11:O111.016717.
142. Bruderer R, Sondermann J, Tsou CC, et al. New targeted approaches for the quantification of data-independent acquisition mass spectrometry. Proteomics 2017;17.
143. Hilpert H, Guba W, Woltering TJ, et al. β-Secretase (BACE1) inhibitors with high in vivo efficacy suitable for clinical evaluation in Alzheimer's disease. Journal of medicinal chemistry 2013;56:3980-95.
144. May PC, Dean RA, Lowe SL, et al. Robust central reduction of amyloid-β in humans with an orally available, non-peptidic β-secretase inhibitor. The Journal of neuroscience : the official journal of the Society for Neuroscience 2011;31:16507-16.
145. Bando H, Brokelmann M, Toi M, et al. Immunodetection and quantification of vascular endothelial growth factor receptor-3 in human malignant tumor tissues. International journal of cancer 2004;111:184-91.
146. Goh JB, Ng SK. Impact of host cell line choice on glycan profile. Critical reviews in biotechnology 2018;38:851-67.
147. Clausen H, Wandall HH, Steentoft C, Stanley P, Schnaar RL. Glycosylation Engineering. In: Varki A, Cummings RD, Esko JD, et al., eds. Essentials of Glycobiology. Cold Spring Harbor (NY): Cold Spring Harbor Laboratory Press

Copyright 2015-2017 by The Consortium of Glycobiology Editors, La Jolla, California. All rights reserved.; 2015:713-28.
148. Jenkins N, Parekh RB, James DC. Getting the glycosylation right: implications for the biotechnology industry. Nature biotechnology 1996;14:975-81.
149. Leppanen VM, Tvorogov D, Kisko K, et al. Structural and mechanistic insights into VEGF receptor 3 ligand binding and activation. Proceedings of the National Academy of Sciences of the United States of America 2013;110:12960-5.
150. Brodney MA, Beck EM, Butler CR, et al. Utilizing structures of CYP2D6 and BACE1 complexes to reduce risk of drug-drug interactions with a novel series of centrally efficacious BACE1 inhibitors. Journal of medicinal chemistry 2015;58:3223-52.
151. Malamas MS, Barnes K, Johnson M, et al. Di-substituted pyridinyl aminohydantoins as potent and highly selective human beta-secretase (BACE1) inhibitors. Bioorganic & medicinal chemistry 2010;18:630-9.
152. Rombouts FK, Ken-ichi; Alexander, Richard; Austin, Nigel; Borghys, Herman; De Cleyn, Michel; Dhuyvetter, Deborah; Gijsen, Harrie; Hrupka, Brian; Jacobs, Tom; Jerhaoui, Soufyan; Lammens, Lieve; Leclercq, Laurent; Tsubone, Koichi; Ueno, Tatsuhiko; Morimoto, Kenji; Einaru, Shunsuke; Sumiyoshi, Hirokazu; Van Den Bergh, An; Vos, Ann; Surkyn, Michel; Teisman, Ard; Moechars, Diederik. JNJ-67569762, a 2-aminotetrahydropyridine based selective BACE1 inhibitor targeting the S3 pocket: from discovery to clinical candidate. Journal of Medicinal Chemistry, submitted for publication 2021.
153. Grüninger-Leitch F, Schlatter D, Küng E, Nelböck P, Döbeli H. Substrate and inhibitor profile of BACE (beta-secretase) and comparison with other mammalian aspartic proteases. The Journal of biological chemistry 2002;277:4687-93.
154. Tvorogov D, Anisimov A, Zheng W, et al. Effective suppression of vascular network formation by combination of antibodies blocking VEGFR ligand binding and receptor dimerization. Cancer cell 2010;18:630-40.
155. Roelfsema PR, Treue S. Basic neuroscience research with nonhuman primates: a small but indispensable component of biomedical research. Neuron 2014;82:1200-4.
156. Capitanio JP, Emborg ME. Contributions of non-human primates to neuroscience research. Lancet (London, England) 2008;371:1126-35.
157. Joukov V, Kumar V, Sorsa T, et al. A recombinant mutant vascular endothelial growth factor-C that has lost vascular endothelial growth factor receptor-2 binding, activation, and vascular permeability activities. The Journal of biological chemistry 1998;273:6599-602.
158. Joukov V, Pajusola K, Kaipainen A, et al. A novel vascular endothelial growth factor, VEGF-C, is a ligand for the Flt4 (VEGFR-3) and KDR (VEGFR-2) receptor tyrosine kinases. The EMBO journal 1996;15:290-98.
159. Wang Y, Nakayama M, Pitulescu ME, et al. Ephrin-B2 controls VEGF-induced angiogenesis and lymphangiogenesis. Nature 2010;465:483-6.
160. Dieterich LC, Ducoli L, Shin JW, Detmar M. Distinct transcriptional responses of lymphatic endothelial cells to VEGFR-3 and VEGFR-2 stimulation. Scientific data 2017;4:170106.
161. Yoneya T, Tahara T, Nagao K, et al. Molecular cloning of delta-4, a new mouse and human Notch ligand. Journal of biochemistry 2001;129:27-34.
162. Brütsch R, Liebler SS, Wüstehube J, et al. Integrin cytoplasmic domain-associated protein-1 attenuates sprouting angiogenesis. Circulation research 2010;107:592-601.
163. Suchting S, Freitas C, le Noble F, et al. The Notch ligand Delta-like 4 negatively regulates endothelial tip cell formation and vessel branching. Proceedings of the National Academy of Sciences of the United States of America 2007;104:3225-30.
164. Wu X, Liu NF. FOXC2 transcription factor: a novel regulator of lymphangiogenesis. Lymphology 2011;44:35-41.
165. Sabine A, Petrova TV. Interplay of mechanotransduction, FOXC2, connexins, and calcineurin signaling in lymphatic valve formation. Advances in anatomy, embryology, and cell biology 2014;214:67-80.

166. Barkovits K, Kruse N, Linden A, et al. Blood Contamination in CSF and Its Impact on Quantitative Analysis of Alpha-Synuclein. Cells 2020;9.
167. Jaros JA, Guest PC, Bahn S, Martins-de-Souza D. Affinity depletion of plasma and serum for mass spectrometry-based proteome analysis. Methods in molecular biology (Clifton, NJ) 2013;1002:1-11.
168. Bekker-Jensen DB, Bernhardt OM, Hogrebe A, et al. Rapid and site-specific deep phosphoproteome profiling by data-independent acquisition without the need for spectral libraries. Nature communications 2020;11:787.
169. Muntel J, Kirkpatrick J, Bruderer R, et al. Comparison of Protein Quantification in a Complex Background by DIA and TMT Workflows with Fixed Instrument Time. Journal of proteome research 2019;18:1340-51.
170. Tsou CC, Avtonomov D, Larsen B, et al. DIA-Umpire: comprehensive computational framework for data-independent acquisition proteomics. Nature methods 2015;12:258-64, 7 p following 64.
171. Muntel J, Gandhi T, Verbeke L, et al. Surpassing 10 000 identified and quantified proteins in a single run by optimizing current LC-MS instrumentation and data analysis strategy. Molecular omics 2019;15:348-60.
172. Jeffs JW, Jehanathan N, Thibert SMF, et al. Delta-S-Cys-Albumin: A Lab Test that Quantifies Cumulative Exposure of Archived Human Blood Plasma and Serum Samples to Thawed Conditions. Molecular & cellular proteomics : MCP 2019;18:2121-37.
173. Mitchell BL, Yasui Y, Li CI, Fitzpatrick AL, Lampe PD. Impact of freeze-thaw cycles and storage time on plasma samples used in mass spectrometry based biomarker discovery projects. Cancer informatics 2005;1:98-104.
174. Schwenk JM, Omenn GS, Sun Z, et al. The Human Plasma Proteome Draft of 2017: Building on the Human Plasma PeptideAtlas from Mass Spectrometry and Complementary Assays. Journal of proteome research 2017;16:4299-310.
175. Pernemalm M, Sandberg A, Zhu Y, et al. In-depth human plasma proteome analysis captures tissue proteins and transfer of protein variants across the placenta. eLife 2019;8.
176. Geyer PE, Voytik E, Treit PV, et al. Plasma Proteome Profiling to detect and avoid sample-related biases in biomarker studies. EMBO molecular medicine 2019;11:e10427.
177. Park J, Kim H, Kim SY, et al. In-depth blood proteome profiling analysis revealed distinct functional characteristics of plasma proteins between severe and non-severe COVID-19 patients. Scientific reports 2020;10:22418.
178. Bian Y, Bayer FP, Chang YC, et al. Robust Microflow LC-MS/MS for Proteome Analysis: 38 000 Runs and Counting. Analytical chemistry 2021;93:3686-90.
179. Bian Y, Zheng R, Bayer FP, et al. Robust, reproducible and quantitative analysis of thousands of proteomes by micro-flow LC-MS/MS. Nature communications 2020;11:157.
180. Meier F, Köhler ND, Brunner AD, et al. Deep learning the collisional cross sections of the peptide universe from a million experimental values. Nature communications 2021;12:1185.
181. Gessulat S, Schmidt T, Zolg DP, et al. Prosit: proteome-wide prediction of peptide tandem mass spectra by deep learning. Nature methods 2019;16:509-18.
182. He W, Hu J, Xia Y, Yan R. β-site amyloid precursor protein cleaving enzyme 1(BACE1) regulates Notch signaling by controlling the cleavage of Jagged 1 (Jag1) and Jagged 2 (Jag2) proteins. The Journal of biological chemistry 2014;289:20630-7.
183. Yan R. Physiological Functions of the β-Site Amyloid Precursor Protein Cleaving Enzyme 1 and 2. Frontiers in molecular neuroscience 2017;10:97.
184. Hampel H, Vassar R, De Strooper B, et al. The β-Secretase BACE1 in Alzheimer's Disease. Biological psychiatry 2021;89:745-56.
185. Pajusola K, Aprelikova O, Korhonen J, et al. FLT4 receptor tyrosine kinase contains seven immunoglobulin-like loops and is expressed in multiple human tissues and cell lines. Cancer research 1992;52:5738-43.
186. Dumont DJ, Jussila L, Taipale J, et al. Cardiovascular failure in mouse embryos deficient in VEGF receptor-3. Science (New York, NY) 1998;282:946-9.

187. Karkkainen MJ, Haiko P, Sainio K, et al. Vascular endothelial growth factor C is required for sprouting of the first lymphatic vessels from embryonic veins. Nature immunology 2004;5:74-80.
188. Kaipainen A, Korhonen J, Mustonen T, et al. Expression of the fms-like tyrosine kinase 4 gene becomes restricted to lymphatic endothelium during development. Proceedings of the National Academy of Sciences of the United States of America 1995;92:3566-70.
189. Antila S, Karaman S, Nurmi H, et al. Development and plasticity of meningeal lymphatic vessels. The Journal of experimental medicine 2017;214:3645-67.
190. Zhang Y, Zhang C, Li L, et al. Lymphangiogenesis in renal fibrosis arises from macrophages via VEGF-C/VEGFR3-dependent autophagy and polarization. Cell death & disease 2021;12:109.
191. Swovick K, Firsanov D, Welle KA, et al. Interspecies Differences in Proteome Turnover Kinetics Are Correlated With Life Spans and Energetic Demands. Molecular & cellular proteomics : MCP 2021;20:100041.
192. Kuhn PH, Wang H, Dislich B, et al. ADAM10 is the physiologically relevant, constitutive alpha-secretase of the amyloid precursor protein in primary neurons. The EMBO journal 2010;29:3020-32.
193. Postina R, Schroeder A, Dewachter I, et al. A disintegrin-metalloproteinase prevents amyloid plaque formation and hippocampal defects in an Alzheimer disease mouse model. The Journal of clinical investigation 2004;113:1456-64.
194. Lahiri DK, Maloney B, Long JM, Greig NH. Lessons from a BACE1 inhibitor trial: off-site but not off base. Alzheimer's & dementia : the journal of the Alzheimer's Association 2014;10:S411-9.
195. Singh N, Tiem M, Watkins R, et al. Soluble vascular endothelial growth factor receptor 3 is essential for corneal alymphaticity. Blood 2013;121:4242-9.
196. Kan CW, Tobos CI, Rissin DM, et al. Digital enzyme-linked immunosorbent assays with sub-attomolar detection limits based on low numbers of capture beads combined with high efficiency bead analysis. Lab on a chip 2020;20:2122-35.
197. Darebna P, Spicka J, Kucera R, et al. Detection and Quantification of Carbohydrate-Deficient Transferrin by MALDI-Compatible Protein Chips Prepared by Ambient Ion Soft Landing. Clin Chem 2018;64:1319-26.
198. Li H, Popp R, Frohlich B, Chen MX, Borchers CH. Peptide and Protein Quantification Using Automated Immuno-MALDI (iMALDI). Journal of visualized experiments : JoVE 2017.
199. Zahedi RP, Parker CE, Borchers CH. Immuno-MALDI-TOF-MS in the Clinic. Clinical Chemistry 2018;64:1271-2.
200. Barão S, Moechars D, Lichtenthaler SF, De Strooper B. BACE1 Physiological Functions May Limit Its Use as Therapeutic Target for Alzheimer's Disease. Trends in neurosciences 2016;39:158-69.
201. Pajusola K, Aprelikova O, Pelicci G, Weich H, Claesson-Welsh L, Alitalo K. Signalling properties of FLT4, a proteolytically processed receptor tyrosine kinase related to two VEGF receptors. Oncogene 1994;9:3545-55.
202. Deng Y, Zhang X, Simons M. Molecular controls of lymphatic VEGFR3 signaling. Arteriosclerosis, thrombosis, and vascular biology 2015;35:421-9.
203. Sarabipour S, Ballmer-Hofer K, Hristova K. VEGFR-2 conformational switch in response to ligand binding. eLife 2016;5:e13876.
204. Makinen T, Veikkola T, Mustjoki S, et al. Isolated lymphatic endothelial cells transduce growth, survival and migratory signals via the VEGF-C/D receptor VEGFR-3. The EMBO journal 2001;20:4762-73.
205. Urner S, Planas-Paz L, Hilger LS, et al. Identification of ILK as a critical regulator of VEGFR3 signalling and lymphatic vascular growth. The EMBO journal 2019;38.
206. Domigan CK, Ziyad S, Iruela-Arispe ML. Canonical and noncanonical vascular endothelial growth factor pathways: new developments in biology and signal transduction. Arteriosclerosis, thrombosis, and vascular biology 2015;35:30-9.

207. Zhang X, Groopman JE, Wang JF. Extracellular matrix regulates endothelial functions through interaction of VEGFR-3 and integrin alpha5beta1. Journal of cellular physiology 2005;202:205-14.
208. Kong LL, Yang NZ, Shi LH, et al. The optimum marker for the detection of lymphatic vessels. Molecular and clinical oncology 2017;7:515-20.
209. Uhlen M, Zhang C, Lee S, et al. A pathology atlas of the human cancer transcriptome. Science (New York, NY) 2017;357.
210. Merilahti JAM, Ojala VK, Knittle AM, Pulliainen AT, Elenius K. Genome-wide screen of gamma-secretase-mediated intramembrane cleavage of receptor tyrosine kinases. Molecular biology of the cell 2017;28:3123-31.
211. Merilahti JAM, Elenius K. Gamma-secretase-dependent signaling of receptor tyrosine kinases. Oncogene 2019;38:151-63.
212. Lichtenthaler SF, Haass C, Steiner H. Regulated intramembrane proteolysis--lessons from amyloid precursor protein processing. Journal of neurochemistry 2011;117:779-96.
213. Lin J, Lalani AS, Harding TC, et al. Inhibition of lymphogenous metastasis using adeno-associated virus-mediated gene transfer of a soluble VEGFR-3 decoy receptor. Cancer research 2005;65:6901-9.
214. Makinen T, Jussila L, Veikkola T, et al. Inhibition of lymphangiogenesis with resulting lymphedema in transgenic mice expressing soluble VEGF receptor-3. Nature medicine 2001;7:199-205.
215. Tammela T, Zarkada G, Wallgard E, et al. Blocking VEGFR-3 suppresses angiogenic sprouting and vascular network formation. Nature 2008;454:656-60.
216. Tammela T, Enholm B, Alitalo K, Paavonen K. The biology of vascular endothelial growth factors. Cardiovascular research 2005;65:550-63.
217. McColl BK, Stacker SA, Achen MG. Molecular regulation of the VEGF family -- inducers of angiogenesis and lymphangiogenesis. APMIS : acta pathologica, microbiologica, et immunologica Scandinavica 2004;112:463-80.
218. Jeltsch M, Kaipainen A, Joukov V, et al. Hyperplasia of lymphatic vessels in VEGF-C transgenic mice. Science (New York, NY) 1997;276:1423-5.
219. Gogineni A, Caunt M, Crow A, et al. Inhibition of VEGF-C modulates distal lymphatic remodeling and secondary metastasis. PloS one 2013;8:e68755.
220. Irrthum A, Karkkainen MJ, Devriendt K, Alitalo K, Vikkula M. Congenital hereditary lymphedema caused by a mutation that inactivates VEGFR3 tyrosine kinase. American journal of human genetics 2000;67:295-301.
221. Karkkainen MJ, Saaristo A, Jussila L, et al. A model for gene therapy of human hereditary lymphedema. Proceedings of the National Academy of Sciences of the United States of America 2001;98:12677-82.
222. Moreno-Zambrano D, Santana D, Avila D, Santibáñez R. Lymphatics of the Central Nervous System: Forgotten first descriptions. (S39.003). Neurology 2018;90:S39.003.
223. Iliff JJ, Wang M, Liao Y, et al. A paravascular pathway facilitates CSF flow through the brain parenchyma and the clearance of interstitial solutes, including amyloid β. Science translational medicine 2012;4:147ra11.
224. Louveau A, Smirnov I, Keyes TJ, et al. Structural and functional features of central nervous system lymphatic vessels. Nature 2015;523:337-41.
225. Aspelund A, Antila S, Proulx ST, et al. A dural lymphatic vascular system that drains brain interstitial fluid and macromolecules. The Journal of experimental medicine 2015;212:991-9.
226. Absinta M, Ha SK, Nair G, et al. Human and nonhuman primate meninges harbor lymphatic vessels that can be visualized noninvasively by MRI. eLife 2017;6.
227. Louveau A, Herz J, Alme MN, et al. CNS lymphatic drainage and neuroinflammation are regulated by meningeal lymphatic vasculature. Nature neuroscience 2018;21:1380-91.
228. Esposito E, Ahn BJ, Shi J, et al. Brain-to-cervical lymph node signaling after stroke. Nature communications 2019;10:5306.

229. Ahn JH, Cho H, Kim JH, et al. Meningeal lymphatic vessels at the skull base drain cerebrospinal fluid. Nature 2019;572:62-6.
230. Da Mesquita S, Louveau A, Vaccari A, et al. Functional aspects of meningeal lymphatics in ageing and Alzheimer's disease. Nature 2018;560:185-91.
231. Ma Q, Ineichen BV, Detmar M, Proulx ST. Outflow of cerebrospinal fluid is predominantly through lymphatic vessels and is reduced in aged mice. Nature communications 2017;8:1434.
232. Patel TK, Habimana-Griffin L, Gao X, et al. Dural lymphatics regulate clearance of extracellular tau from the CNS. Molecular neurodegeneration 2019;14:11.
233. Mahoney ER, Dumitrescu L, Moore AM, et al. Brain expression of the vascular endothelial growth factor gene family in cognitive aging and alzheimer's disease. Molecular psychiatry 2019.
234. Siekmann AF, Lawson ND. Notch signalling and the regulation of angiogenesis. Cell adhesion & migration 2007;1:104-6.
235. Zhang Y, Ulvmar MH, Stanczuk L, et al. Heterogeneity in VEGFR3 levels drives lymphatic vessel hyperplasia through cell-autonomous and non-cell-autonomous mechanisms. Nature communications 2018;9:1296.
236. Hellström M, Phng LK, Hofmann JJ, et al. Dll4 signalling through Notch1 regulates formation of tip cells during angiogenesis. Nature 2007;445:776-80.
237. Ju S, Xu C, Wang G, Zhang L. VEGF-C Induces Alternative Activation of Microglia to Promote Recovery from Traumatic Brain Injury. Journal of Alzheimer's disease : JAD 2019;68:1687-97.
238. Alishekevitz D, Gingis-Velitski S, Kaidar-Person O, et al. Macrophage-Induced Lymphangiogenesis and Metastasis following Paclitaxel Chemotherapy Is Regulated by VEGFR3. Cell reports 2016;17:1344-56.
239. Kiesewetter A, Cursiefen C, Eming SA, Hos D. Phase-specific functions of macrophages determine injury-mediated corneal hem- and lymphangiogenesis. Scientific reports 2019;9:308.
240. Narimatsu A, Hattori T, Koike N, et al. Corneal lymphangiogenesis ameliorates corneal inflammation and edema in late stage of bacterial keratitis. Scientific reports 2019;9:2984.
241. Yen YC, Kammeyer AM, Tirlangi J, Ghosh AK, Mesecar AD. A Structure-Based Discovery Platform for BACE2 and the Development of Selective BACE Inhibitors. ACS chemical neuroscience 2021.
242. Díaz-Catalán D, Alcarraz-Vizán G, Castaño C, et al. BACE2 suppression in mice aggravates the adverse metabolic consequences of an obesogenic diet. Molecular metabolism 2021;53:101251.
243. Munir H, Jones JO, Janowitz T, et al. Stromal-driven and Amyloid β-dependent induction of neutrophil extracellular traps modulates tumor growth. Nature communications 2021;12:683.
244. Chen Z, Wang H, Zhang Z, et al. Cell surface GRP78 regulates BACE2 via lysosome-dependent manner to maintain mesenchymal phenotype of glioma stem cells. Journal of experimental & clinical cancer research : CR 2021;40:20.
245. Wang H, Chen Z, Wang S, et al. TGFβ1-induced beta-site APP-cleaving enzyme 2 upregulation promotes tumorigenesis through the NF-κB signalling pathway in human gliomas. Molecular oncology 2020;14:407-25.
246. Matafora V, Farris F, Restuccia U, et al. Amyloid aggregates accumulate in melanoma metastasis modulating YAP activity. EMBO reports 2020;21:e50446.
247. Paris D, Quadros A, Patel N, DelleDonne A, Humphrey J, Mullan M. Inhibition of angiogenesis and tumor growth by beta and gamma-secretase inhibitors. European journal of pharmacology 2005;514:1-15.
248. Peters HL, Tuli A, Wang X, et al. Relevance of amyloid precursor-like protein 2 C-terminal fragments in pancreatic cancer cells. International journal of oncology 2012;41:1464-74.
249. Farris F, Matafora V, Bachi A. The emerging role of β-secretases in cancer. Journal of experimental & clinical cancer research : CR 2021;40:147.
250. Tsang JYS, Lee MA, Chan TH, et al. Proteolytic cleavage of amyloid precursor protein by ADAM10 mediates proliferation and migration in breast cancer. EBioMedicine 2018;38:89-99.

251. Paavonen K, Puolakkainen P, Jussila L, Jahkola T, Alitalo K. Vascular endothelial growth factor receptor-3 in lymphangiogenesis in wound healing. The American journal of pathology 2000;156:1499-504.
252. Baeyens N, Nicoli S, Coon BG, et al. Vascular remodeling is governed by a VEGFR3-dependent fluid shear stress set point. eLife 2015;4.
253. Laakkonen P, Waltari M, Holopainen T, et al. Vascular endothelial growth factor receptor 3 is involved in tumor angiogenesis and growth. Cancer research 2007;67:593-9.
254. Burton JB, Priceman SJ, Sung JL, et al. Suppression of prostate cancer nodal and systemic metastasis by blockade of the lymphangiogenic axis. Cancer research 2008;68:7828-37.
255. Mouawad R, Spano JP, Comperat E, Capron F, Khayat D. Tumoural expression and circulating level of VEGFR-3 (Flt-4) in metastatic melanoma patients: correlation with clinical parameters and outcome. European journal of cancer (Oxford, England : 1990) 2009;45:1407-14.
256. Labani-Motlagh A, Ashja-Mahdavi M, Loskog A. The Tumor Microenvironment: A Milieu Hindering and Obstructing Antitumor Immune Responses. Frontiers in immunology 2020;11:940.
257. Rabinovici GD. Controversy and Progress in Alzheimer's Disease - FDA Approval of Aducanumab. The New England journal of medicine 2021.
258. Lalli G, Schott JM, Hardy J, De Strooper B. Aducanumab: a new phase in therapeutic development for Alzheimer's disease? EMBO molecular medicine 2021;13:e14781.
259. Da Mesquita S, Papadopoulos Z, Dykstra T, et al. Meningeal lymphatics affect microglia responses and anti-Aβ immunotherapy. Nature 2021.

8. List of publications

Not applicable

9. Affidavit

Hiermit versichere ich an Eides statt, dass ich die vorliegende Dissertation „Identification and validation of vascular endothelial growth factor receptor 3 (VEGFR3) as an in vitro and in vivo substrate of the Alzheimer's disease-linked protease BACE2" selbstständig angefertigt habe, mich außer der angegebenen keiner weiteren Hilfsmittel bedient und alle Erkenntnisse, die aus dem Schrifttum ganz oder annähernd übernommen sind, als solche kenntlich gemacht und nach ihrer Herkunft unter Bezeichnung der Fundstelle einzeln nachgewiesen habe.

I hereby confirm that the dissertation „Identification and validation of vascular endothelial growth factor receptor 3 (VEGFR3) as an in vitro and in vivo substrate of the Alzheimer's disease-linked protease BACE2" is the result of my own work and that I have only used sources or materials listed and specified in the dissertation.

München, den 17.03.2022

Andree Schmidt

Munich, date Unterschrift signature

10.Declaration of author contributions

Andree Schmidt, Brian Hrupka, Stephan Müller, Mana Ito, Iryna Voytyuk, Bart de Strooper, Dieder Moechars, Stefan Lichtenthaler

A.S. performed the MS and immunological validation in the different mouse models (Fig. 06); *in vitro* validation in overexpression and endogenous conditions (Fig. 07-10), MS sequencing of VEGFR3 fragments; cleavage site determination (Fig. 12-13), MS validation in NHP (Fig. 16); functional consequences *in vitro* (Fig.17-18), was involved in designing the study.

A.S. and B.H. collaborated in the generation of inhibitor dose response curves (Fig. 11), *in vivo* monitoring of SEZ6L and VEGFR3 (Fig. 14), VEGFR3 comparison to fur pigmentation (Fig. 15) and analysing data on clinical trial participants (Fig. 16). B.H., D.M. and Janssen pharmaceutica provided murine plasma of inhibitor treated mice (Fig. 06B-C); were involved in designing the study.

S.M. performed the initial MS screening of glycoprotein enriched plasma (Fig 05), was involved in designing the study

A.S. and M.I. collaborated on the generation of NHP ELISA data (Fig. 16). M.I. and Shionogi provided the NHP and clinical trial participant plasma (Fig. 16)

I.V. and B.S. provided murine plasma samples from WT, self-generated B1KO and B2KO mice (Fig. 05) and commercial Riken B2KO mice (Fig. 06A,E-F)

S.L. supervised and designed the study

München, den 17.03.2022

Andree Schmidt

Munich, date Unterschrift signature